UiT
THE ARCTIC UNIVERSITY OF NORWAY

Faculty of Health Sciences
Department of Pharmacy

Melt processability of amorphous solid dispersions during hot-melt extrusion

Screening using vacuum compression moulding and evaluation by rheology and solid-state analysis

Nicklas Ekblad

Master's thesis in Pharmacy 2018

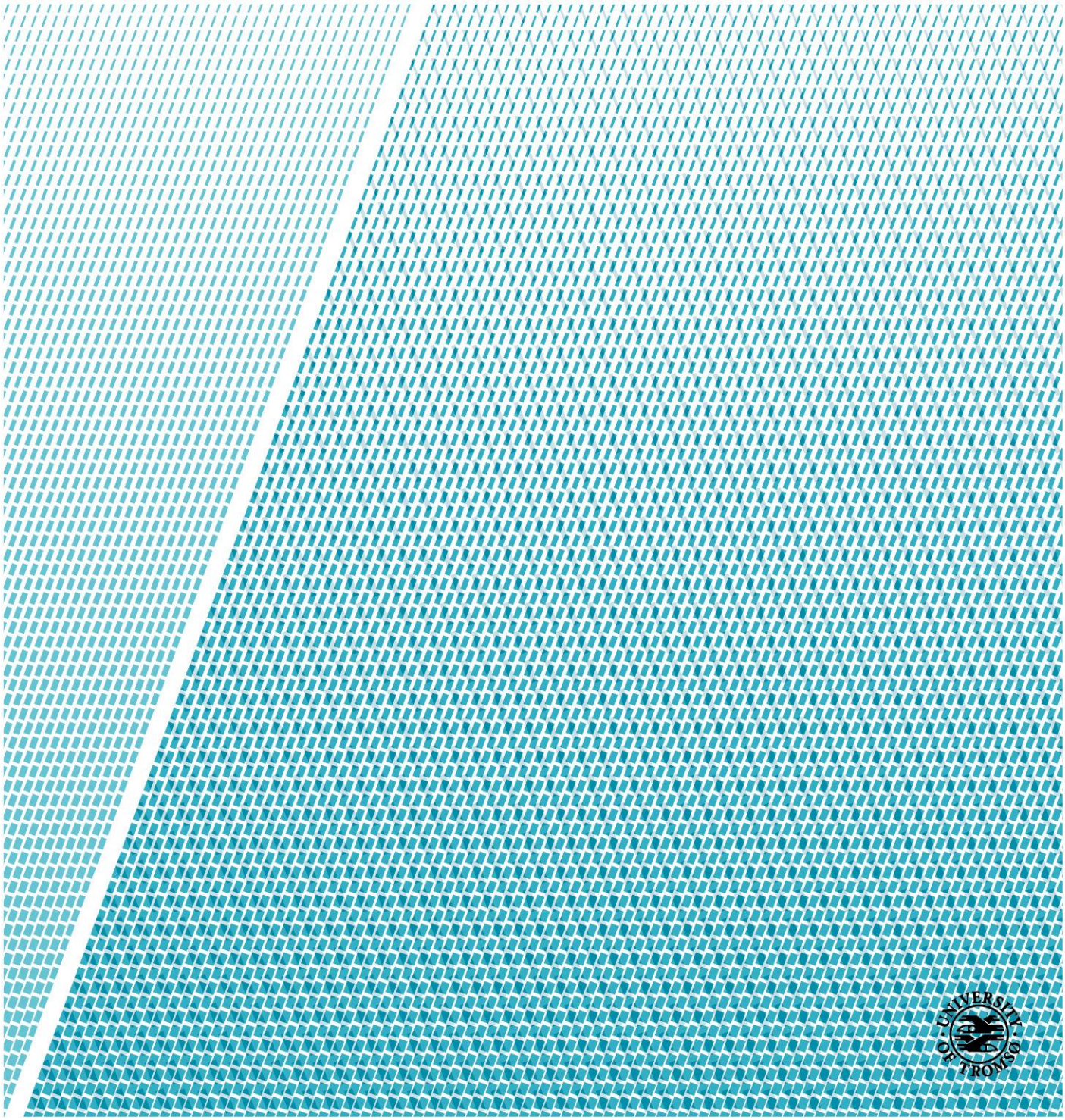

Foreword

I would like to thank my academic supervisors, Professor Jukka Rantanen and Professor Natasa Skalko-Basnet for giving me the opportunity to do this project and my co-supervisor Magnus Edinger for endless support and guidance. A big thanks to Jacob Bannow for guidance with the MeltPrep equipment, to Matthias Manne Knopp for help and guidance with the solubility determinations and Ana Calduch Arques for assisting me with sample preparation. Thanks to Johan Bøtker for helping with the extrusion process whenever problems arouse. A special thanks to Tomas Lövdahl for our time spent together as roommates, as classmates and as friends during our student years.

Lastly, I want to thank my family for their never-ending support through my many years of studying. Finally, I am extremely grateful and happy for the invaluable support and patience from my beloved girlfriend Nadja Soukka who is always there for me.

Abstract

Soluplus is a suitable excipient for innovative manufacturing techniques such as hot-melt extrusion (HME). While Soluplus is useful for forming amorphous solid dispersions (ASD's) during HME, the resulting extrudates are often stiff and brittle. In order to achieve suitable dosage forms, with optimal downstream processability, an efficient screening for suitable formulations is required. Vacuum compression moulding (VCM) is a rapid, cost-efficient sample preparation method for thermoplastic materials that could possibly be used as a reliable screening tool.

Solid dispersions with 10%, 30% and 50% w/w drug load of naproxen (NAP) or celecoxib (CCX) in Soluplus were prepared by HME and VCM under controlled conditions (HME: 120°C, 0 and 5 min recirculation, 50RPM, VCM: 120°C, 15 min). Melt processability and the effect of drug load were evaluated using rheology, subjecting the samples to a frequency sweep from 100-0.01 Hz at 120°C within the linear viscoelastic region. The samples were also analysed using differential scanning calorimetry (DSC), polarized light microscopy (PLM) and Raman Spectroscopy. The stability during storage of the solid dispersions prepared using HME was also investigated.

The complex viscosity (η*) between the different preparative methods varied considerably especially at the higher drug-loads. The lack of mixing and shear forces in VCM leads to less amorphisation and higher crystal content of drug in the mixture, which increases the melt viscosity. The difference is especially evident at higher drug loads where the mixing is critical for forming an ASD. The results also show that the dissolved NAP can act as a plasticizer lowering the melt viscosity of the API-polymer mixture. VCM should be used with consideration when predicting melt properties of melt extrudates, especially at higher drug loads.

List of Abbreviations

API – Active pharmaceutical ingredient

ASD – Amorphous solid dispersion

AUC – Area under the curve

BCS – Biopharmaceutical classification system

CCX – Celecoxib

CMC – Critical micelle concentration

COX – Cyclooxygenase inhibitor

C_{max} – Maximum plasma concentration

DSC – Differential scanning calorimetry

DMSO – Dimethyl sulfoxide

FDA – Food and Drug Administration

GFA – Glass forming ability

GI – Gastro-intestinal

HME – Hot-melt extrusion

HPMC – Hydroxypropyl methylcellulose

HSM – Hot Stage Microscopy

HTS – High throughput screening

IR – Infrared

LBDDS – Lipid based drug delivery system

LVR – Linear viscoelastic region

MP – MeltPrep®

NAP – Naproxen

NCE – New chemical entity

NSAID – Nonsteroidal anti-inflammatory drug

PAT – Process analytical technology

PEG – Polyethylene glycol

PEO – Polyethylene oxide

PTFE – Polytetrafluoroethylene

PVCL – Polyvinyl chloride

RPM – Rounds per minute

T_g – Glass transition temperature

T_m – Melting temperature

TPGS – d-α-Tocopheryl polyethylene glycol 1000 succinate

PCA – Principal component analysis

PLM – Polarized light microscopy

PVAc – Polyvinyl-acetate

PVCL – Polyvinyl-caprolactame

PVP – Polyvinyl pyrrolidone

SAOS – Small amplitude oscillatory shear

SNV – Standard normal variate

TGA – Thermogravimetric analysis

VCM – Vacuum compression moulding

XRPD – X-ray powder diffraction

Hz – Hertz

Pa – Pascal

s – Seconds

w/w – Weight to weight ratio

η* – Complex viscosity

η_s – Shear viscosity

γ – Strain

γ_0 – Strain amplitude

$\dot{\gamma}$ – Shear (strain) rate

τ – Shear stress

δ – Phase angle

ω – Angular frequency

t – Time

F – Force

A – Area

v – Velocity/volume

h – Gap / slit height

G' – Storage modulus

G" – Loss modulus

λ – wavelength

d – crystalline lattice spacing

θ – angle of diffraction

R – Gas constant

ρ – Density

χ – Flory-Huggins parameter

ΔH_m – Enthalpy of fusion

Table of Contents

1 Introduction

Soluplus is a polymer suitable for innovative manufacturing techniques such as hot-melt extrusion (HME)(Ali, Langley, Djuric, & Kolter, 2015). While Soluplus is useful for forming amorphous solid dispersions (ASD's) during HME, the resulting extrudates are often stiff and brittle. To achieve suitable dosage forms, with optimal downstream processabilities, an efficient screening for suitable formulations is required. Vacuum compression moulding (VCM) is a rapid, cost-efficient sample preparation method for thermoplastic materials that could possibly be used as a reliable screening tool (Treffer, Troiss, & Khinast, 2015).

This thesis has focused on investigating if VCM can be used as an appropriate tool for assessing the melt behaviour of HME formulations and as a screening tool for finding suitable formulations for HME. Rheological analysis, Raman spectroscopy, differential scanning calorimetry (DSC) and polarized light microscopy (PLM) has been evaluated as tools for assessing the quality and melt processability of solid dispersions prepared by HME. Naproxen (NAP) and celecoxib (CCX) were chosen as model compounds. Soluplus was chosen as the model polymer.

2 Litterature review

2.1 Solubility of drugs

The oral route of drug administration remains the preferred and most used method due to its non-invasive and patient oriented nature, improving the long term compliance of patients (Shaji & Patole, 2008). For an oral dosage form to have a clinical effect and enter the systemic circulation it must pass certain barriers. First the drug must be released from the carrier system (for example from a tablet). Then the drug must dissolve in the gastro-intestinal (GI) fluids during the short timeframe the drug travels through the GI-tract. After that the dissolved drug must permeate through the intestinal membrane into the blood stream (Ruiz-Garcia, Bermejo, Moss, & Casabo, 2008).

2.1.1 The Biopharmaceutics Classification System

The Biopharmaceutics Classification System (BCS) is a classification system suggested by Amidon and Lennernäs in 1995, classifying drugs into four categories based on their solubility and intestinal permeability (Table 1)(Amidon, Lennernäs, Shah, & Crison, 1995). The BCS has since been widely accepted as a guideline in lead detection and development of drugs and their appropriate dosage forms. The BCS has been introduced to the guidelines of the Food and Drug Administration (FDA) and is being used by regulatory agencies in the process of new drug approvals. (Löbenberg & Amidon, 2000).

Table 1 The Biopharmeceutics Classification System

Class	Solubility	Permeability
I	High	High
II	Low	High
III	High	Low
IV	Low	Low

Solubility issues are affecting the bioavailability of oral drugs. For drugs in the biopharmaceutical classification system (BCS) class II (high permeability, low solubility) solubility is the limiting factor (Amidon et al., 1995). The introduction of high throughput screening (HTS) has led from the traditional method of drug solubilisation to a massive increase in screening capacity for new chemical entities (NCE). Today in vitro assays are used to screen for activity of compounds from large chemical libraries with hundreds of thousands of compounds (Mayr & Bojanic, 2009). In these libraries compounds are often dissolved in aprotic solvents, for example dimethyl sulfoxide (DMSO), as stock solutions. This has led to water solubility not being as relevant in HTS lead detection as it used to be and thus, even a higher percentage of lead compounds are poorly soluble in aqueous media (Burbaum, 1998). This has led to approximately 30-40% of marketed oral drugs with instant release profile being practically insoluble in water with a solubility of less than 0.01 mg/mL (Takagi et al., 2006).

Today, the BCS and thus, determination of in vivo solubility and permeability has been incorporated in HTS and lead detection by most pharmaceutical companies (Ku, 2008).

2.1.2 Solubilisation techniques

With increased complexity and specificity of new drugs and receptors there has been an increase in formulation research in delivery systems and in increasing the solubility of poorly water-soluble drugs (Singh, Worku, & Van den Mooter, 2011). Different solubilisation techniques have been developed to tackle the challenge of poorly soluble drugs. These include solid dispersions, cyclodextrin complexes, lipid based systems and nanocrystals (Y. Huang & Dai, 2014).

Cyclodextrins are cyclic oligosaccharides with a hydrophobic core and hydrophilic shell (Fig 1). Cyclodextrins form complexes with hydrophobic compounds enhancing solubility and thus bioavailability of poorly soluble drugs (Loftsson & Duchêne, 2007).

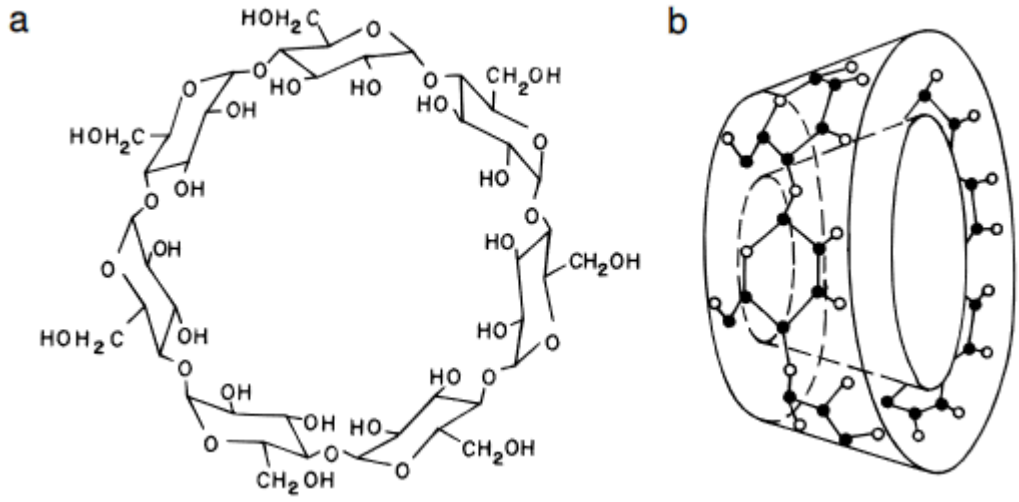

Figure 1 (a) The chemical structure and (b) the toroidal shape of the β-cyclodextrin molecule. (Loftsson & Brewster, 1996)

Lipid based drug delivery systems (LBBDS) for oral preparations have shown to increase bioavailability of poorly soluble drugs by stimulating gallbladder contractions and increasing secretion of bile salts and phospholipids in the GI tract. This increases solubilisation of the hydrophobic drug. Lipids can also increase the residence time in the GI tract (Dahan & Hoffman, 2008).

Nanocrystals are crystalline drug particles at nanoscale (<1μm). Nanocrystals can be produced either by precipitation techniques using solvents or by disintegration techniques such as ball milling (Keck & Müller, 2006). Nanocrystals improve dissolution by the significant surface area enlargement according to the Noyes-Whitney equation (Noyes & Whitney, 1897). Nanocrystals also increase the apparent solubility, which at nanorange is also a function of particle size (Junghanns & Müller, 2008).

While improving solubility using methods such as cyclodextrins, LBDDS, or surfactants these methods have the tendency to decrease the apparent permeability. Amorphous solid dispersions show a solubility enhancing effect while having limited or no effect on permeability while increasing the solubility (Miller, Beig, Carr, Spence, & Dahan, 2012). Within the recent years solid dispersion has been firmly established as a platform technology, when working with formulations of poorly soluble drugs.

2.2 Solid dispersions

Solid dispersions and especially amorphous solid dispersions (ASD's) is a promising method to improve bioavailability of poorly soluble drugs. It is common census that by reducing the particle size of drugs, where the dissolution of the drug in the GI-tract is the limiting factor, it generally increases absorption and bioavailability (Fincher, 1968). Amorphous drugs have shown to have a higher saturation solubility compared with crystalline drugs due to the lack of a crystalline lattice (Hancock & Parks, 2000). For a drug to dissolve from a crystalline state, energy is required. By transforming the drug to the amorphous form, it enters a higher energy state. As the crystalline state is a lower energy state it is the thermodynamically favoured state and thus amorphous compounds tend to recrystallize. ASD's utilize an excipient, usually a polymer, to fix the drug in its amorphous dispersed state by hydrogen bonding and a high glass transition temperature (T_g) (Yu, 2001). The glass transition can be described as the transition of an amorphous solid from a hard and brittle glassy state, into a rubbery viscous state (Forrest, Dalnoki-Veress, Stevens, & Dutcher, 1996).

Most solid dispersions used today can be defined as dispersions of drug in an amorphous polymer matrix, where the drug is preferably in the molecular dispersed state. The hydrophobic drug is molecularly dispersed by melting or dissolving it in a hydrophilic carrier, for example

a polymer. At storage conditions the polymer matrix is in a solid-state, suspending the drug inside it (Fig 2). The solid dispersions can be prepared to oral formulations such as tablets or capsules (Y. Huang & Dai, 2014).

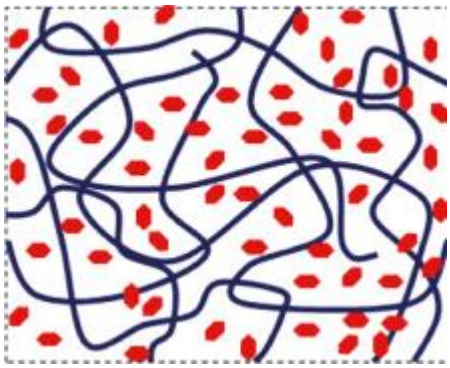

Figure 2 The ideal structure of a solid dispersion where the drug (red) is molecularly dispersed in the polymer matrix (blue) (Y. Huang & Dai, 2014)

In solid dispersions the drug is highly dispersed in the polymer matrix, ideally on a molecular level. By dispersing the drug molecules, solid dispersion systems provide a large surface area of the drug, which increases the dissolution rate. By dispersing the drug in the polymer, the crystalline lattice of the drug is removed and the crystal packing energy is reduced, thus reducing the energy required to dissolve the drug in aqueous media (Jermain, Brough, & Williams III, 2018). The solid dispersion contains stored potential energy that releases when the system gets in contact with the gastrointestinal fluids and works as a spring, producing a supersaturation of the drug (Jermain et al., 2018). The drug is then absorbed from the supersaturated state into the systemic circulation. As the supersaturation is in a thermodynamically unstable state, the hydrophilic carrier must work as a stabilizer or so-called parachute, prolonging the absorption by inhibiting precipitation of the drug in the GI-fluids for the time it takes to be absorbed into the body. (Brouwers, Brewster, & Augustijns, 2009; Guzman et al., 2007). Polymers such as polyvinylpyrrolidone (PVP), hydroxypropylmethylcellulose (HPMC) and poly-ethylene glycol (PEG) have shown stabilizing effect in solid dispersions (Jermain et al., 2018). Newman et al. (Newman, Knipp, & Zografi, 2012) evaluated research papers on amorphous solid dispersions and showed that in approximately 80% of the publications showed increased bioavailability in comparison to their references.

Today the use of solid dispersions is an established technique to improve bioavailability with several products on the market (Table 2). At least three methods of producing solid dispersions are used in commercial products. These are hot melt extrusion (HME), spray drying, and solvent co-precipitation (Y. Huang & Dai, 2014).

Table 2 Examples of FDA approved solid dispersions on the market (adapted from Y. Huang & Dai, 2014)

Product name	API	Polymer	API Tm (°C)	SD preparation method	Year of approval
Cesamet	Nabilone	PVP	160		1985
Sporanox	Itraconazole	HPMC	166	Spray drying on sugar beads	1992
Prograf	Tacrolimos	HPMC	128	Spray drying	1994
Kaletra	Lopinavir/ritonavir	PVP/VA	125/122	Melt extrusion	2005
Intelence	Etravirine	HPMC	265	Spray drying	2008
Zotress	Everolimus	HPMC	115	Spray drying	2010
Novir	Ritonavir	PVP/VA	122	Melt extrusion	2010
Onmel	Itraconazole	HPMC	166	Melt extrusion	2010
Incivek	Telaprevir	HPMCAS	246	Spray drying	2011
Zelboraf	Vemurafenib	HPMCAS	272	Co-precipitation	2011
Kalydeco	Ivacaftor	HPMCAS	291	Spray drying	2012

Itraconazole is a good example of the benefits of solid dispersions. Itraconazole is a broad-spectrum antifungal drug that is insoluble in water and was commercialized using solid dispersion technology. The first marketed product was Sporanox® using spray drying method to significantly improve the bioavailability of the drug. Later Onmel® came on the market with a melt extrusion formulation of itraconazole, eliminating the use of solvents and reducing the dosage frequency. The results of these studies and other marketed solid dispersions are reviewed by Jermain et al. (Jermain et al., 2018)

Other interesting studies of possible products from solid dispersion technology include:

Solid dispersions of rebamipide, an antiulcer drug in BCS class IV, and poloxamer showed improved bioavailability in rats, compared to tablets with conventional rebamipide, by enhancing the solubility of the drug (Tung et al., 2011). Albendazole is used to treat a variety of parasitic worms. Solid dispersions of albendazole, showed a 2,4-fold increase in bioavailability in rabbits compared to a commercial product (Kalaiselvan, Mohanta, Madhusudan, Manna, & Manavalan, 2007). Solid dispersion granules of curcumin showed an

approximately 10-fold increase in both area under the plasma concentration-time curve (AUC) and maximum plasma concentration (Cmax) in rats compared with curcumin (Jang, Kim, Lee, & Oh, 2014). An HIV-attachment inhibitor, BMS-488043 prepared into amorphous dispersion using spray-drying showed a 15–18-fold improvement in Cmax and 7–9-fold in AUC relative to a crystalline capsule formulation in dogs (Fakes et al., 2009)

A challenge with ASD's is that as the API is in an amorphous state, which is a metastable state and not as energetically favourable as the crystalline state. This leads to risk of recrystallization or precipitation of the API in the polymer matrix, which provides challenge for preparing ASD's with reliable shelf life. ASD's can also phase separate over time, which can lead to further recrystallization (Vasanthavada, Tong, Joshi, & Kislalioglu, 2005). Another challenge is to avoid precipitation of the drug in the GI-tract after its been released from the carrier matrix.

2.2.1 Glass forming ability of amorphous drugs

Amorphous drugs can be classified by assessing the glass forming ability (GFA) or the tendency to recrystallize. The classification system classifies amorphous drugs into three classes depending on the cooling rate required to inhibit recrystallization from the heated molten state of the drug. Class I drugs require very rapid cooling >750°C/min. Class II drugs require modest cooling at rates of 10-20°C/min from the molten state to recrystallize while class III drugs can stay amorphous at low cooling rates (approx. 1°C/min). The model compounds used in this thesis are class I (naproxen) and class II (celecoxib). (Baird, Van Eerdenbrugh, & Taylor, 2010; Blaabjerg, Lindenberg, Löbmann, Grohganz, & Rades, 2016)

2.2.2 Hot-melt Extrusion

Hot-melt extrusion (HME) is a processing technique that has widely been used in the plastic, rubber and food industry since the 1930's (Chokshi & Zia, 2010). The process of HME was originally introduced to prepare polymeric coatings for wires in the mid-nineteenth century. (Crowley et al., 2007). Today, a large part of all plastic products is manufactured by HME. The HME technique was introduced to the pharmaceutical industry in the 1960's and is today an established method for producing different dosage forms of solid dispersions.

In HME the active pharmaceutical ingredient (API) and a polymer or combination of polymers are melted and mixed at elevated temperature. The heat combined with the shear force generated by the screws cause the crystalline drug to convert into amorphous form. The resulting mixture is cooled and solidified before downstream processing into for example tablets or capsules. HME requires the API and polymer to be miscible and thermodynamically stable at processing parameters (temperature, shear forces, residence time) (Crowley et al., 2007). Today many companies produce a plethora of different polymers specially designed for a certain manufacturing method. For example, Soluplus® by BASF (PEG6000/vinylcaprolactam/vinylacetate copolymer, Soluplus®, BASF, Germany) is especially developed for use in hot melt extrusion thanks to its suitable process behaviour. (Kolter, Karl, Gryczke, & Ludwigshafen am Rhein, 2012).

The extruder consists of the feeder or hopper, a barrel with controllable conditions including temperature and screw speed, and a die (Fig 3). Extruders are available in single screw or multi screw configurations. Twin-screw extruders are the most used extruders because of their dispersive and distributive mixing, conveying high shear to break up particles while dispersing them (Wilson, Williams, Jones, & Andrews, 2012). The two screws are usually aligned side by side and give the extruder configurability and improved mixing and conveying capabilities compared to a single-screw extruder. The screws can either be co-rotating or counter-rotating. (Crowley et al., 2007).

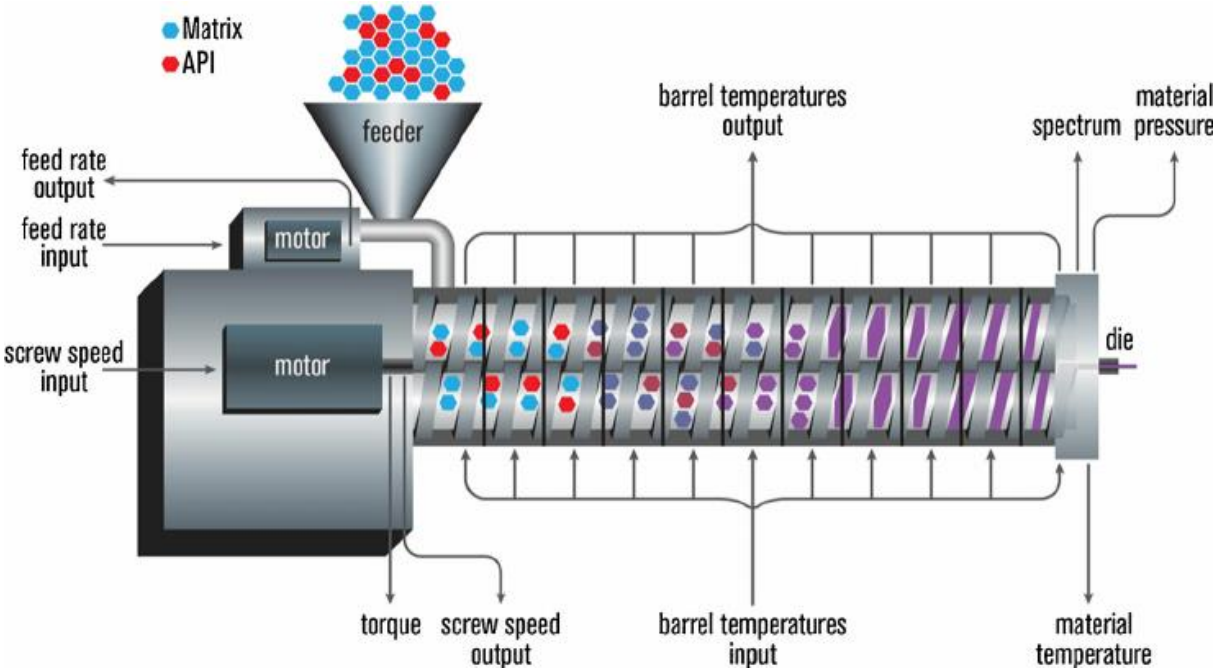

Figure 3 Schematic of an extruder (Patil, Tiwari, & Repka, 2016)

The HME process can be divided into the following sections: 1) feeding of material into the extruder through the feeder, 2) melting, mixing and conveying of the melt, 3) extrusion through a die and 4) cooling and down-stream processing. Process parameters include flow of powder, shear force, residence time and pressure, cooling rate and shaping of the extrudate. HME requires in process monitoring of parameters such as heat, torque and pressure to ensure uniformity of the product. (Breitenbach, 2002). The extruder can also be equipped with in line monitoring such as Raman spectroscopy to monitor API concentration and solid-state characteristics of the API-polymer melt (Saerens et al., 2011).

HME offers certain advantages to other manufacturing methods. HME is a relatively simple processing method with few processing steps. It requires no solvent in producing ASD's and is suitable for continuous manufacturing at relatively high throughput rate. HME is very versatile with modulated extruders with customizable screws and adjustable screw speed, shear rate and temperature. The temperature can also be adjusted in different parts of the extruder. However, HME is not suitable for production of all drugs. HME is performed at elevated temperatures so it is not suitable for thermal sensitive drugs or excipients (Chokshi & Zia, 2010).

The glass transition temperature (T_g) affects the stability of the ASD. The T_g allows the entrapment of the drug in the polymer in a "glassy" solid state below the T_g. Above the T_g the

drug-polymer mixture enters a viscous, rubbery state. When temperature is further increased the viscosity lowers towards liquid-like properties. The T_g should be 40-50 °C higher than the storage temperature (Yoshioka, Hancock, & Zografi, 1995). With a low T_g the extrudate will be softer and more prone to recrystallization and phase separation at storage temperatures. BASF Pharma Polymers, producer of polymers for HME suggests that a suitable T_g for thermoplastic polymers used in HME should be 50 – 180 °C (Kolter et al., 2012) For optimal melt extrusion the carrier polymer has to be workable at relatively low temperatures due to thermal degradation of several drugs at higher temperatures.

During HME, polymers may be subjected to different types of degradation. Sources of degradation may include mechanical degradation from shear forces by the rotating screws, thermal degradation by the elevated process temperature and oxidative degradation. It is possible to stabilize polymers using antioxidants. Crowley and his co-workers (2002) states that Vitamin E, Vitamin E succinate and Vitamin E polyethylene glycol 1000 succinate (TPGS) were found to be suitable stabilizers for PEO during processing. TPGS is obtained by the esterification of Vitamin E succinate with polyethylene glycol 1000 (Crowley, Zhang, Koleng, & McGinity, 2002). HME have been used to produce granules, pellets, capsules, sustained release tablets, transdermal and transmucosal drug delivery systems and implants (Crowley et al., 2007)

2.2.3 Spray drying and co-precipitation

In spray drying the components are dissolved together and then dispersed into droplets by atomization. The droplets are rapidly dried using a hot gas, often air or nitrogen. The dried powder is then collected for further processing (Singh & Van den Mooter, 2016).The rapid evaporation during the process causes kinetic trapping of the API in the carrier matrix resulting in a supersaturated molecular dispersion (Paudel, Worku, Meeus, Guns, & Van den Mooter, 2013).

Another technique to produce solid dispersions is co-precipitation, where a non-solvent is added to the API and the polymeric carrier solution under mixing. The API and polymer co-precipitate forming microparticles. The microparticles are filtered and dried for further processing (J. Huang, Wigent, Bentzley, & Schwartz, 2006).

2.2.4 Polymers in hot-melt extrusion

Polymers are large molecules consisting of repeating subunits called monomers. Due to the macromolecular structure of polymers, containing long polymeric chains with different lengths and morphology, different polymers exhibit very different properties (Rudin, 1998). Polymers range from synthetic plastics to natural occurring polymers such as cellulose. Polymers can have characteristics optimal for entrapping drugs in their amorphous state and are often used as the carrier matrix in the manufacturing of ASD's. This is due to amorphous polymers having a glass-transition temperature (T_g). At temperatures below the T_g, polymers are in a glassy, solid like state, where there is no mobility between the polymeric chains. At the T_g of the polymer, it transitions from a glassy state to a rubbery state with limited mobility between the chains. As the temperature is further increased, the polymer transitions into a molten state with free mobility between chains. When the ASD's prepared by HME are cooled below the T_g of the drug-polymer melt, the drug becomes entrapped in the glassy state of the polymer matrix meaning that the drug is molecularly dispersed within the matrix.

2.2.4.1 Polymeric melts

Many small-molecule drugs act as plasticizers in the polymeric melt, increasing the free volume and decreasing the friction between the polymer molecules. The plasticizing effect be observed as a decrease in T_g for the API-polymer melt and a decrease in brittleness of the finished extrudates. (Aho, Edinger, Botker, Baldursdottir, & Rantanen, 2016)

2.2.5 Advantages and limitations of solid dispersions

The most obvious advantage of using solid dispersions is the improved bioavailability due to the improved solubility in the GI-tract. The preparation of solid dispersions using methods such as HME is rather simple with few processing steps. Preparation of solid dispersions using HME enables for continuous manufacturing, which is more economical and time saving compared to conventional batch by batch processing (Schaber et al., 2011). Solid dispersions can be prepared without solvents that can be expensive and bad for the environment. There are several ways to

produce solid dispersions that suits different types of drugs and excipients. Solid dispersions can be produced into powders, granules, pellets, films, patches and can even be molded into desired shapes and sizes with techniques such as injection molding and 3d-printing (Kolter et al., 2012)

Recrystallization is the biggest problem of solid dispersions. Solid dispersions tend to recrystallize since that is the favored energy state. An inert carrier matrix with a high enough glass transition temperature and viscosity at storage temperature is required to avoid recrystallization during storage. Solid dispersions can also absorb moisture, which can result in phase separation and recrystallization (Vasconcelos, Sarmento, & Costa, 2007). The pharmaceutical industry is still adapting to continuous manufacturing and more in-line analytical tools need to be developed and validated before it can be utilized fully. Analytical tools such as Raman spectroscopy show promise for use as process analytical tools (PAT) (Wahl et al., 2013). Heat sensitive drugs have a risk of degrading during processing at elevated temperatures. The process temperatures can be lowered by using plasticizers lowering the viscosity of the melt. Some drugs can work as plasticizers themselves (Repka, Gerding, Repka, & McGinity, 1999).

Solid dispersions show great promise in improving bioavailability of poorly soluble drugs. There are several products already on the market and with the industry seemingly willing to go into continuous manufacturing instead of just traditional batch to batch manufacturing, solid dispersions (especially produced by melt extrusion) offer products that are suitable for continuous manufacturing and downstream processing into wanted dosage forms. The biggest challenge seems to be the risk of recrystallization of the drug in the carrier matrix. This can be reduced by polymer selection, appropriate drug loading and packaging of the product. By overcoming challenges of storage and process recrystallization, solid dispersions will hopefully remain as an established method for overcoming solubility limitations of drugs.

2.2.6 Safety

The use of polymers in medicine is not new. Natural polymers have been used as components in traditional medicine for thousands of years (Satchi-Fainaro & Duncan, 2006). With the surge in polymer technology in the 20th century several synthetic polymers have become available for

drug development. Potential issues relating to the suitability of polymers in the development of nanomedicine are reviewed by Ruth Duncan (Duncan, 2011). Duncan mentions safety issues such as potential toxicity of polymers and their metabolites, stability during storage and administration (i.e. recrystallization, phase separation) and reproducibility in manufacturing in terms of molecular weight, branching or other forms of heterogeneity. An issue with biodegradable polymers is the uncertainty of the safety of the degradation products. Especially at chronic use of solid dispersions it is important that the polymer is not accumulated in the body but is eliminated. The degradation and elimination of polymers from the body is still not completely certain. However, most polymers used in solid dispersions have already been approved by regulatory agents such as FDA and EMA and are generally regarded as safe. The route of administration also plays a role as for example some polymers such as PVP does not get absorbed from the GI tract due to the high molecular weight (Leuner & Dressman, 2000).

2.3 Rheology

Rheology is the study of deformation and flow of matter (Barnes, Hutton, & Walters, 1989). In the food industry for example rheology is used to analyze properties such as mouth feel, chewability and ease to swallow (Aho, Hvidt, & Baldursdottir, 2016). To understand the flow properties of the polymeric melts during HME, a proper understanding of the rheological properties should be known (Aho, 2011).

The framework for rheology is set by Newtons law of viscosity for Newtonian fluids and Hooke's Law for ideal solids. Newtons law of viscosity states that the shear viscosity, or ratio of shear stress to shear rate, is constant. This law is only valid for Newtonian fluids such as for example water or glycerin. In contrast to Newtonian fluids, fully elastic, or ideal solid materials, such as metals, follow Hooke's Law. Hooke's Law states that the stress applied to a material is proportional to the strain (George & Qureshi, 2013). Ideal solids deform elastically where the material return to its original state after the stress is removed. Newtonian or ideal fluids deform irreversibly, when stress is applied they flow and do not return to the original state after the stress is removed. Ideal fluids follow Newton's law and ideal solids follow Hooke's.

However, materials often have both solid and liquid-like properties when undergoing deformation. and exhibit rheological characteristics of interest. These materials are called

viscoelastic materials (Ferry, 1980) Rheology focuses mainly on so called non-Newtonian fluids. The viscosity of non-Newtonian fluids is not constant and the viscosity is dependent on the shear rate (George & Qureshi, 2013).

Shear stress and shear rate can be described mathematically using a two-plate model as an example (Fig 4). Considering a sample between two plates where the upper plate is moved by a given force F. Shear stress, τ is defined as the force applied to the plate divided by the area of the plate, A (Eq 1). Using the same model shear rate, $\dot{\gamma}$ can be defined as the velocity, v of the upper plate divided by the distance, h between the two plates (Eq 2).

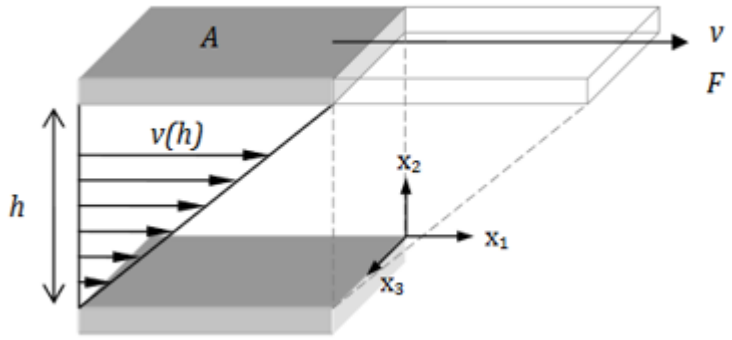

Figure 4 Visualization of the two plate model (Aho, 2011)

$$\tau = \frac{F}{A} \qquad \text{(Pa)} \qquad [1]$$

$$\dot{\gamma} = \frac{v}{h} \qquad (s^{-1}) \qquad [2]$$

From the shear stress and shear rate the shear viscosity, η_s can be calculated by

$$\eta_s = \frac{\tau}{\dot{\gamma}} \qquad (Pa \times s) \qquad [3]$$

The shear viscosity gives a measure of the thickness, or resistance to flow of the material. Polymers are viscoelastic and thus the melt properties are somewhere between those of ideal

liquids and ideal solids. The viscoelasticity means the material responds to stress-strain behavior time dependent and the deformation is partially reversible. Most polymers exhibit a property called shear-thinning. The viscosity decreases as a function of shear rate (Fig 5). This is due to the disentanglement of the entangled polymer chains (Aho, 2011). The shear thinning of polymers is an important characteristic during HME, where the shear forces of the screws together with the elevated temperature significantly lowers the viscosity of the polymer melt, allowing the drug to be dispersed within the polymer.

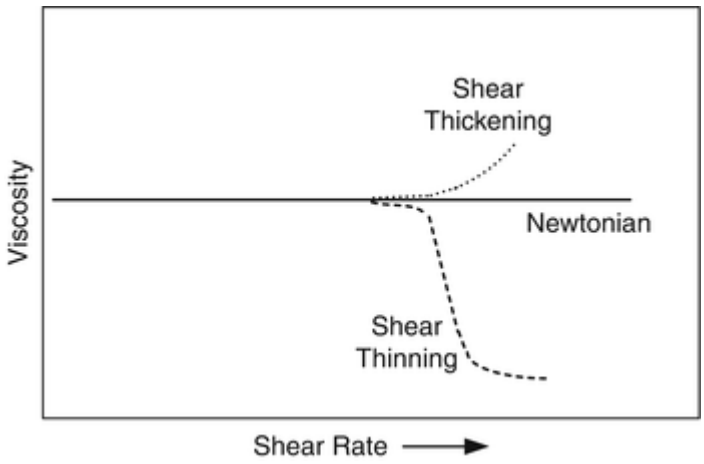

Figure 5 Visualization of shear thinning. At higher shear rates a decrease in viscosity is observed (shear thinning). The viscosity of Newtonian fluids is not affected by the shear rate. Some materials such as slurries can exhibit shear thickening, where higher shear rates increases the viscosity of the melt. (May & Henderson, 2013)

For reliable rheological data, the experiments should be conducted in the linear viscoelastic region of the polymer before plastic, irreversible deformation occurs. The linear viscoelastic region is the region where the deformation applied on the sample is reversible (elastic deformation) and the polymeric structure remains unchanged. This usually encompasses a very small force of deformation. Small amplitude oscillatory shear rheology is used to characterize properties of the polymers in the linear viscoelastic region (Aho, Boetker, Baldursdottir, & Rantanen, 2015).

2.3.1 Small amplitude oscillatory shear rheology

To better understand the properties of polymers in the viscoelastic region small amplitude oscillatory shear (SAOS) rheology can be used. SAOS applies a small pre-defined strain at a changing frequency to the sample. The viscoelasticity is measured as the phase lag between the applied stress and the corresponding strain. One type of SAOS measurement is the parallel-plate model (Fig 6), where the sample is placed between two circular plates, one stationary and one performing oscillating strain on the sample and the resulting stress response is measured. It is also possible to use SAOS in stress-controlled mode where the strain response to the applied stress is measured.

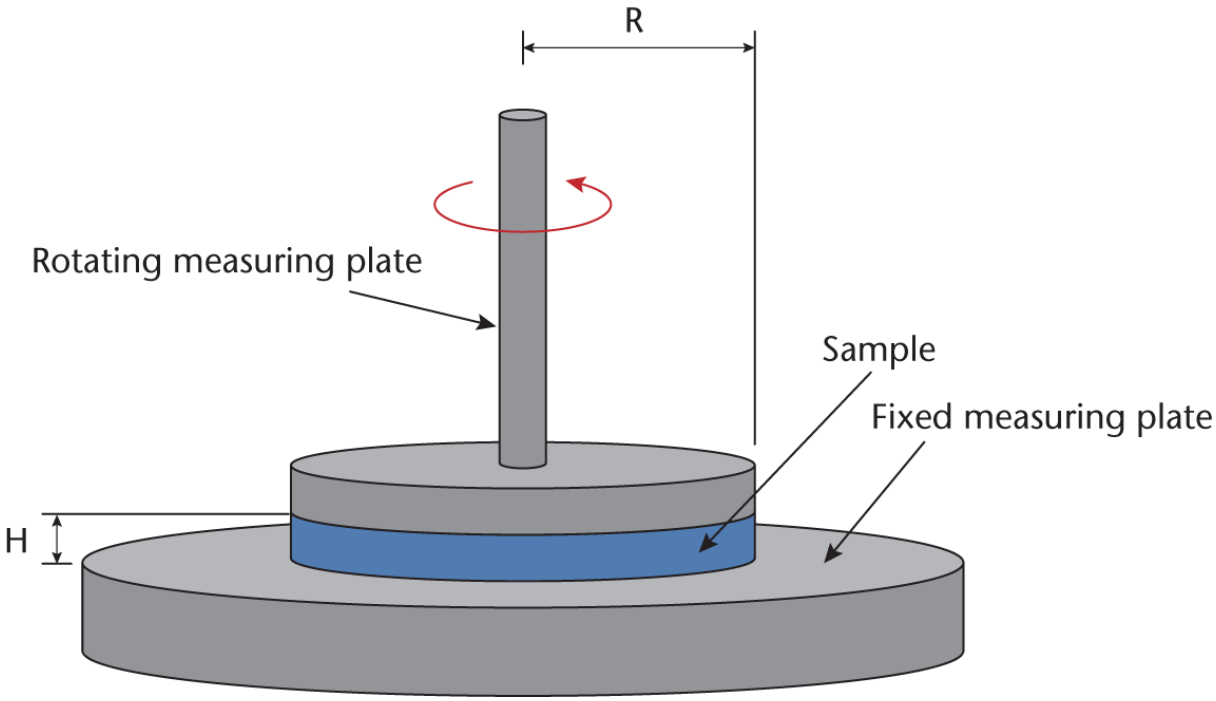

Figure 6 Schematic of a rotational parallel-plate geometry used in SAOS rheological measurements (Leizea et al., 2017)

The strain function can be described as:

$$\gamma(t) = \gamma_0 sin\,(\omega t) \qquad [4]$$

where ω is the angular frequency and γ_0 is the strain amplitude. The corresponding stress response can be described as:

$$\tau = \tau_0 \sin(\omega t + \delta) \quad [5]$$

In the viscoelastic region the deformation of the sample is sinusoidal where the response of the material is in a lag phase behind the stress (Fig 7) The lag between stress and strain is defined as the phase angle, δ. The phase angle δ is related to the viscoelasticity of the sample. For an ideal elastic sample δ=0° and for an ideal viscous material δ=90°. A viscoelastic sample has a phase lag between 0° and 90°.

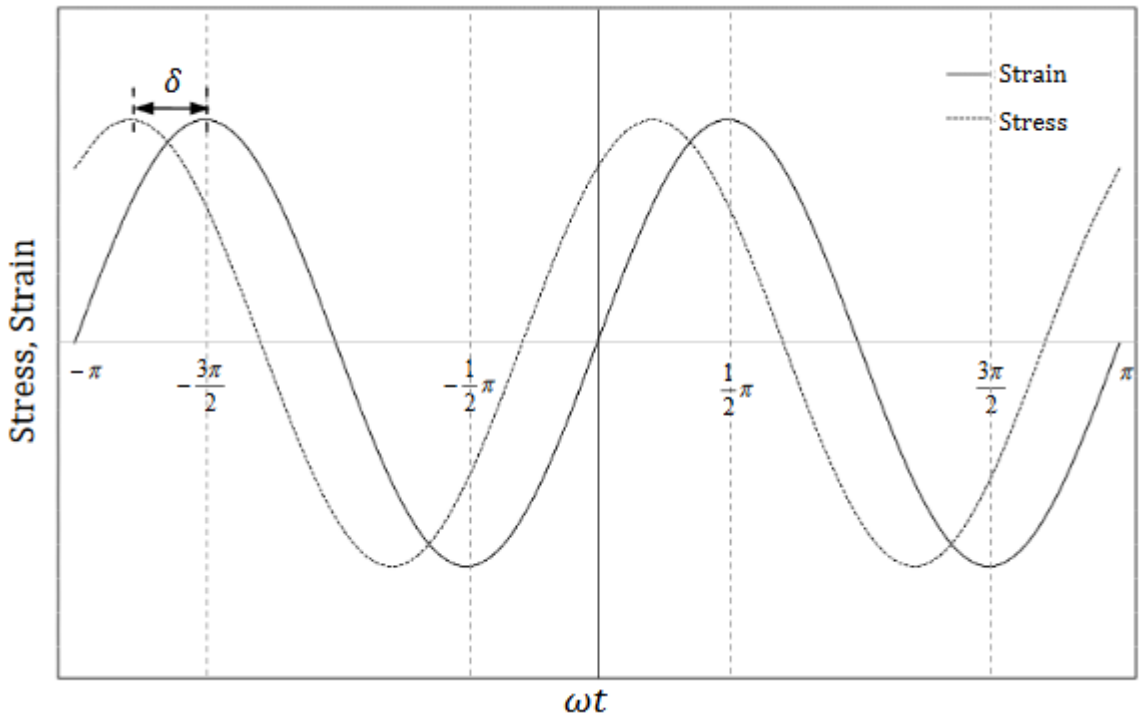

Figure 7 The phase angle between the applied stress and the measured strain in a stress controlled SAOS measurement (Aho, 2011)

From the phase angle the viscoelastic moduli can be calculated. The elastic, reversible characteristics are represented by the storage modulus, G', describing the amount of energy stored in the sample. The loss modulus G'' represents the viscous characteristics describing the energy lost in the deformation of the sample.

$$G' = \frac{\tau}{\gamma_0} \cos(\delta) \quad [6]$$

$$G'' = \frac{\tau}{\gamma_0}\sin(\delta) \quad [7]$$

the relationship between the storage and loss moduli can be described as

$$\tan\delta = \frac{G'}{G''} \quad [8]$$

From the storage and loss moduli the complex modulus also referred to as complex viscosity:

$$|\eta^*| = \sqrt{\left(\frac{G'}{\omega}\right)^2 + \left(\frac{G''}{\omega}\right)^2} \quad [9]$$

The complex viscosity gives an understanding of the rheological properties of the sample and can help to give an assessment for drug-polymer melts during HME.

2.4 Vacuum compression moulding

For reliable rheological results homogenous sample preparation is important. Traditionally samples have been prepared by compression or injection moulding. Treffer et al. have introduced a novel vacuum compression moulding (VCM) tool for preparing homogenous thermoplastic samples for rheological measurements (Treffer et al., 2015). The MeltPrep® tool (Fig 8) offers certain advantages such as simple, fast sample preparation at a low-cost. The vacuum removes excess air preventing the formation of air bubbles in the sample, which can lead to erroneous results when doing rheological analysis. The small chamber reduces heat load and mechanical stress reducing degradation.

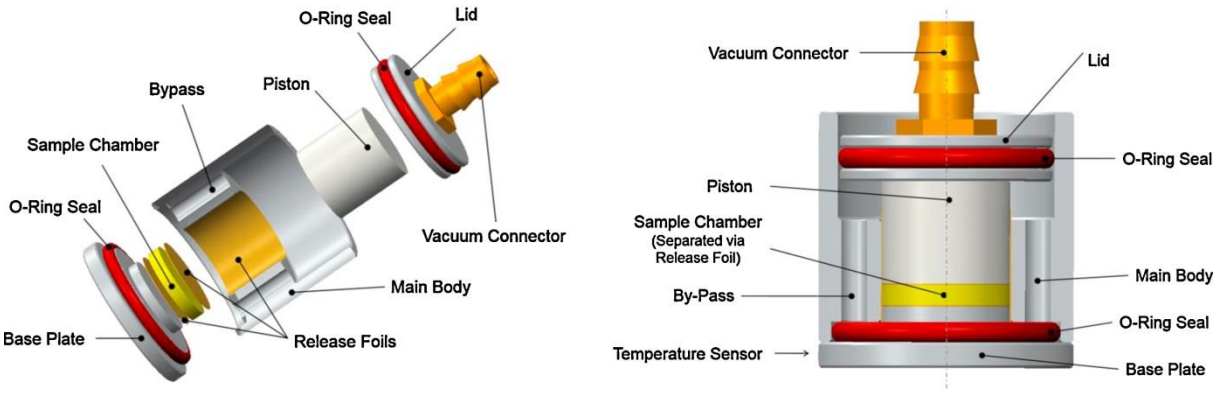

Figure 8 The VCM tool (Treffer et al., 2015)

The tool consists of a cylindrical base plate, a main body, a piston and a lid. The o-ring seals provide a gas-tight chamber together with the main body. The sample can be loaded into the chamber as a powder. The tool is then connected to a vacuum source producing a lower pressure than the surrounding atmospheric pressure. The vacuum forces the piston to compress the sample. The tool is then heated using a hot-plate. The heat melts the sample producing a uniform, bubble-free sample. The sample is then cooled and removed from the tool. Separation foils with a Polytetrafluoroethylene (PTFE) coating prevents sticking of material to the tool.

2.5 Analytical methods

2.5.1 Thermogravimetric analysis

Thermogravimetric analysis (TGA) measures change in weight as a function of increasing temperature. A small amount of sample is placed on a tared heat resistant pan, for example platinum and heated up in a furnace. The weight loss of the sample is measured. The obtained data from the TGA can be used to determine degradation temperature and solvent evaporation from solid materials (Coats & Redfern, 1963).

2.5.2 DSC

Differential Scanning Calorimetry (DSC) is a quantitative analytical method for detailed thermal and physical analysis of chemicals. DSC measures energy difference as a function of temperature or time. The difference in amount of energy required to increase the temperature of a sample and a reference pan is measured. DSC can provide information such as the purity of a drug or phase transitions such as melting temperature. The T_g of an amorphous drug can also be observed. In DSC the T_g can be observed as a change in heat capacity and thus a change in the baseline can be observed in the DSC curve (Clas, Dalton, & Hancock, 1999).

2.5.3 Polarized Light Microscopy

Polarized Light Microscopy (PLM) is an optical microscopy method utilizing polarized light to detect or determine the crystallographic properties of compounds (Carlton, 2011). Natural light or non-polarized light vibrates in random directions, while linear polarized light travels within a single plane (Fig 9). By using a polarizing filter the natural light is converted into polarized light by only letting through light of a single orientation (Kliger & Lewis, 2012). By using two perpendicular polarizing filters no light waves are let through the PLM. When a crystalline, birefringent sample is placed between the filters it will diffract the light. The diffracted light can pass the second polarizing filter and the crystals can be visualized and characterized. (Carlton, 2011; Wolman & Kasten, 1986)

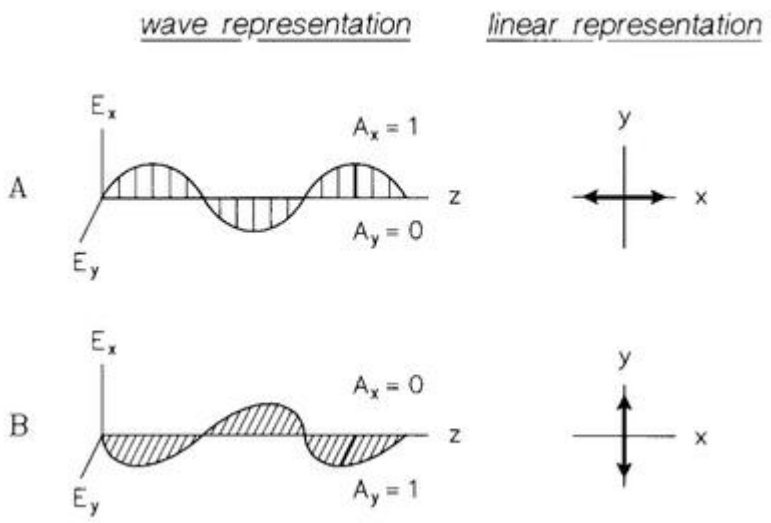

Figure 9 Representation of linearly polarized light. Examples of polarization oriented along the x axis (A) or y axis (B) (Kliger & Lewis, 2012).

2.5.4 X-ray Powder Diffraction

X-ray Powder Diffraction (XRPD) is a fast, non-destructive analytical method for structural characterization of materials. It can be used to determine crystallographic density and the crystalline structure of a sample and is an effective tool for confirming amorphous structure of the prepared ASD's. X-ray wavelengths are diffracted by a crystalline sample. The crystalline sample acts as a diffraction grating allowing the X-rays to reinforce each other by constructive interference, when Bragg's law is satisfied:

$$n\lambda = 2d\sin(\theta) \qquad [10]$$

Where n is an integer, λ is the wavelength of the x-ray, d is the spacing between the the planes of the crystalline lattice and θ is the angle of diffraction (Fig 10). The pattern of scattering is unique to each crystalline structure.

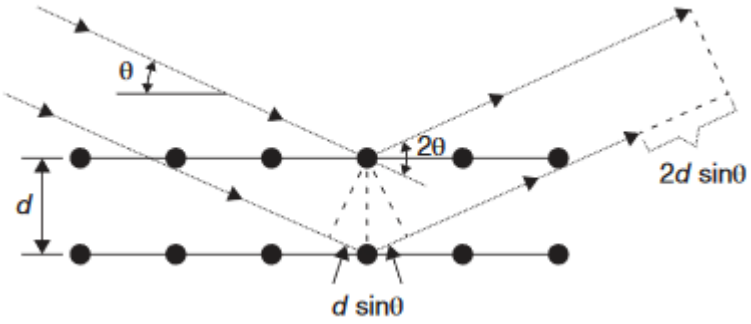

Figure 10 Bragg's law of diffraction. X-rays diffracted by planes with the interplanar spacing d at a diffraction angle of θ. The lower ray travels an extra distance of 2d sin θ (Byrn, Zografi, & Chen, 2017)

In XRPD the powdered sample have the crystals oriented randomly in all directions along a single dimension. By measuring the diffraction along this dimension, a diffractogram representing all crystal orientations can be observed. The x-rays are emitted at a constant intensity and wavelength while changing the angle θ between the sample and the source (Fig 11). A detector moves similarly at an angle of 2θ detecting the intensity of the diffracted x-rays. The resulting diffractogram is a plot of intensity as a function of 2θ (Byrn et al., 2017).

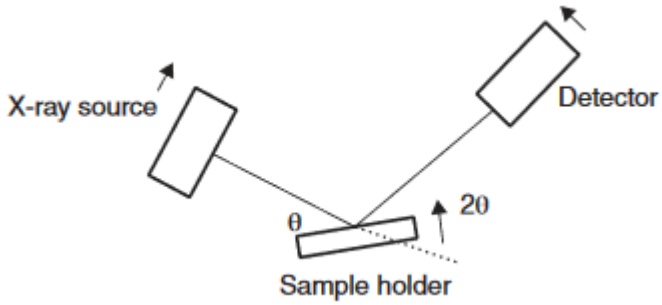

Figure 11 Principle of the XPRD equipment. (Byrn et al., 2017)

In XRPD, amorphous material tend to express a diffuse halo due to no long range order in the sample, while crystalline material express sharper peaks (Fig 12) (Andrews et al., 2010).

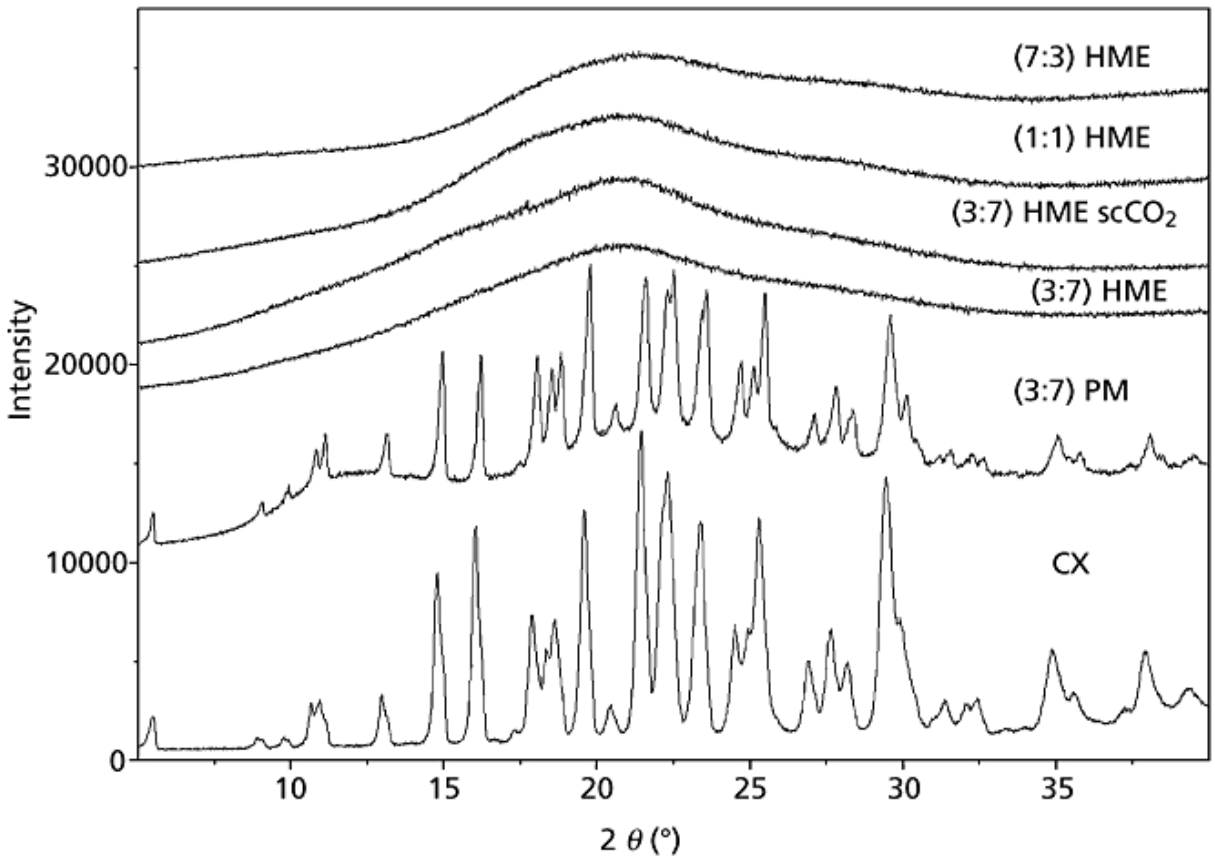

Figure 12 Powder X‐ray diffractometry patterns for crystalline CCX, physical mixture of crystalline CCX and PVP and hot‐melt extruded samples containing amorphous CCX (Andrews et al., 2010)

The XRPD is a common tool for confirming the amorphisity of ASD's. However, the XRPD was unavailable during the time of this thesis.

2.5.5 Raman spectroscopy

Raman spectroscopy is a vibrational spectroscopy that measures the inelastic scattering of monochromatic light from a sample. Inelastic scattering refers to the part of scattering where the emitted light photon from the sample has either a higher or lower energy than the source photon. The light, typically from a monochromatic laser, interacts with the molecular bonds within the sample and excites a given bond to a temporary virtual state. The bond then scatters the photon back with either the same amount of energy (called Rayleigh scattering or elastic scattering), with a lower energy (stokes scattering) or with higher energy (anti-stokes scattering) (Fig 13). The inelastic stokes and anti-stokes scattered photons can then be observed with a detector. The energy shift of the photon gives information about vibrational modes in the

sample. Rayleigh scattering is the dominant form and only a small part of the scattering is inelastic. Approximately only one in every 10^6 -10^8 photon is inelastic or Raman active. Due to this weak signal from the Raman scattering the Rayleigh scattering must be filtered out using a filter. Raman spectroscopy also require a powerful laser to be able to detect the Raman scattering (Smith & Dent, 2013).

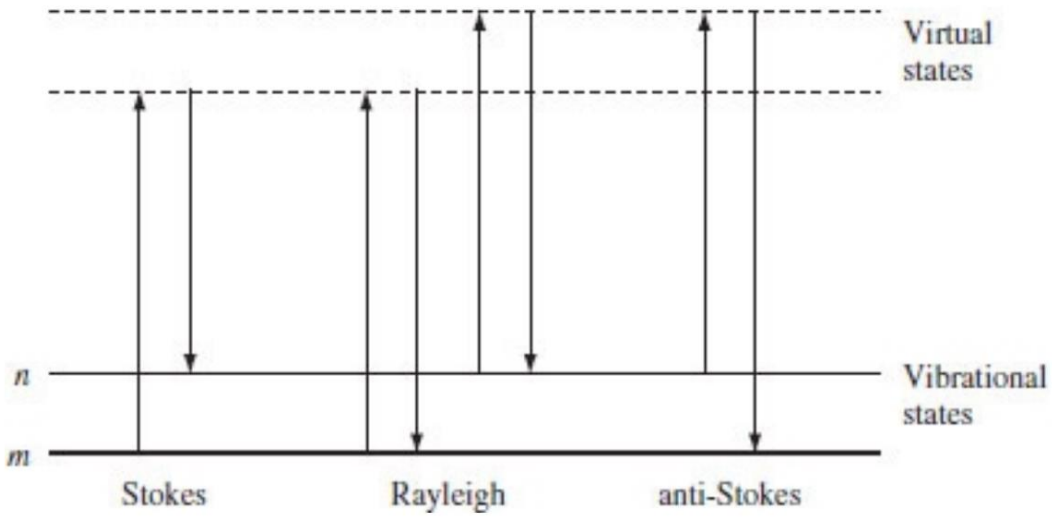

Figure 13 The Rayleigh and Raman scattering presented as Stokes and anti-Stokes scattering.(Smith & Dent, 2013)

Raman is a scattering technique in contrast to absorption techniques such as X-ray absorption, fluorescence emission and infrared (IR) absorption. In absorption techniques instead of scattering the photon it is absorbed and the electron/molecule is moved to an excited energy state, n causing vibrations in the molecules. Raman data is obtained due to the polarizability of the electrons in the sample molecules. After the sample has been subjected to the inelastic scattering, the sample enters a different rotational or vibrational state. The scattering intensity is proportional to the change in polarizability. The energy loss (or gain) of the scattered photon is characteristic for a specific bond in the molecule, thus Raman provides a structural fingerprint which can be used to identify the molecular structure of the sample. (Smith & Dent, 2013)

Paired with complementary techniques such as infrared (IR) spectroscopy, Raman provides us with characteristics of fundamental vibrations that are extensively used in characterization of molecular structures. (Larkin, 2017; Smith & Dent, 2013). Raman spectroscopy can be used as In-line characterization tools in pharmaceutical manufacturing during for example hot melt extrusion to characterize the miscibility of API and polymer, as well as the amorphous/crystalline structure of the melt. (Saerens et al., 2011).

After the data has been obtained it is often necessary to apply a range of preprocessing steps to extract the relevant data. Standard normal variate transformation (SNV) is a common method for normalising the data. SNV normalizes the spectra to unit standard deviation, correcting for intensity of the peaks making the spectra easily comparable.

Principal component analysis (PCA) is an eigenvalue-based statistical method for finding the main sources of variance a dataset, in this case the spectral data. It takes the variance between the observations and decomposes them into principal components, each describing the main sources of variation within the data. Principal component 1 (PC-1) explains the main part of the variance and succeeding variance is explained by PC-2, PC-3 and so forth. The level of variance explained is given by a percentage. PCA helps cluster the data into subgroups making it easier to separate the differences within the obtained data. The data are also separated into a loadings plot, showing the nature of the variation in the principal component. If the loadings plot of a PC looks similar to a feature in the spectra, it is highly likely that the principal component describes the variation related to that feature (eg. if the loadings plot looks similar to the amorphous peak, the PC likely describes the level of amorphicity within the samples) (Abdi & Williams, 2010).

2.5.6 Prediction of drug-polymer solubility (Flory-Huggins model)

To ensure the stability of the ASD's during storage it is important to assess the solubility of the drug in the polymer. To keep the ASD stable and prevent recrystallization during shelf life, it is essential that the drug is molecularly dispersed below its saturation solubility allowing a molecularly dispersed ASD. As most relevant drugs and polymers are in the solid state or highly viscous state at room temperature the assessment is often carried out at higher temperatures and then extrapolated down to room temperature (Knopp et al., 2016) (Knopp et al., 2015). The Flory-Huggins model (Flory, 1953) can be used to predict the drug-polymer solubility, using a melting point depression for oversaturated drug-polymer ratios in the DSC. The melting of the crystalline drug should occur when the chemical potential of the crystal equals the chemical potential of the melt. The amorphous polymer should reduce the chemical potential of the crystalline drug, lowering the melting point. By fitting the model by Flory-Huggins to the drug-polymer system the melting point depression can be related to the solubility of the drug in the polymer (Knopp et al., 2015). Accurate, known ratios of drug-polymer are mixed gently to reduce particle size but to avoid amorphisation of the drug. The mixtures are slowly heated in

the DSC. The onset of the endothermic melting of the mixture can be considered the solubility temperature of the mixture.

$$\frac{\Delta H_m}{R}\left(\frac{1}{T_m}-\frac{1}{T}\right)=\ln\left(v_{drug}\right)+\left(1-\frac{1}{\lambda}\right)\left(1-v_{drug}\right)+\chi\left(1-v_{drug}\right)^2 \qquad [11]$$

Where ΔH_m is the enthalpy of fusion for the pure drug, T_m is the melting temperature for the pure drug. R is the gas constant, λ is the molar volume ratio of the polymer and drug. χ is the Flory-Huggins interaction parameter. T is the onset of melting temperature. v_{drug} is the volume fraction of drug derived from:

$$v_{drug}=\frac{\frac{X_{drug}}{\rho_{drug}}}{\frac{X_{drug}}{\rho_{drug}}+\frac{1-X_{drug}}{\rho_{polymer}}} \qquad [12]$$

where ρ_{drug} and $\rho_{polymer}$ are the densities of the drug and polymer. X_{drug} is the mass fraction of the drug.

The results of melt point depression at elevated temperatures can be extrapolated down to room temperature using a statistical model presented by Knopp et al. (Knopp et al., 2015) to estimate the drug solubility in the polymer at room temperature which is the preferred storage temperature. The estimates were reported as central estimates (the least-squares estimate) with a 95% confidence interval.

3 Aims

The aim of this project was to investigate different preparative methods of solid dispersions to evaluate them as possible screening tools for the quality and melt processability of API-polymer mixtures. HME and VCM was chosen as the preparative methods.

This thesis has focused on investigating if rheological analysis can be used as an appropriate tool for assessing the quality and melt processability of solid dispersions prepared by HME. The effect of drug load on rheological properties of API-polymer mixtures have also been investigated. VCM has been evaluated as a screening tool for HME and for assessing the

miscibility of drug-polymer mixtures. The suitability of VCM for finding the optimal temperature and process parameters for HME was evaluated.

Different analytical methods were used for determining the physiochemical properties and formation of amorphous solid dispersions (ASD's) of the prepared API-polymer mixtures including Raman spectroscopy, differential scanning calorimetry (DSC), thermogravimetric analysis (TGA) and polarized light microscopy (PLM). The benefits of other methods such as X-ray powder diffraction was also discussed. The Flory-Huggins model was used to determine solubility of API in polymer and compared with the analytical data obtained through other methods.

4 Materials

4.1 Raw materials

4.1.1 Naproxen

Naproxen was purchased from Fagron Nordic A/S (Copenhagen, Denmark). Naproxen, (2S)-2-(6-Methoxynaphthalen-2-yl)propanoic acid is a non-steroid anti-inflammatory drug (NSAID) with both antipyretic and anti-inflammatory effects and is used in treatment various pain and inflammatory conditions (Fig 14). Naproxen is a nonselective cyclooxygenase inhibitor (COX) inhibiting both enzymes COX-1 and COX-2. (Ta & Dionne, 2004). Naproxen is practically insoluble in water and is soluble in ethanol. The sodium salt of naproxen is being used commercially to improve water solubility. Naproxen has a melting point of 153°C. Naproxen is a weak acid with pKa 4.15. Naproxen is classified as class II in the BCS and as class I by GFA. The limiting factors for the bioavailability of Naproxen is the solubility and the dissolution rate. The naphthalene ring causes strong π–π interactions and the carboxylic acid groups form hydrogen bonds which makes naproxen very prone to recrystallization and amorphous naproxen is very physically unstable by itself. (Liu, Zhou, & Zhang, 2017).

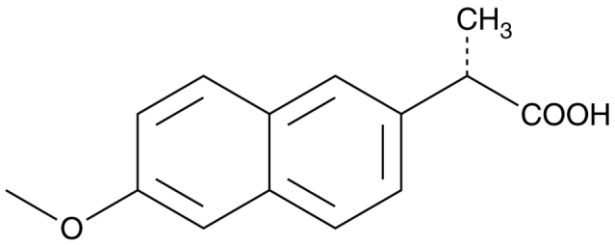

Figure 14 (s)-Naproxen (Cayman Chemical)

4.1.2 Celecoxib

Celecoxib (CCX, Mw = 381.37 g/mol) was purchased from AK Scientific, Inc. (Union City, CA, USA). Celecoxib (Fig 15), 4-[5-(4-methylphenyl)-3-(trifluoromethyl)-1*H*-pyrazol-1-yl] is a NSAID selectively inhibiting COX-2. Celecoxib is used to treat symptoms of osteoarthritis and rheumatoid arthritis (Paulson et al., 2001). Celecoxib is a weak acid with a pKa of 11.1 and is classified as BCS II drug due to its poor water solubility (≅5 μg/ml). The melting temperature of celecoxib is 158°C. Crystalline Celecoxib form long, needle like crystals. (Chawla, Gupta, Thilagavathi, Chakraborti, & Bansal, 2003)

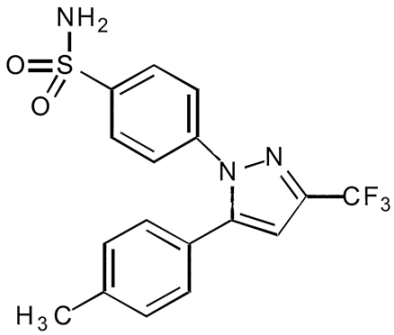

Figure 15 Celecoxib (Paulson et al., 2001)

4.1.3 Soluplus

Soluplus® was purchased from BASF SE (Ludwigshafen, Germany). Soluplus is a graft copolymer consisting of a polyethylene glycol (PEG) 6000 backbone with polyvinylcaprolactam (PVCL) and polyvinyl acetate (PVAc) side chains. Soluplus is an amphiphilic polymer, where PEG functions as hydrophilic part and the PVCL/PVAc side chains function as lipophilic part. This allows Soluplus to form micelles in aqueous solutions

above the critical micelle concentration (CMC) of 7.6 mg/ml (Ali et al., 2015). Soluplus consists of white to yellowish free-flowing granules and has a Mw of 118 000 g/mol.Soluplus was developed for use in solid dispersions and shows good extrudability and flowability. (Tsinman, Tsinman, & Shaukat, 2015). Soluplus has a reported T_g of approximately 70 °C (Caron et al., 2013).

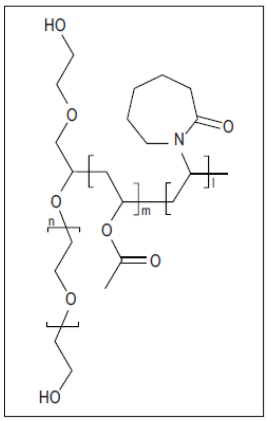

Figure 16. Soluplus

5 Methods

5.1 Hot Melt Extrusion

The extrusions were conducted using a lab-scale twin screw extruder with two co-rotating conical mixing screws (DSM Xplore Micro Compounder) (Fig 17).

The API-polymer mixtures were manually mixed using a mortar and pestle in weight to weight (w/w) ratios of 10:90, 30:70 and 50:50 to investigate the influence of drug-polymer ratio in the extrudates. The API-polymer mixtures were extruded at 120 °C with a screw speed of 50 rounds per minute (RPM). The three heating zones of the extruder were set to 120 °C and allowed to equilibrate. Approximately 5-10g of the API-polymer mixture was fed manually through a hopper. The mixtures were extruded using different circulation times, in which the mixtures were melted and recirculated inside the extruder. The mixtures were extruded either without recirculation as continuous manufacturing or as a batch with a 5-minute recirculation time to investigate how the time of exposure to the heat in the molten state affects the extrudates.

The extrudates were manually collected and cooled at ambient conditions. The collected extrudates were grinded using a mortar and pestle for further analysis. Some strands were also collected for a stability study.

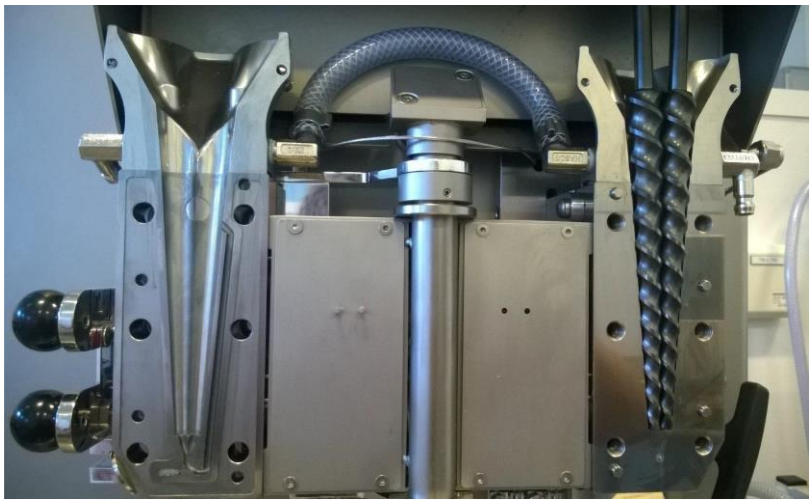

Figure 17 Laboratory scale extruder with a co-rotating twin-screw setup (DSM Xplore Micro Compounder)

5.2 Stability study

Strands and grinded extrudates produced using HME were stored at a 95% relative humidity at 40 °C. The extrudates were analysed using Raman spectroscopy and PLM at d0, d30, d60. The samples are presented in Table 3.

Table 3 List of samples chosen for stability studies.

API	Polymer	%API	%Polymer	Method	Recirculation time (min)
NAP	Soluplus	10	90	HME	0
NAP	Soluplus	10	90	HME	5
NAP	Soluplus	30	70	HME	0
NAP	Soluplus	30	70	HME	5
NAP	Soluplus	50	50	HME	0
NAP	Soluplus	50	50	HME	5
CCX	Soluplus	10	90	HME	0
CCX	Soluplus	10	90	HME	5
CCX	Soluplus	30	70	HME	0
CCX	Soluplus	30	70	HME	5
CCX	Soluplus	50	50	HME	0
CCX	Soluplus	50	50	HME	5

5.3 Vacuum compression moulding

API-polymer disks for rheological studies and DSC were prepared using VCM. The disks were prepared using a MeltPrep® tool (MeltPrep GmbH, Austria). The samples were prepared at 120 °C with a dwell time of 15 minutes to mimic the HME process. Some samples were also prepared using higher temperatures and analysed using PLM and Raman to determine the effect of temperature on the API-polymer disks.

For the rheological studies samples of grinded extrudates were prepared into suitable 25mm disks using VCM. The process temperature was set to 100 °C. The temperature was chosen as lower than the extrusion temperature so as not to affect the samples further after the extrusion process.

5.4 Rheological analysis

The rheological analyses were conducted using an AR-G2 rotational rheometer (TA Instruments) (Fig 18) with a heating test chamber. 25-mm parallel-plate geometries were selected for the analyses based on the viscosity of the samples. The linear viscoelastic region (LVR) was determined for Soluplus using s a strain sweep at the strain amplitude range of 0.015% to 15% at 120°C at a constant angular frequency of 10 Hz.

SAOS frequency sweeps were run in the LVR at 120°C at a constant strain amplitude $\gamma = 0.5\%$ and decreasing angular frequency from 100 to 0.01 Hz. The experiments were ran using 25mm disks prepared using VCM and weighing approximately 500mg. A gap of 0.75mm between the parallel plates was used for all sample measurements.

Supporting temperature sweep measurements in SAOS were run at constant strain amplitude $\gamma = 0.5\%$ (within the LVR) and constant angular frequency $\omega = 1$ Hz. The measurements were run from 100°C to 180°C. The complex viscosity was used to assess the melt processability of the samples and to assess if the VCM samples showed similar rheological properties as the extruded samples.

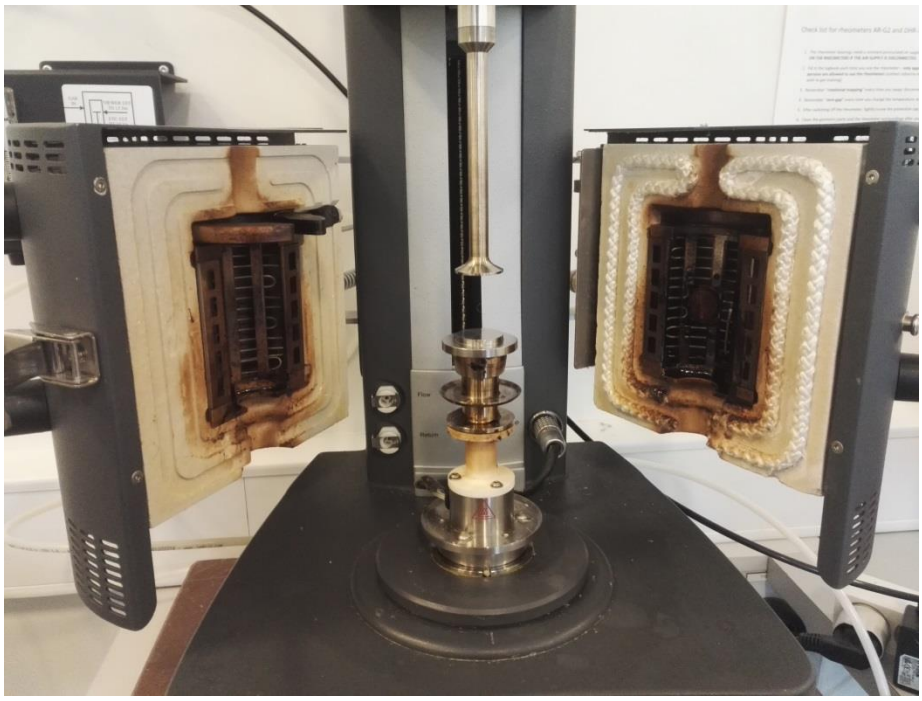

Figure 18 AR-2 Rheometer (Trios)

5.5 Thermogravimetric analysis

Thermogravimetric analysis (TGA) was performed using a Discovery TGA (TA Instruments, New Castle, DE, USA) controlled by TRIOS software (TA Instruments, New Castle, DE, USA). Samples were analysed in flame-cleansed open platinum pans. TGA was used to determine degradation temperatures of NAP and CCX to ensure that no significant degradation occurred at used process temperatures. The samples of pure crystalline API were heated up to 300°C.

5.6 Differential Scanning Calorimetry

Thermal analyses were performed using a modulated differential scanning calorimetry (MDSC, Q100, TA Instrument, Elstree, UK). Modulated temperature DSC was used to determine the T_g of the samples prepared by HME and VCM. Physical mixtures of the same ratios were also used as a reference. 2-11 mg of sample were packed into an aluminium pan with a non-hermetic lid. For HME the extrudates were ground using a mortar and pestle before sampling. VCM

samples were prepared using the pan-sized 5mm disk tool on the MeltPrep weighing approximately 10mg. Physical mixtures were manually mixed.

The inflection Tg's were determined from the reversing heat flow in the modulated DSC to avoid interference from enthalpic relaxation. This was done by taking the derivative and selecting the minimum value.

The samples were heated to 100° (Ramp 1) and kept isothermal for 2 min to get rid of moisture and reduce the effect of enthalpic relaxation. The samples were cooled down to -50°C before heating up to 170°C at 5°C/min (Ramp 2). After Ramp 2 the samples were cooled back down to -50 and heated up to 170°C for a second time (Ramp 3) to see if the T_g would be affected of heating above the T_m of the API. The DSC program is summarized in Table 4.

Table 4 Modulated DSC program for T_g determination

Step	Description
1	Equilibrate -50,00 °C
2	Modulate Temperature Amplitude 0,5310 °C , Period 40,0 s
3	Ramp 5,00 °C/min to 100,00 °C
4	Isothermal 2,00 min
5	Equilibrate -50,00 °C
6	Modulate Temperature Amplitude 0,5310 °C , Period 40,0 s
7	Ramp 5,00 °C/min to 170,00 °C
8	Equilibrate -50,00 °C
9	Modulate Temperature Amplitude 0,5310 °C , Period 40,0 s
10	Ramp 5,00 °C/min to 170,00 °C

5.6.1 Solubility determination

200mg of high drug load drug-polymer mixtures were manually mixed using a mortar and pestle with low force (Table 5). The melting point depression was measured using DSC. Approximately 2 mg of powder were packed in aluminium pans. The lid was pinholed for moisture to escape. The samples were heated above the melting point up to 170°C by 1°C/min. The onset of melting for each sample was determined using Trios software and was used to calculate solubility of the APIs in polymer. The results were extrapolated to room temperature using the Flory-Huggins equation described earlier in this thesis. The volume fractions of the drug and polymer were calculated by dividing the weight fractions by the amorphous densities of the materials. For NAP the crystalline density was used instead due to the difficulty of producing a amorphous sample of pure NAP.

Table 5 API:polymer fractions used for the solubility determination of NAP and CCX in Soluplus

NAP	Soluplus
75	25
80	20
85	15
90	10
100	0

CCX	Soluplus
70	30
75	25
80	20
85	15
100	0

The sample preparation for solubility determination of CCX in Soluplus was performed by Ana Calduch Arques.

5.7 Stability study

Strands and grinded extrudates were stored at a 95% relative humidity at 40 °C. The extrudates were analysed using Raman spectroscopy and PLM at day 0, 30 and 60.

5.8 Raman spectroscopy

Raman spectroscopy was performed using a Kaiser RXN1 Microprobe (Kaiser Optical Systems, Ann Arbor, MI, USA) equipped with a PhaT-probe (Kaiser Optical Systems). The laser wavelength was 785 nm and the Raman shifts were measured from 150 to 1900 cm^{-1} with each spectrum comprising of 5801 data points. The exposure time was 5 seconds with 1 accumulation. Triplicates of each sample were gathered from different parts of the samples. The optimal region for predicting amorphisity of the samples were selected and confirmed by literature. For CCX the region from 770 to 840 cm^{-1} was selected. The amorphisity can be observed as a peak shift from 810 cm^{-1} for crystalline CCX to 798 cm^{-1} for the amorphous CCX. The 798 cm^{-1} peak seems to merge with a peak observed at 794 cm^{-1}. This shift has also been observed by Edinger et al. (Edinger et al., 2018) The shift is explained as a change in the intermolecular structure surrounding the phenyl ring in CCX. For NAP a region from 1610 to 1650 cm^{-1} was selected. The amorphization of NAP causes a minor peak shift from 1630 for crystalline NAP to 1634 cm^{-1} for amorphous NAP. This shift is due to the change in the intermolecular structure surrounding the aromatic ring structure of NAP. This shift has also been presented by Allesø et al. (Allesø et al., 2009).

The obtained Raman spectra were pre-processed using Standard normal variate correction (SNV) and trends were visualised using Principal component analysis (PCA).

5.9 Polarized light microscopy

Polarized light microscopy (PLM) was performed using a Leica DM LM microscope (Leica Microsystems GmbH, Wetzlar, Germany) equipped with a 40× objective. Microscope images were obtained using an Evolution MP camera (Media Cybernetics, Rockville, MD, USA) controlled by Image-Pro Insight software (Media Cybernetics).

6 Results

6.1 Stability of raw materials

Before starting the HME process and the rheological studies, stability of the raw materials at the process temperatures had to be ensured. The degradation temperatures for NAP, CCX and Soluplus were established by thermogravimetric analysis. Results are shown in Figure 19. No significant weight loss could be observed at the chosen extrusion temperatures of 120-130°C. The initial weight loss of Soluplus is due to water evaporating from the sample. NAP starts degrading at temperatures over 150°C. CCX an Soluplus appear to be stable at temperatures exceeding 200ºC. Therefore, the chosen extrusion temperature was regarded as safe.

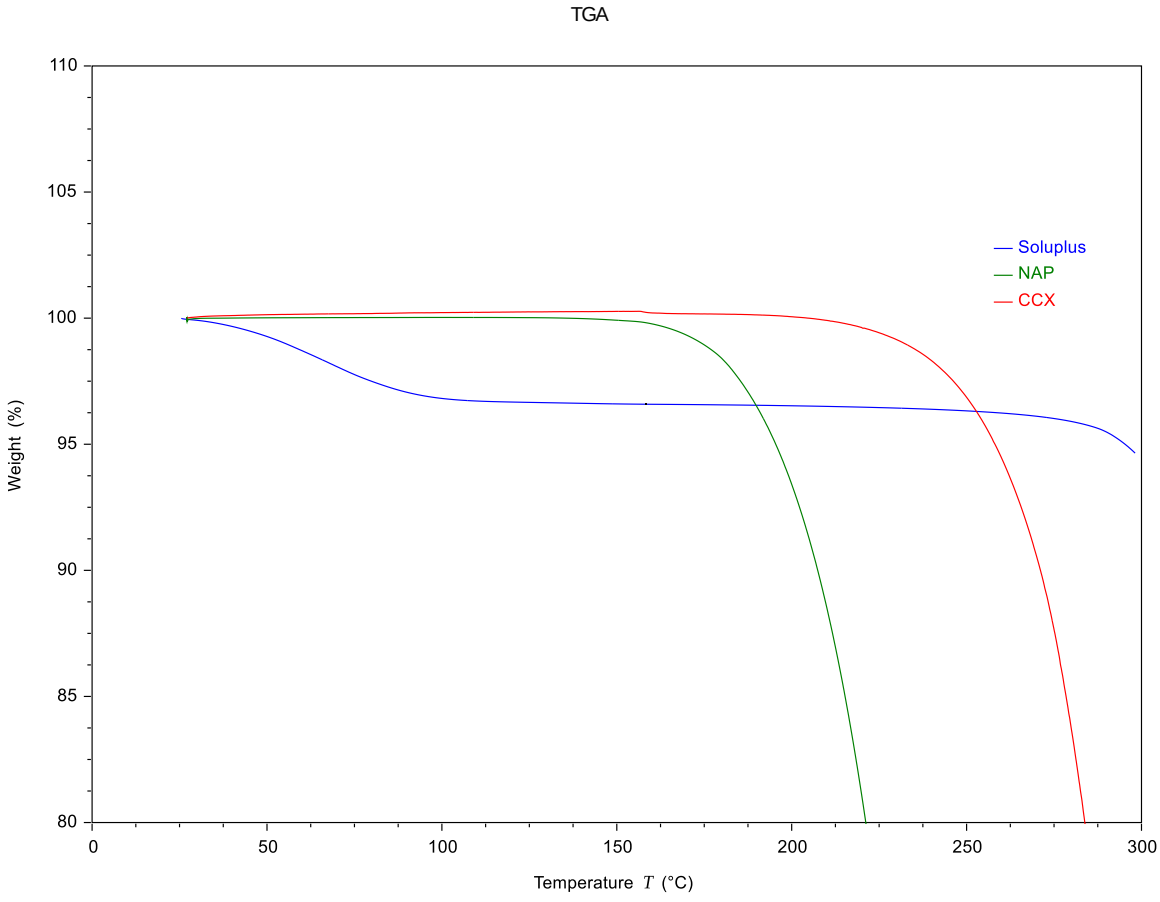

Figure 19 Thermogravimetric analysis diagram of CCX(blue), NAP(green) and Soluplus(red) showing weight loss in percent as a function of temperature. Heating rate 10°C/min

6.2 Solubility determination

Using the Flory-Huggins theory and melting point depression in oversaturated API-polymer samples in the DSC, an estimate of the solubility of API in Soluplus for both NAP and CCX were determined. The fraction of drug that will fully dissolve in Soluplus at a given temperature is presented in Figure 20& Figure 21. At the chosen process temperature for HME and VCM at 120°C an estimated 61% (53-67%, 95% confidence) of NAP will be soluble in Soluplus. In other words in a 61:39 NAP:SP ratio all NAP should be soluble and able to disperse in the polymer mixture. The corresponding amount of soluble CCX at 120°C is 32% (13-45%, 95% confidence).

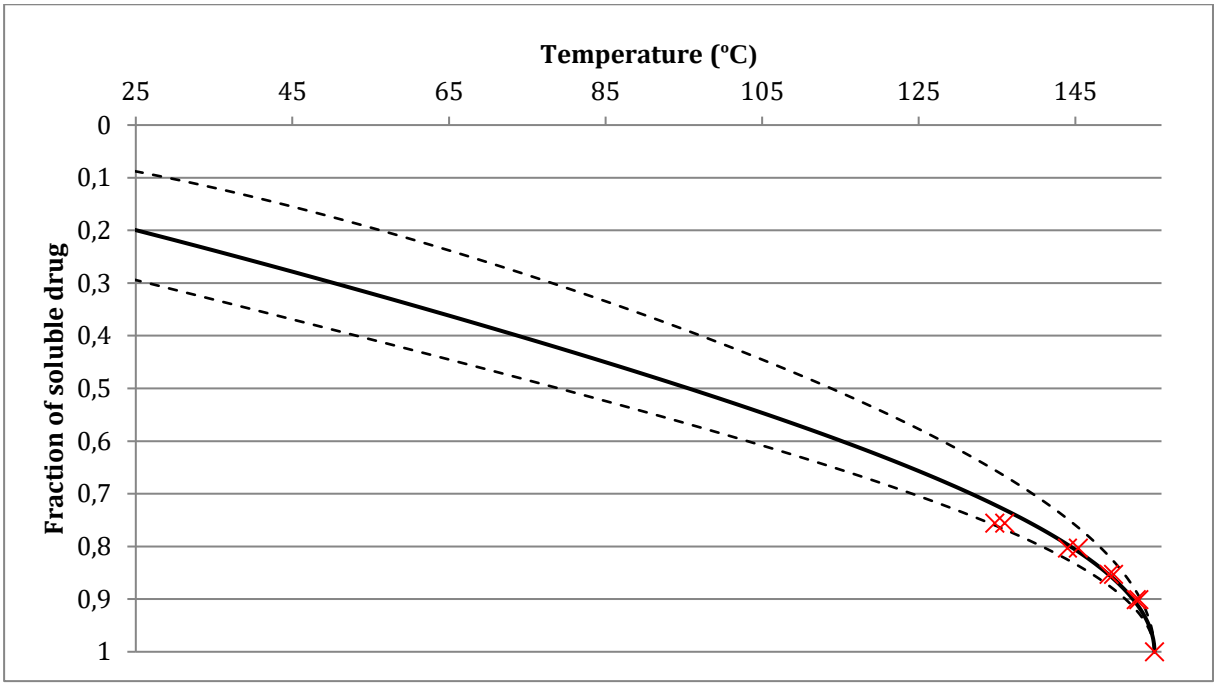

Figure 20 Solubility estimation of NAP in Soluplus with 95% confidence intervals.

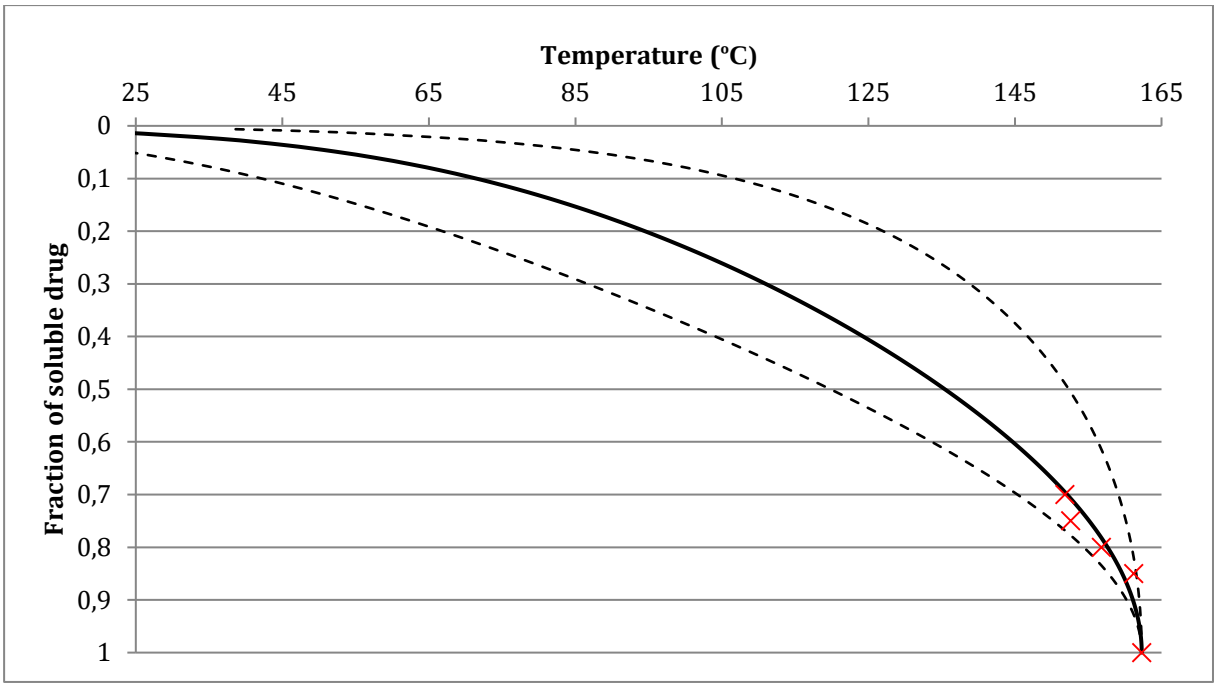

Figure 21 Solubility estimation of CCX in Soluplus with 95% confidence intervals.

NAP shows a high solubility in Soluplus and show good extrusion characteristics at the chosen process temperatures. The extrapolation of solubility would indicate that even at room temperature approximately a 20% NAP content would be fully soluble in Soluplus. The low solubility of CCX, closing at a 0-5% estimated solubility at room temperature indicates that Soluplus is not an ideal polymer for producing ASD's with CCX, especially at higher drug contents.

6.3 Preparation of solid dispersions

6.3.1 Hot-melt extrusion

The chosen API-polymer mixtures showed good extrudability at the chosen process temperature of 120ºC and the screw speed of 50 RPM, allowing for both continuous extrusion with immediate collection of the extrudates, as well as extrusion prepared by batch processing with a 5-minute recirculation within the extruder, before opening of the extrusion valve. However the 50:50 NAP:Soluplus extrudates exhibited low viscosity and were sticky at collection. This indicates that NAP has a plasticising effect on the API-polymer melt. For future extrusions of

50:50 NAP:Soluplus, change of process parameters (lower temperature or screw speed) or improved collection of the extrudates from the die, to prevent lumping of the sample, is recommended.

Approximately 5-10 grams powder mixture was used for each batch produced. The powder was manually fed into the extruder until the chamber was considered full and a stable melt pressure was obtained. The recirculation time was recorded from the end of feeding to start of extrusion, thus the time inside the extruder is more than 5 minutes for the batch manufactured extrudates. During some of the extrusions the chamber reached a maximum melt pressure of 5000N, activating a safety setting and shutting off the engine. In this case the motor was restarted and some of the sample allowed to exit the extruder. All parameters of the extruder were recorded and stored including melt pressure and temperature.

For the batch produced, 5-minute recirculated samples the melt pressure quickly dropped after opening the valve and forming the extruded strand from the die. This led to a slowing of the extrusion after the initial start. The first and last part of the extrudates were discarded and the rest were chosen for further analysis.

Upon exiting the die, the extrudates ranged from clear to opaque (Fig 22&23). The extrudates containing CCX were stiff and brittle. Extrudates containing NAP were more flexible at higher drug content, but still exhibited brittleness when force was applied.

The produced extrudates of NAP in Soluplus (Fig 22) decreased in thickness with increased drug content even though the same die was used for all samples. This was probably due to lower viscosity of the melt. The extrudates with 10% and 30% NAP content were clear, while the 50% NAP exhibited cloudiness possibly indicating residual crystals in the solid dispersion.

The corresponding extrudates with CCX in Soluplus showed a more opaque, cloudy appearance (Fig 23). The extrudates were also thicker and having a higher viscosity in the extrusion process compared with extrudates containing NAP. This would indicate that CCX does not have a plasticizing effect of the same magnitude as NAP. The opaque nature of the extrudates can indicate crystallinity but may also be due to characteristics of the raw materials. This can be correlated with the poor solubility of CCX in Soluplus shown by the Flory-Huggins model. It is possible the opaque nature is due to undissolved CCX in the extrudates.

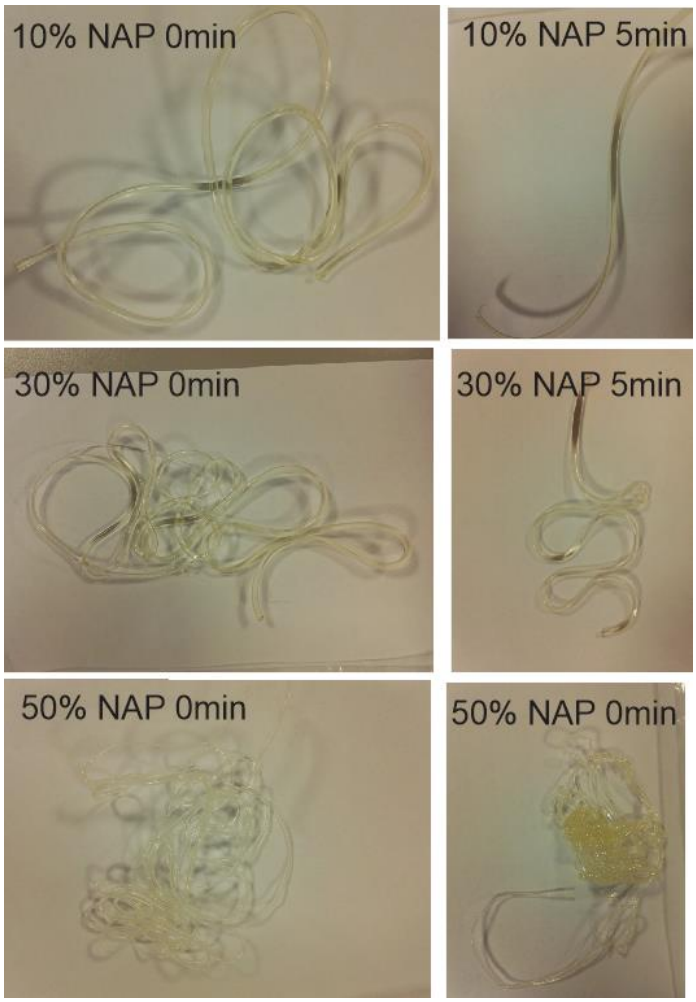

Figure 22 Extrudates of NAP in Soluplus. Fraction of NAP and the recirculation time in the extruder given for each picture

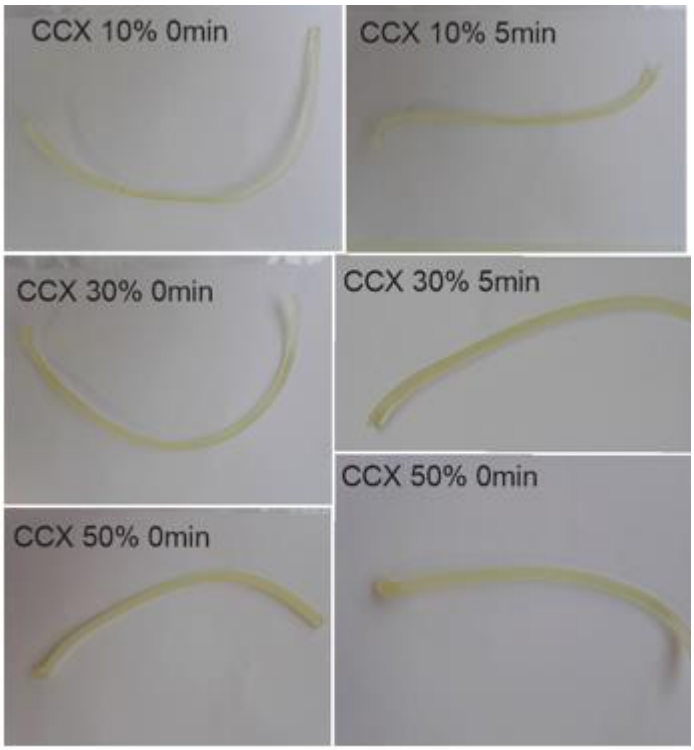

Figure 23 Extrudates of CCX in Soluplus. Fraction of CCX and the recirculation time in the extruder given for each picture

Due to the high viscosity and opaque appearance of the extrudates containing CCX, a test extrusion with 50:50 CCX:Soluplus was done at 130°C with a 5 minute recirculation. The elevated temperature together with the recirculation time in the extruder seemed to give the extrudate a clearer appearance (Fig 24). The extrudate was included in further analytical studies to see if the amount of amorphous API had increased by elevated temperature.

Figure 24 Comparison of exrudates of 50:50 CCX:Soluplus at different temperatures. 120ºC with no recirculation (left) and 130ºC with 5 minute recirculation in the extruder

All the extrusions were conducted well under the melting temperature of the API's. NAP has a reported melting point of 153ºC and CCX 158ºC.

6.3.2 Vacuum compression moulding

To mimic the extrusion process corresponding API-polymer samples were prepared using VCM. API-polymer disks were prepared from physical mixtures using the MeltPrep®-tool at elevated pressure and temperature. The goal was to obtain homogenous samples of solid dispersions, optimal for rheological analysis and DSC that could be used for screening mixtures before commencing large-scale extrusions. The temperature was chosen as 120°C, same as the process temperature in the extruder. Some test samples were also prepared at elevated temperatures of 130°C and 170°C.

Due to the lack of mixing and shear in the VCM the disks did not appear homogenous. The disks showed drug rich deposits when visually inspecting them, while other parts were clear. Both for CCX and NAP 50% disks were flaky and white, powdery on the surface, indicating high crystal content.

VCM was also used to produce disks of the extrudates from the melt-extrusion. The grinded extrudates were heated up to 100°C at elevated pressure in order to produce 25mm disks similar

to the disks prepared from the raw materials. The disks prepared from extrudates had a much clearer appearance compared with the disks from raw materials (Fig 25&26).

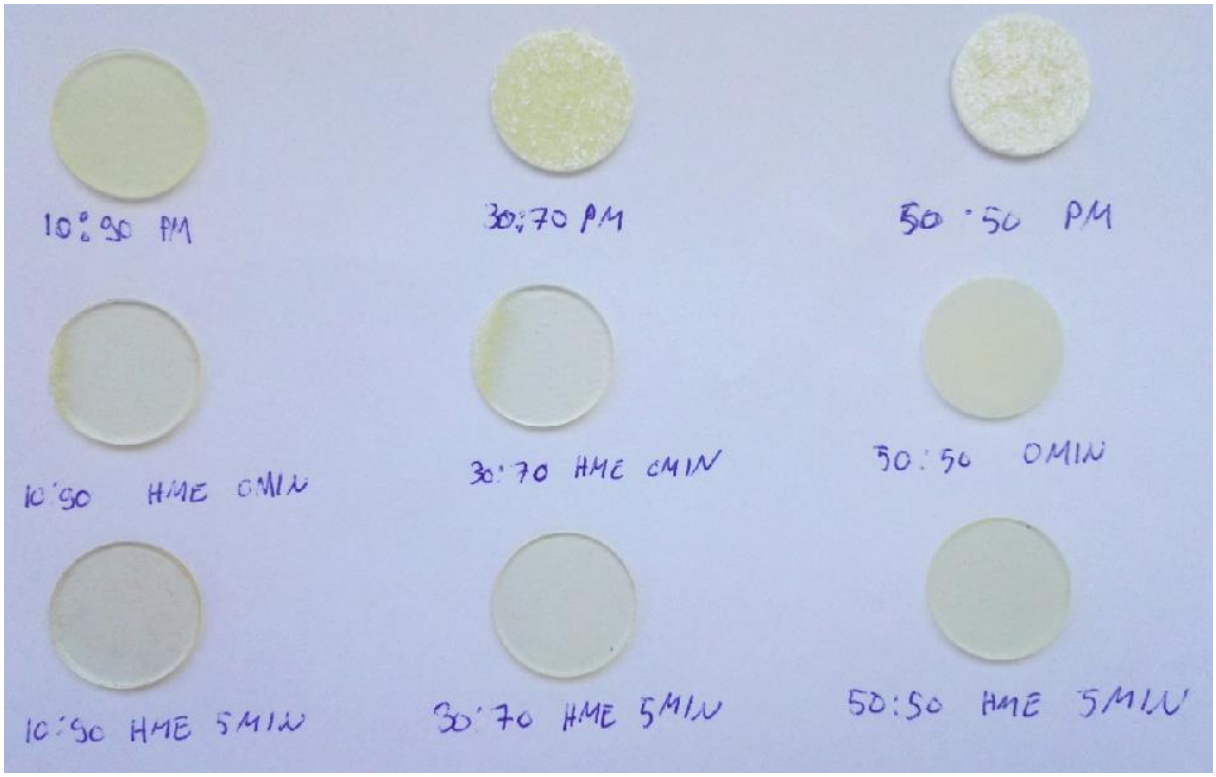

Figure 25 VCM disks of CCX:Soluplus. Top row is prepared from physical mixture(PM) .Second row is extruded without recirculation at 120°C and third row is extruded with 5 minute recirculation time. Samples prepared using MeltPrep®

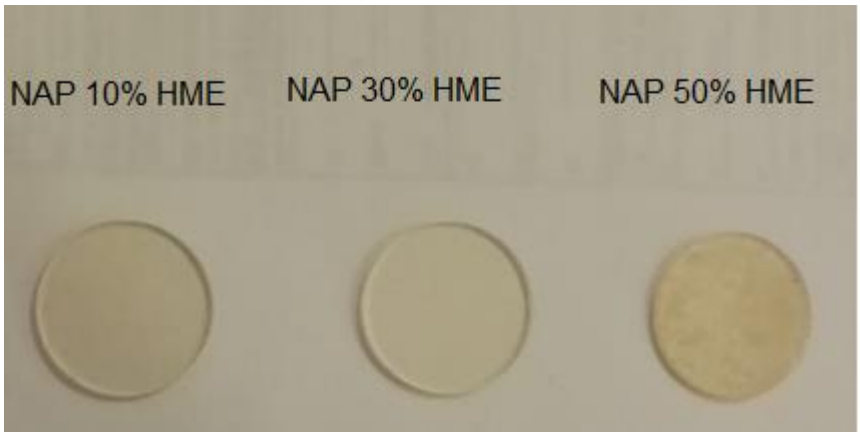

Figure 26 VCM disks of NAP:Soluplus. Prepared of grinded extrudates using the MeltPrep at 100°C. The extrudates were extrudet at 120°C without recirculation

For a rheological temperature sweep measurement samples from physical mixtures were prepared at 100°C for 15 minutes using the VCM. All the samples were white non-transparent (Fig 27&28). A sample of 50% CCX would not melt together at 100°C and was left out of the temperature sweep measurements. The disks containing CCX seemed to have a more crystalline structure compared to disks containing NAP when visually inspecting them.

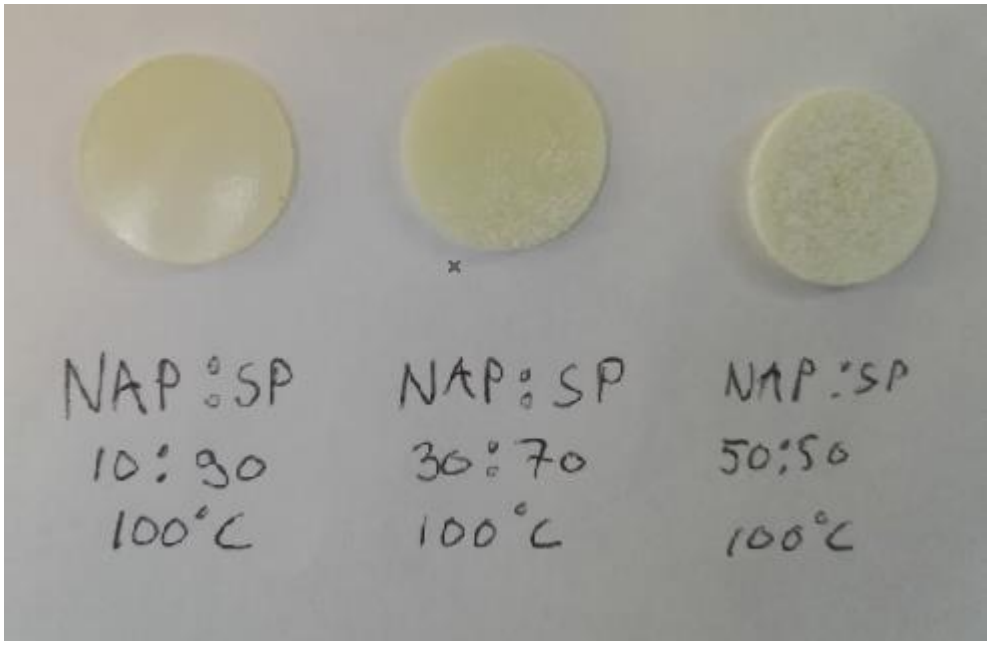

Figure 27 VCM-disks of NAP:Soluplus 10-30-50% API content. Prepared at 100°C from physical mixtures for temperature sweep analysis

Figure 28 VCM-disks of CCX:Soluplus. 10% CCX (left) and 30% CCX (right). Prepared at 100°C from physical mixtures for temperature sweep analysis

6.4 Raman spectroscopy

Raman spectroscopy was evaluated as a technique for determining amorphicity of the samples. Due to the speed of measurements, Raman spectroscopy could potentially be used as a PAT tool for HME.

6.4.1 Naproxen

Naproxen as a GFA class I compound has a tendency to rapidly recrystallize from its amorphous state. Therefore naproxen is very difficult to make amorphous by itself. The polymer matrix of Soluplus however "locks" NAP in its amorphous state due the the high glass-transition temperature of Soluplus.

In Figure 29 a comparison of the crystalline and amorphous Raman shift of NAP can be seen. The amorphisation of NAP causes a minor peak shift from 1630 for crystalline NAP to 1634 cm^{-1} for amorphous NAP.

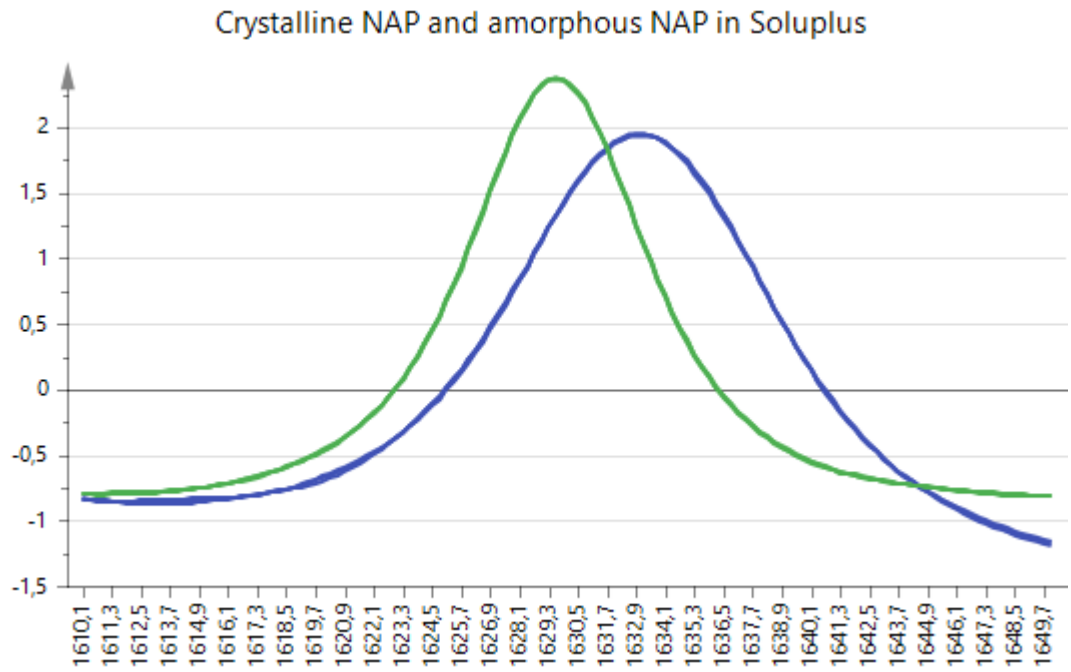

Figure 29 Crystalline NAP (green) and amorphous NAP in Soluplus (blue).

The chosen region for NAP was 1610 to 1650 cm^{-1} and the obtained spectra were preprocessed using SNV. The results are presented in Figure 30. Here, a comparison between the solid dispersions prepared by HME and VCM (MeltPrep®, MP) were compared. Spectra of corresponding physical powder mixtures were also measured.

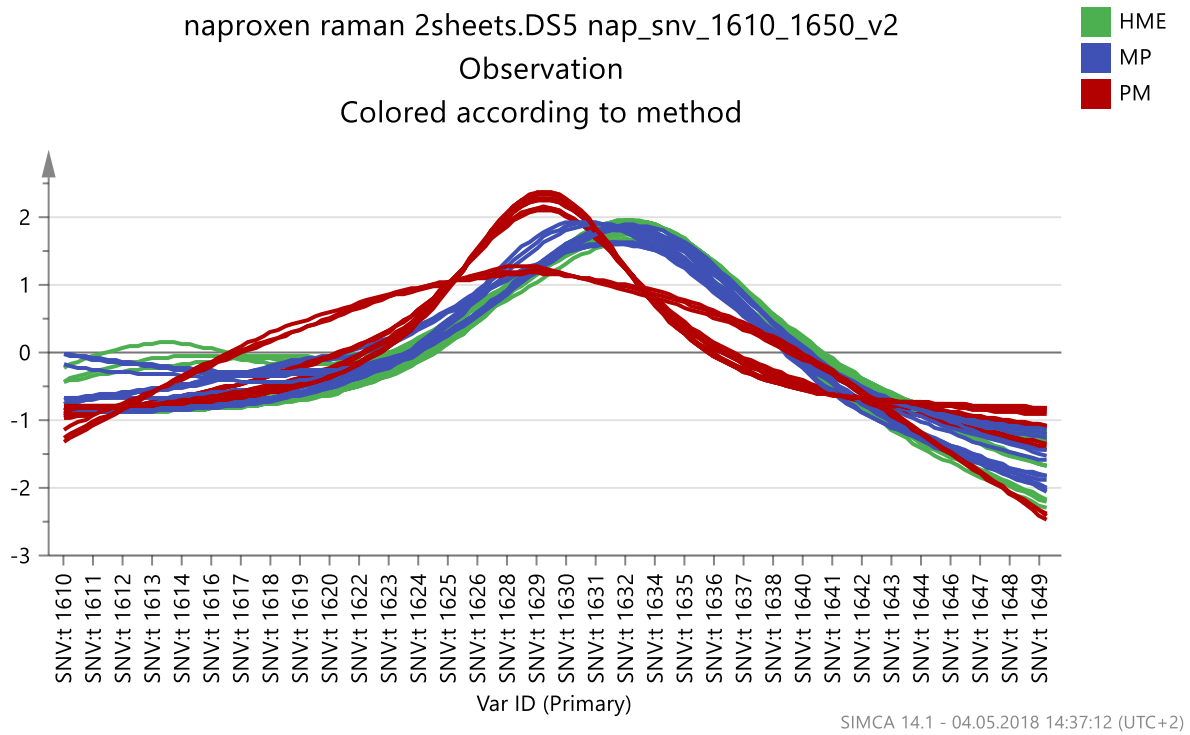

Figure 30 SNV corrected Raman spectra of NAP:Soluplus solid dispersions. Coloured according to manufacturing method. HME (green) MeltPrep (blue) and physical mixtures for reference (red)

By using the statistical method of PCA of the interesting region in the spectra some further data can be obtained. By comparing the SNV processed spectra for the chosen Raman region of 1610-1650 cm^{-1} for NAP, with the loadings plot for PCA-1 (Fig 31) a negative correlation between the crystallinity of the sample and the PC-1 plot can be observed. By visualizing the data in a scores plot plotting PC-1 against PC-2 the observed data points show a tendency towards increased amorphous content along the x-axis (PC-1), with crystalline physical mixtures giving a negative result (Fig 32). The PC-2 is not conclusive in this context and will not be analysed further. PCA indicate that there is a difference between the solid dispersions prepared by HME compared to VCM, especially at higher drug loads. However, it appears that the use of high temperature VCM can yield similar results to extrudates prepared using HME. Further experiments with varying process parameters are required to better assess the suitability of VCM as a screening tool.

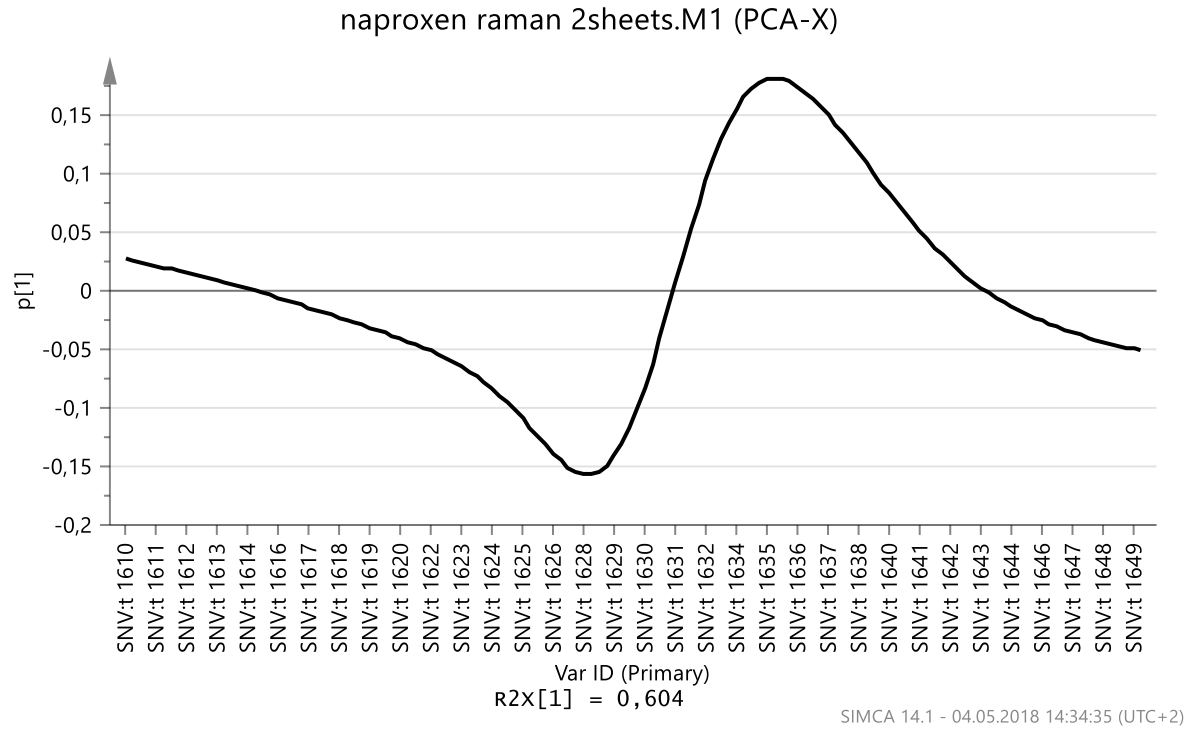

Figure 31 Loadings plot of the first component (PC-1) 60,4% explained variance

When comparing HME and VCM using PCA, some of the samples prepared by VCM are more towards the crystalline reference. Especially at 50% NAP content the HME seems to have more amorphous content compared to VCM (Fig 32-34). Due to the partial overlapping of the Raman shifts and low signal to noise ratio a quantitative estimation is difficult to make. In thee PLM pictures crystals can be observed in all the samples containing 50% NAP.

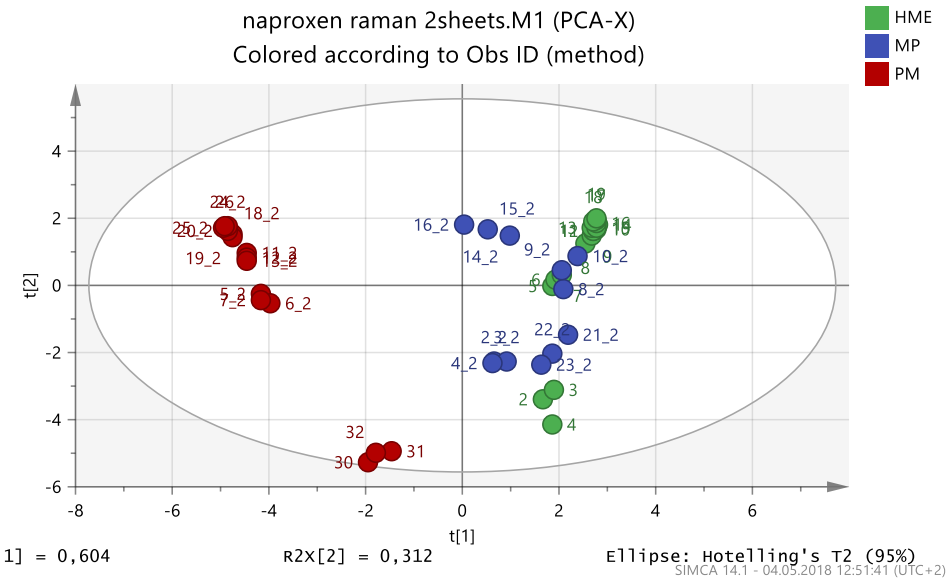

Figure 32 PCA of NAP:Soluplus. Coloured according to preperative method. HME (green) VCM (blue) and physical mixtures as referene (red)

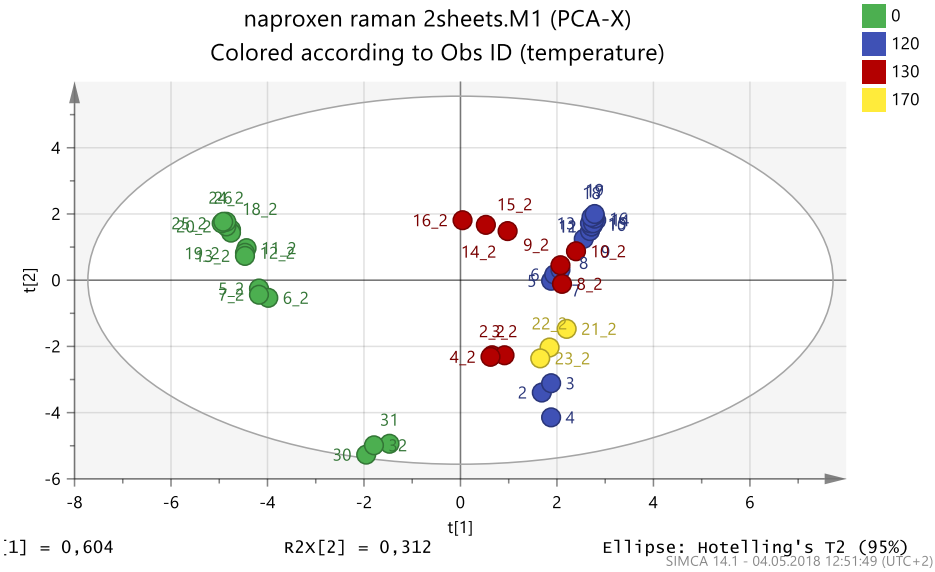

Figure 33 PCA of NAP:Soluplus. Coloured according to process temperature. 120ºC (blue) 130ºC (red) and 170°C (yellow). Physical mixtures as reference (green)

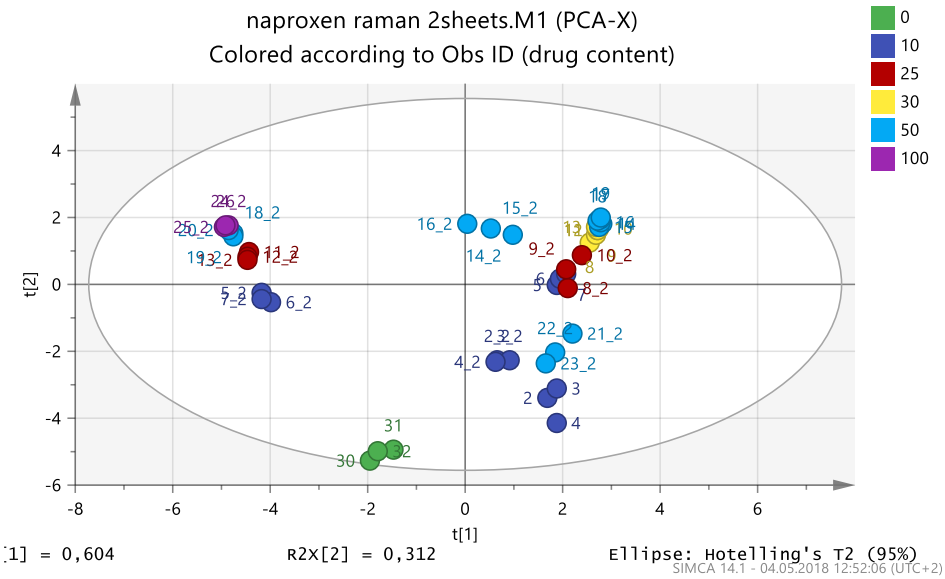

Figure 34 PCA of NAP:Soluplus. Coloured according to naproxen content. 10% (dark blue) 25% (red) 30% (yellow) 50% (teal). Crystalline NAP as reference (purple). Soluplus as reference (green)

6.4.2 Celecoxib

For celecoxib the chosen Raman shift can be observed as a peak shift from crystalline CCX at 810 cm^{-1} to amorphous CCX at 798 cm^{-1} for the amorphous CCX. The 798 cm^{-1} peak merges with a peak observed at 794 cm^{-1} (Fig 35).

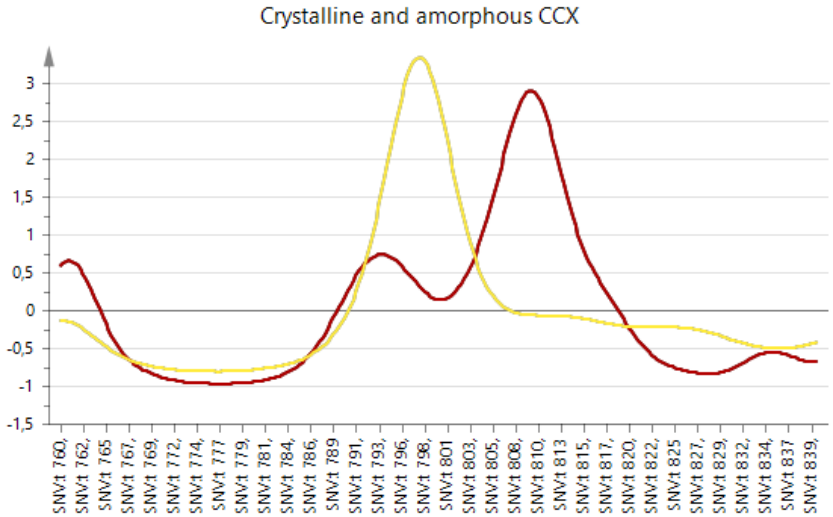

Figure 35 SNV spectra of 100% crystalline (red) and 100% amorphous (yellow) CCX.

When comparing the spectra of the different preparative methods (Fig 36&37), the solid dispersions prepared by VCM show a higher crystalline content while the solid dispersions prepared by HME seem to be mainly amorphous. Both the 30% and 50% CCX content VCM disks show crystallinity prepared at 120°C. 50% CCX was also prepared using VCM above the melting point of CCX at 170°C for 15 minutes. The results indicate that the elevated temperature manages to amorphise the CCX in the VCM tool.

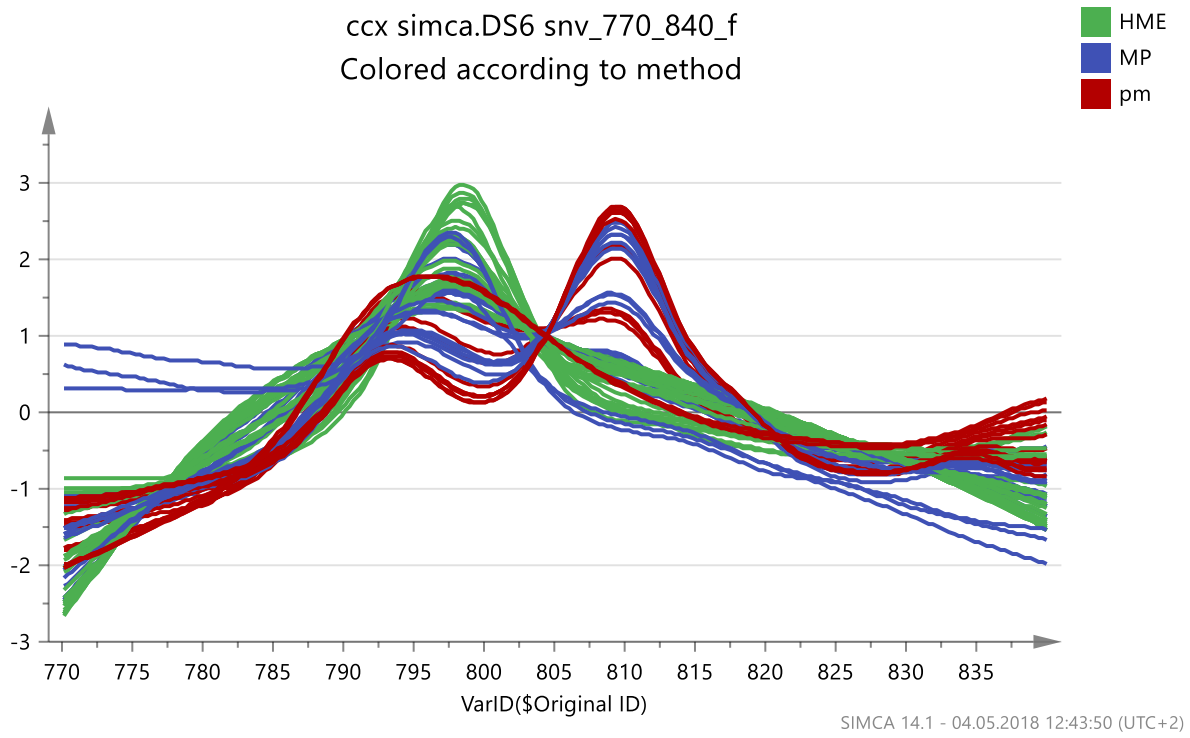

Figure 36 SNV corrected Raman spectra of CCX:Soluplus solid dispersions. Coloured according to manufacturing method. HME (green) MeltPrep (blue) and physical mixtures for reference (red)

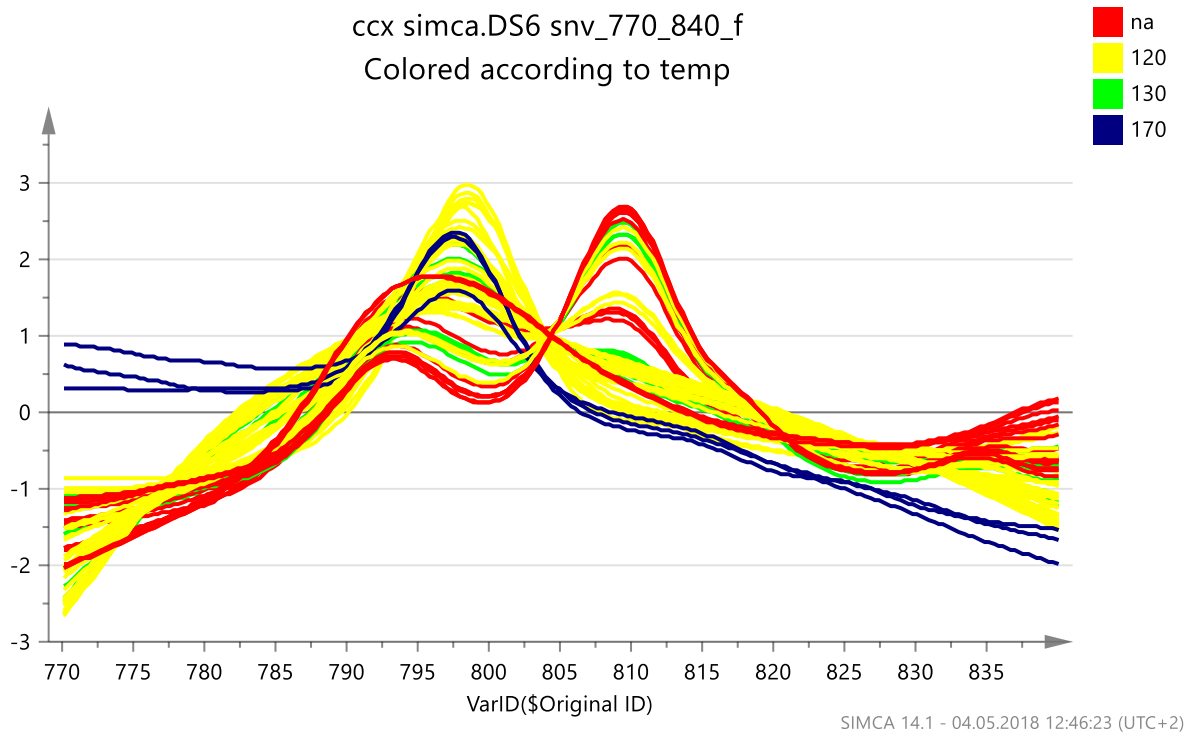

Figure 37 SNV corrected Raman spectra of CCX:Soluplus solid dispersions. Coloured according to process temperature. 120°C(yellow) 130°C(green) 170°C (blue) and physical mixtures for reference (red)

By comparing the SNV processed spectra for the chosen Raman region of 760-840 cm^{-1} with the loadings plot for PCA-1 (Fig 38), a positive correlation between the crystallinity of the samples and the PC-1 plot can be observed. By visualizing the data in a scores plot plotting PC-1 against PC-2 the observed data points show a tendency towards increased crystalline content along the x-axis (PC-1), with crystalline physical mixtures giving a positive result (Fig 39). The PC-2 is not conclusive in this context and will not be analysed further.

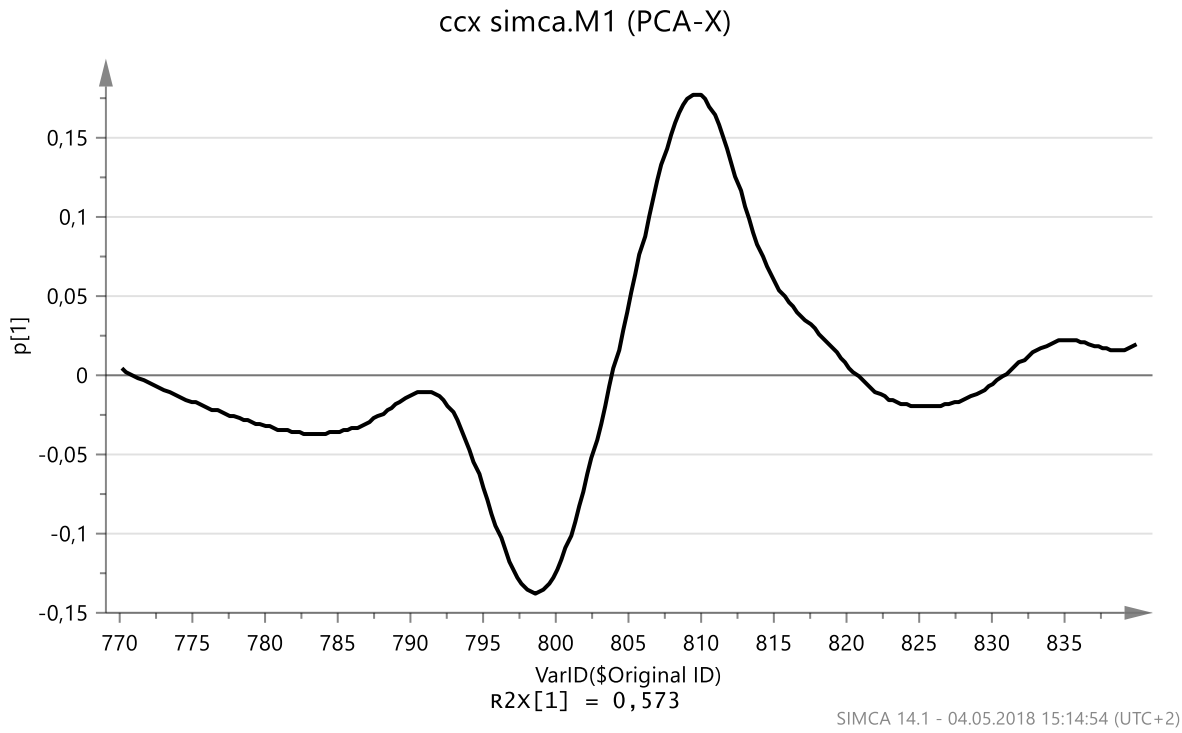

Figure 38 Loadings plot of the first component (PC-1) 57,3% explained variance

The PCA further visualises the Raman data. As seen in Figure 39 all the samples prepared by HME are aligned on the negative side of PC-1 indicating amorphous CCX. The physical mixtures confirm the positive correlation between crystallinity as they contain crystalline CCX. Some samples prepared by VCM also align towards the crystalline side of PC-1. The samples containing 30% and 50% CCX prepared at 120 or 130°C seem to be crystalline while the 50% CCX prepared with VCM at 170°C for 15 minutes seem to be mainly amorphous (Fig 40 & 41). The samples prepared at 170°C can be observed in the top left corner with numbers 57-59.

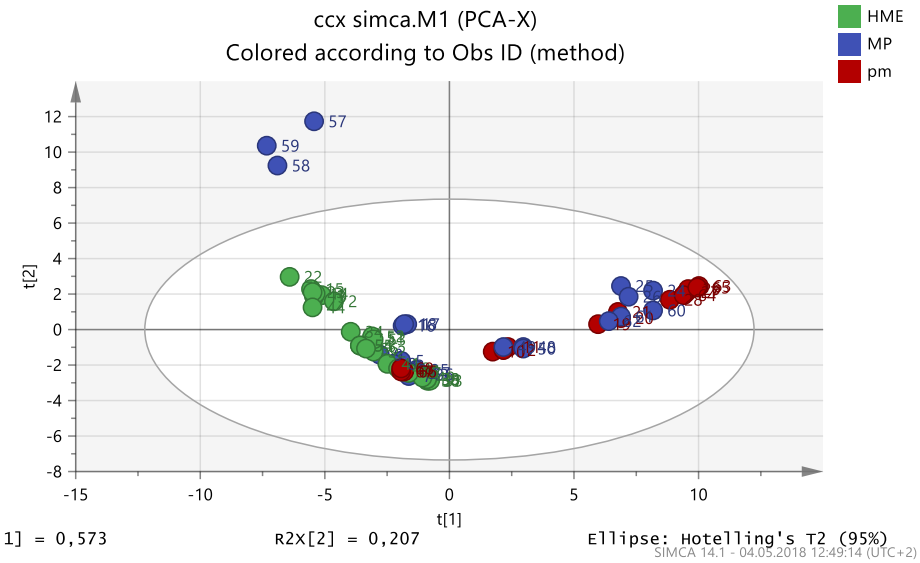

Figure 39 PCA of CCX:Soluplus. Coloured according to manufacturing method. HME (green) MeltPrep (blue) and physical mixtures for reference (red)

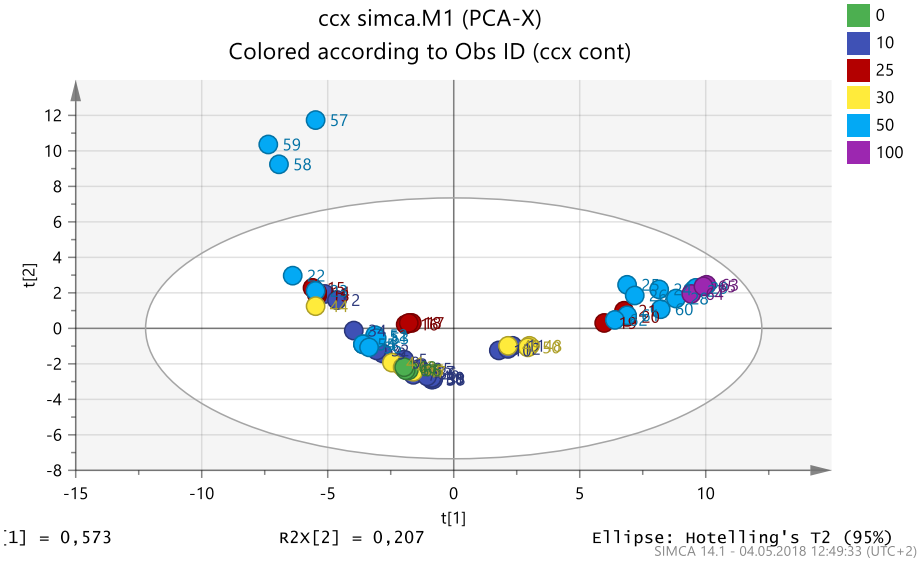

Figure 40 PCA of CCX:Soluplus. Coloured according to CCX content. 10% (blue) 25% (red) 30% (yellow) 50% (teal). 100% crystalline CCX (purple) and Soluplus (green) for reference

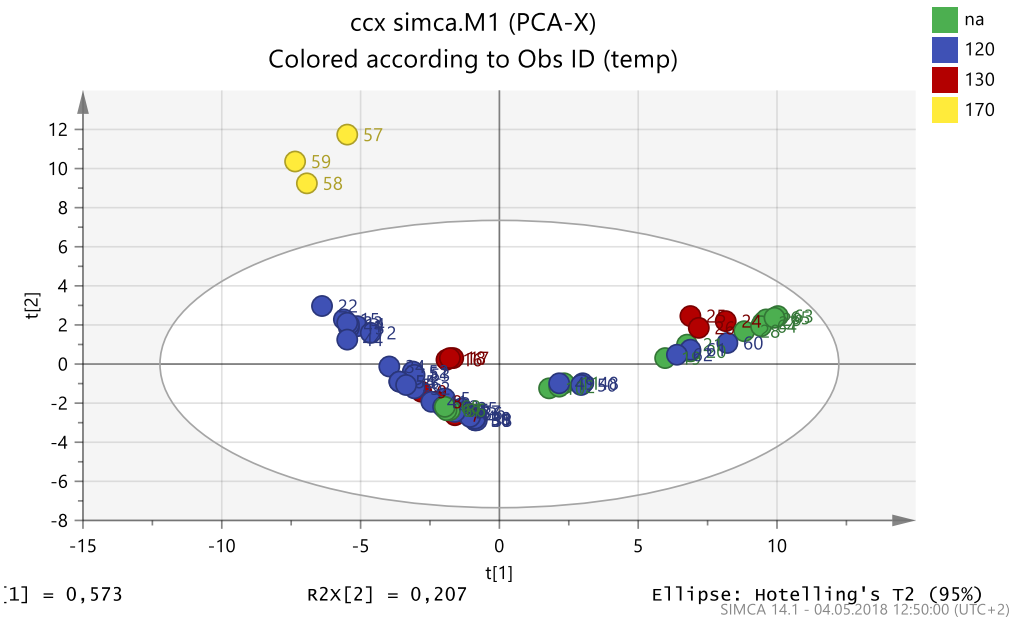

Figure 41 PCA of CCX:Soluplus. Coloured according to process temperature. 120°C (blue) 130°C (red) and 170°C (yellow). Physical mixtures as reference, na (green)

6.5 Rheological properties

Small amplitude oscillatory shear (SAOS) rheology was used to compare solid dispersions prepared by HME and VCM. The effect of recirculation time in the extruder was also evaluated. Rheology was used to assess the plasticizing effect of the model API's in Soluplus, as well as to investigate the solubility of API in Soluplus. The extent of shear thinning of the API-polymer melt in the extruder due to shear forces from the rotating screws was investigated but no correlation was observed between shear thinning and API content. The measured force within the extruder was fluctuating and no conclusive data was obtained. However, the shear forces within the extruder can be expected to contribute to the forming of ASD's in the extruder due to the shear thinning of the melt.

6.5.1 Determination of linear viscoelastic region

The LVR was determined using a strain sweep with increasing oscillation strain on the sample. The LVR for Soluplus range from 0-1.44% oscillation strain (Fig 42) where the polymer structure remains unaltered. When exceeding the LVR the melt structure is destroyed as the molecule chains start to reorganize. A strain of 0.5% was selected for further rheological analyses.

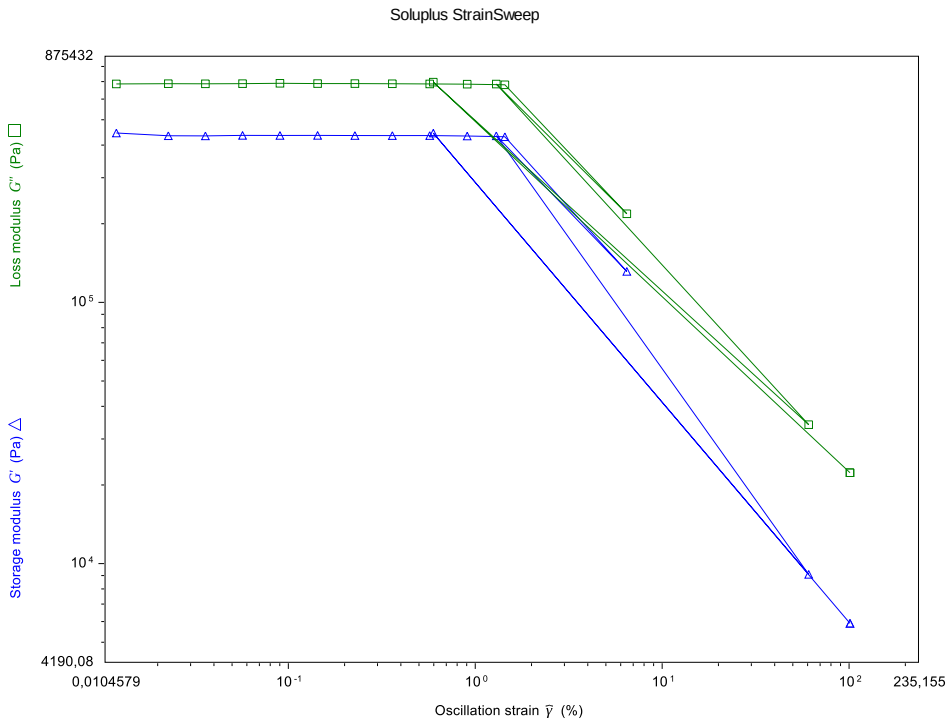

Figure 42 Strain sweep of Soluplus. The LVR can be observed from 0-1.44% where the polymer structure remains unaltered. When exceeding the LVR the melt structure is destroyed as the molecule chains start to reorganize.

SAOS frequency sweeps were run in the LVR at 120°C at a constant strain amplitude γ = 0.5% and decreasing angular frequency from 100 to 0.01 Hz. The complex viscosity of the samples was measured.

6.5.2 Naproxen

The complex viscosity (η*) between the different preparative methods varied considerably especially at the higher drug-loads (Fig 43). The lack of mixing and shear forces in VCM leads to less amorphization and higher crystal content of drug in the mixture, which can be observed as an increased melt viscosity. The difference is especially evident at higher drug loads where

the mixing is critical for forming an ASD. The results also indicate that the extrusion process with a 5-minute recirculation shows lower complex viscosity compared with the extruded samples without recirculation indicating further amorphisation during recirculation within the extruder. However, both extrusion samples show lower viscosity compared to the VCM samples at 50% drug load. The results also show that the dissolved NAP can act as a plasticizer lowering the melt viscosity of the API-polymer mixture.

The results show the effect of the mixing and shear of the screws inside the extruder. Also at higher drug loads by increasing the dwell time inside the extruder by 5 minutes with continuous mixing it seems to further dissolve and disperse the API inside the polymer matrix.

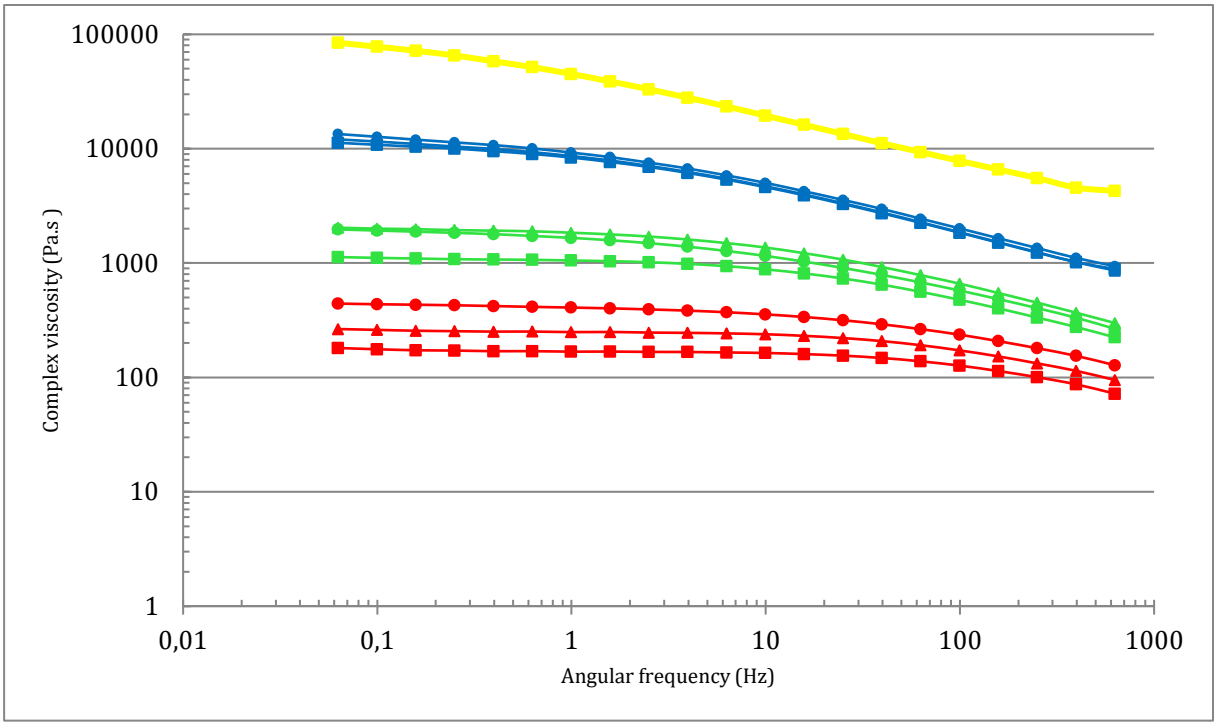

Figure 43 Complex viscosity of NAP-Soluplus solid dispersions. API content 10% (blue) 30% (green) 50% (red). Preparative methods: HME without recirculation (▲), HME with 5 min recirculation time (■) and VCM (●). Soluplus (yellow) for reference

The PLM pictures of the rheological disks prior to the experiments support the findings (Fig 44). It seems at 10% the crystal content is low in all the samples and even VCM alone manages to turn the majority of NAP amorphous. At 30% a much larger difference between the different preparative methods can be seen, as the VCM sample with only MeltPrep® show a much higher crystallinity compared to the extrudates. At 50% NAP content plenty of crystalline NAP can be observed in all three samples. However, the rheological data would indicate that the extruded samples would have a lower crystalline content and a much lower complex viscosity compared

with the MeltPrep® sample. The rheological data also show an increased importance of recirculation time in the extruder allowing for further melting and amorphisation of NAP.

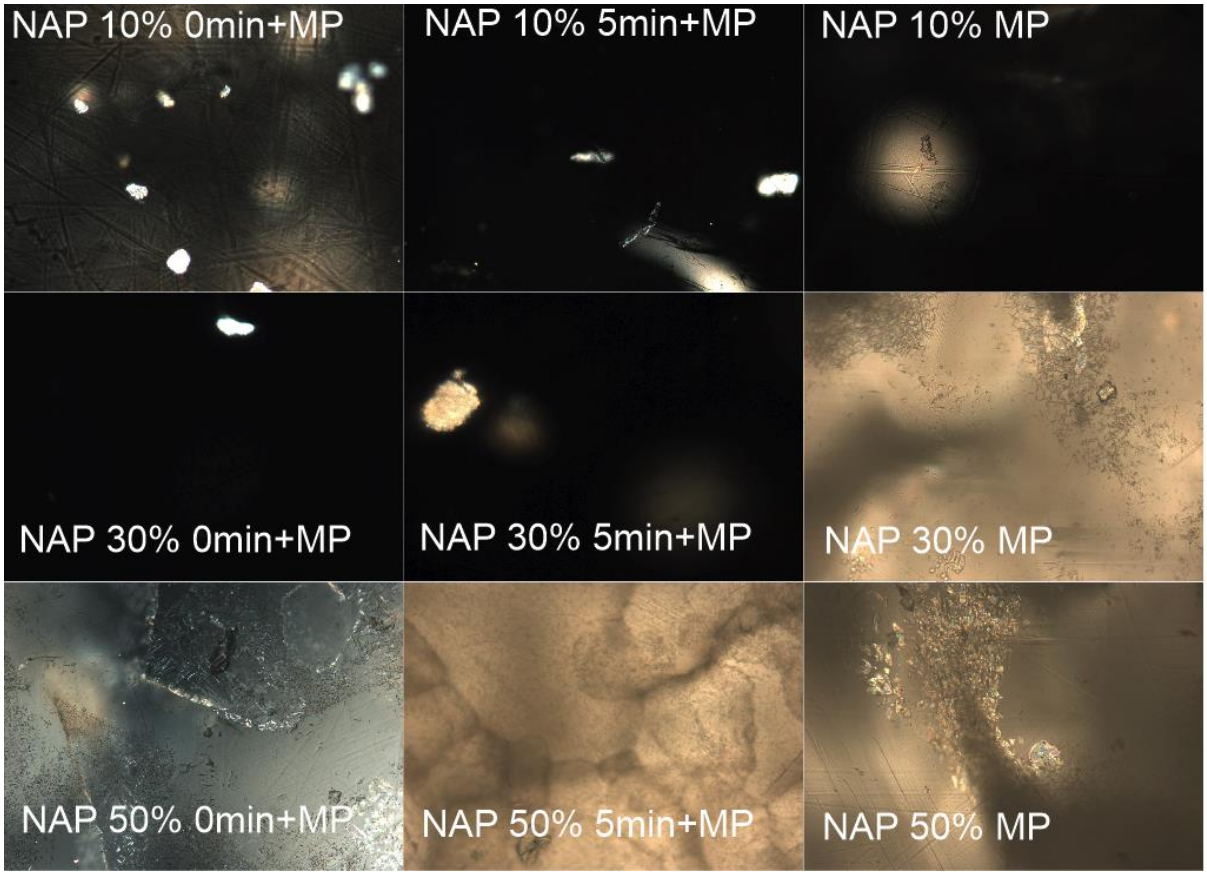

Figure 44 PLM pictures of 25mm disks prepared with MeltPrep® (MP). Left column is from grinded extrudates from HME without recirculation, middle column with 5-minute recirculation within the extruder and right column disks from physical mixtures. Amount of NAP in Soluplus given as percent.

Due to lack of experience in the use of the PLM, the settings between the pictures as well as the magnification of the samples might vary. The lack of scaling for each picture also makes the results shown less quantitative and more speculative in nature. However, it is apparent that some assumptions can be made on basis of the PLM data. To further support the rheological results and PLM data, Raman spectroscopy was used. The Raman data as presented in chapter 6.4.1. suggest that all HME samples and most VCM samples are amorphous. Due to the close proximity of the Raman shifts together with slight overlapping it is unsure how reliable the data is. PLM clearly show crystals on all samples containing 50% NAP. Due to the contradicting nature repeating of samples should be conducted and the crystallinity re-evaluated. What clearly can be concluded is that drug content ant preparative method have an effect on the viscosity of the drug-polymer melt.

6.5.3 Celecoxib

For samples containing CCX the complex viscosity of the prepared VCM disks were higher compared to the disks containing NAP. Some of the samples showed higher viscosity compared with pure Soluplus (Fig 45). This indicates that CCX does not have a significant plasticising effect on the melt in contrast to samples containing NAP, which showed a decrease in viscosity with increased drug load even at drug loads of 50%. The rheological data show a very big difference between the preparative methods of HME and VCM at 50% drug content. This would indicate that the VCM sample contains a much higher crystal content compared to the extruded samples and thus increasing the melt viscosity.

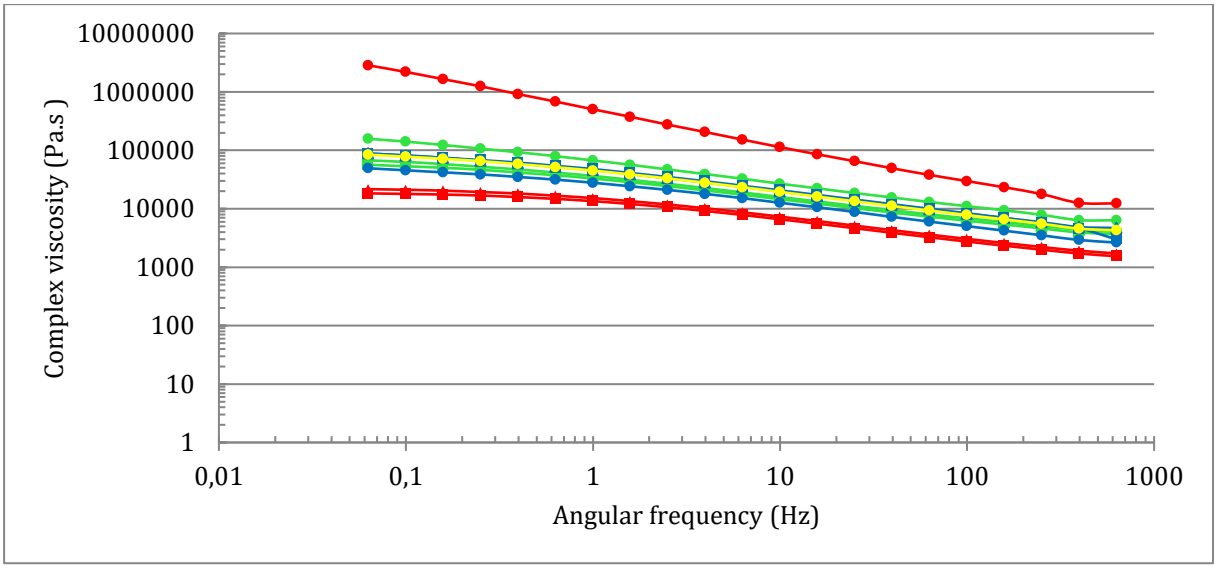

Figure 45 Complex viscosity of CCX-Soluplus solid dispersions. API content 10% (blue) 30% (green) 50% (red). Preparative methods: HME without recirculation (▲), HME with 5 min recirculation time (■) and VCM (●). Soluplus (yellow) for reference

For CCX a significant difference of crystallinity observed using PLM could be seen already at 10% CCX content (Fig 46). The disk prepared from physical mixture using only MeltPrep® showed plenty of crystals while the continuously extruded sample showed a few crystals and the extruded sample with recirculation time within the extruder showed even less or possibly no crystals in the sample disk. The trend continues throughout all of the samples, where the samples prepared by VCM show highest crystallinity, then the non-recirculated extrudates and finally the recirculated extrudates with the lowest crystal content.

Figure 46 PLM pictures of 25mm disks prepared with MeltPrep® (MP). Left column is from grinded extrudates from HME without recirculation, middle column with 5-minute recirculation within the extruder and right column disks from physical mixtures. Amount of CCX in Soluplus given as percent.

The Raman data for CCX presented in chapter 6.4.2. supports the PLM data where both 30% and 50% CCX solid dispersions prepared by VCM show significantly higher crystal content when comparing to the extruded samples. When comparing with the solubility estimation of CCX in Soluplus done using the Flory-Huggins model it is possible that the disks remain highly crystalline in the rheological analysis thus increasing the viscosity of the sample. The 50% sample prepared by VCM show the highest viscosity throughout and it is significantly higher than that of Soluplus alone.

6.5.4 Temperature sweep

Temperature sweeps of disks prepared using VCM at 100°C were performed from 100°C to 180°C to see the effect of temperature on the melt viscosity of the API-polymer mixtures. However the data cannot be relied heavily on due to the runny nature of Soluplus at high temperatures preventing the sample from staying between the geometries and running along the

sides of the lower geometry. This can be observed in the raw data included in the appendix where the storage modulus shows heavy fluctuation. A fast lowering of the viscosity of Soluplus after 150°C can be observed. (Fig 47) For samples containing NAP the inflection happens earlier. The temperature sweeps support the plasticising effect of NAP, but the data are somewhat inconclusive.

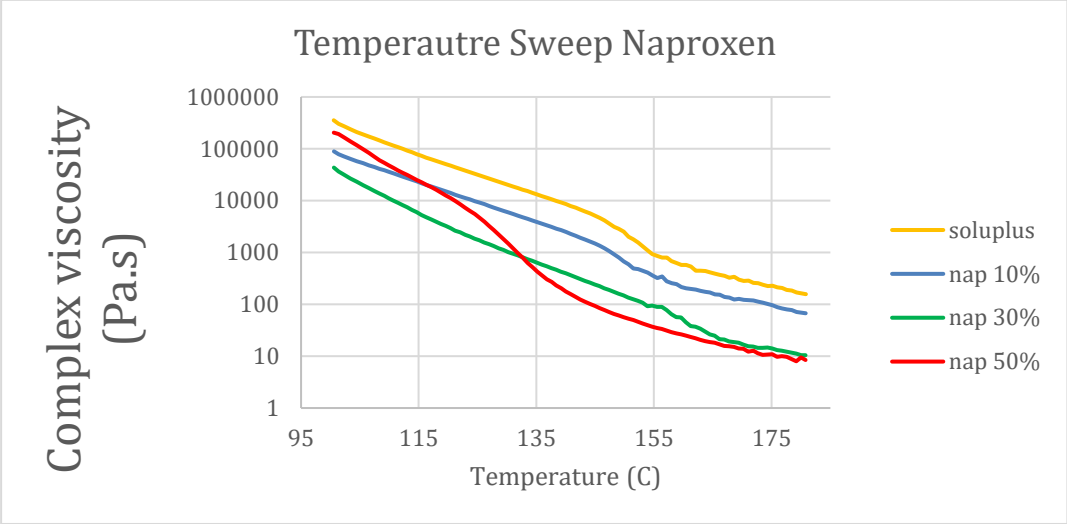

Figure 47 Temperature sweep of NAP:Soluplus mixtures prepared on MeltPrep® at 100°C

For CCX the complex viscosity remained higher than the complex viscosity of Soluplus alone (Fig 48).

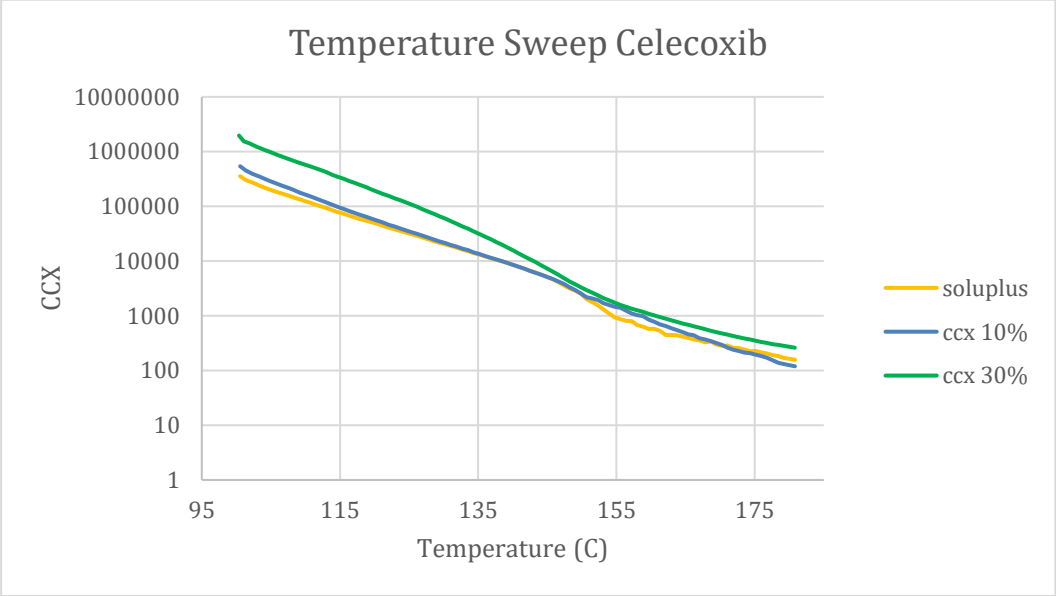

Figure 48 Temperature sweep of CCX:Soluplus mixtures prepared on MeltPrep® at 100°C

6.6 DSC

Modulated temperature DSC was used to determine the T_g of the samples prepared by HME and VCM. The results are presented in Table 6.

Table 6 Tg (inflection) of prepared solid dispersions using reversing heat flow on the DSC. API fraction in Soluplus given as %. Preparative methods Hot-melt extrusion (HME) or VCM using MeltPrep (MP). Phyiscal mixtures and Soluplus standard as reference.

	Tg inflection			Tg inflection	
	Ramp 2	**Ramp 3**		**Ramp 2**	**Ramp 3**
Soluplus std	74,2	78	**Soluplus std**	74,2	78
HME NAP 10% 0min	66,1	62	**HME CCX 10% 0min**	77,6	79,3
HME NAP 10% 5min	66,3	67,5	**HME CCX 10% 5min**	71,9	79,7
HME NAP 30% 0min	54,4	51,8	**HME CCX 30% 0min**	72,2	79,1
HME NAP 30% 5min	52,6	46,5	**HME CCX 30% 5min**	87,1	77,5
HME NAP 50% 0min	44,1	37,9	**HME CCX 50% 0min**	75,4	74,3
HME NAP 50% 5min	37,8	36,8	**HME CCX 50% 5min**	75,5	81
MP NAP 10%	50,9	60	**MP CCX 10%**	75,2	76
MP NAP 30%	39,1	43,2	**MP CCX 30%**	70,6	76,1
MP NAP 50%	34,4	32,7	**Physical mixture CCX 10%**	74,5	84,5
Physical mixture NAP 10%	74,6	70,1	**Physical mixture CCX 30%**	75,1	70,4
Physical mixture NAP 30%	112,7	55	**Physical mixture CCX 50%**	108,1	59,7
Physical mixture NAP 50%	82,3	46,5			

With increased NAP content in the samples the $T_{g\ inflection}$ dropped. This would further confirm that NAP acts as a plasticizer within the mixture lowering the glass transition temperature and the melt viscosity. This was also observed in the behaviour of the drug-polymer melt during extrusion. CCX does not show the same trend in declining $T_{g\ inflection}$.The $T_{g\ inflection}$ remains similar to that of pure Soluplus. It is worth noting that due to the broad glass transition temperature of Soluplus, the determination of Tg was not considered very accurate. As seen in Figure 49 the glass transition temperature can be seen as a broad slope ranging for a broad temperature spectrum with local inflection points. It could be suggested that the Tg should be given as a range instead of a specific value for API-polymer mixtures containing Soluplus. However, in this thesis the determination of glass transition temperature has been chosen as the inflection point of the transition with the steepest curve as seen in Figure 49. This was done by derivatising the observed DSC curve and choosing the signal minimum

in the range of glass-transition. The results are summarised in Table 6 and the corresponding curves can be found in the Appendix

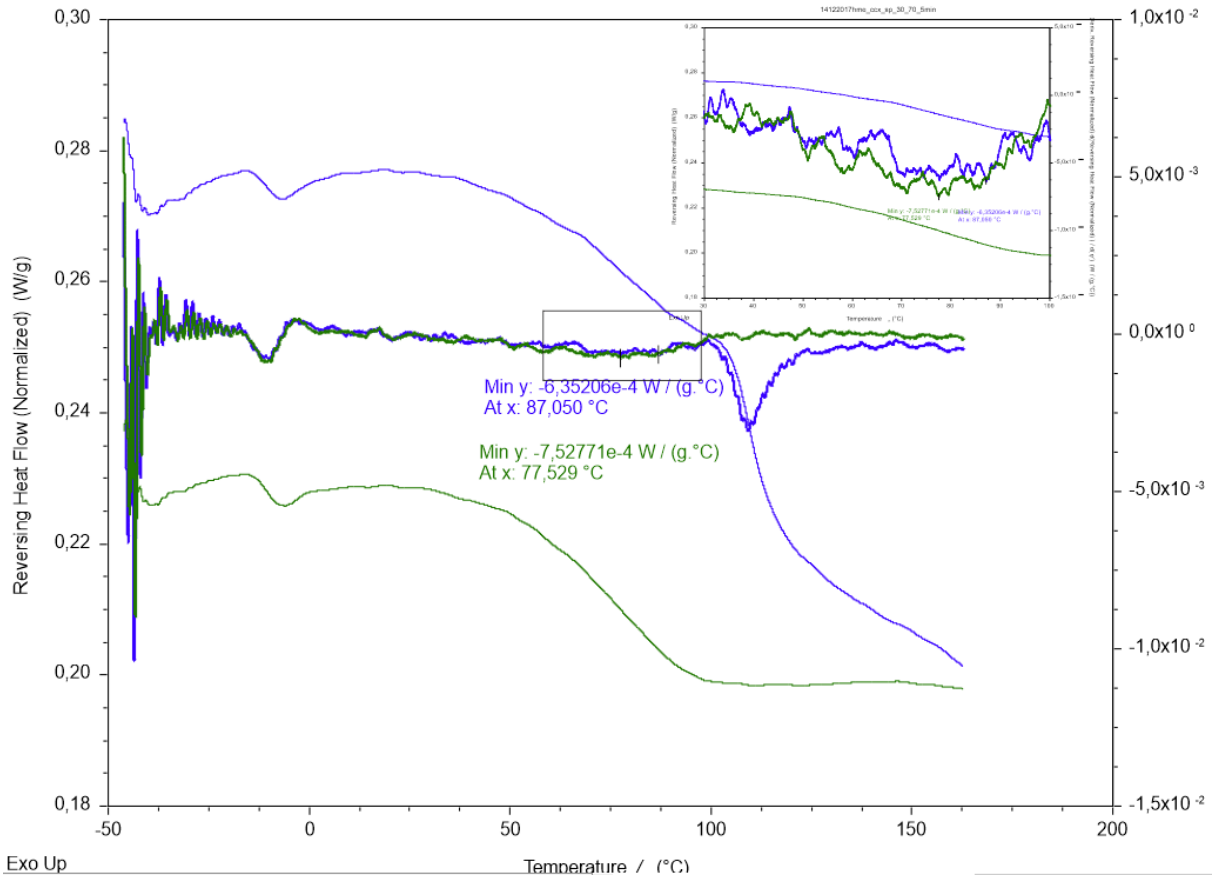

Figure 49 50 Reversing heat flow of Ramp 2 (blue) & Ramp 3 (green) with corresponding derrivatives and Tg inflection point. HME CCX:Soluplus 30:70 5min recirculation

For samples containing CCX the T_g is partially merged with a broad endotherm reaction occurring after the T_g further complicating the estimation of the T_g . This was thought to be the melting of the mixture.

6.7 Influence of storage

Raman and PLM were used to determine the stability of the solid dispersions prepared by HME. The samples were stored at 95% relative humidity at a temperature of 40°C and measured at day 0, day 30 and day 60.

6.7.1 Naproxen

For NAP all samples seemed to be mainly amorphous at day 0 right after the extrusion. The Raman data indicates that already at day 30 of storage, the extrudates containing 50% NAP have turned crystalline. The shift left towards crystalline state can be observed in the SNV enhanced Raman spectra (Fig 51&52). The crystalline peak for NAP can be observed at 1630 cm^{-1}. This occurred for both the non-recirculated one as well as the 5-minute recirculated sample. The spectra indicate that the rest of the extrudates containing NAP have remained mainly amorphous. To further analyse the Raman data PCA was used. By using PCA, a positive correlation between PC-2 and crystallinity of NAP can be observed (Fig 53). The PCA results support the spectral data in grouping 50% NAP samples measured at day 30 and day 60 to the right giving them a positive value while all the other samples group up on the negative side, indicating that NAP is still in its amorphous state within the polymer matrix (Fig 54).

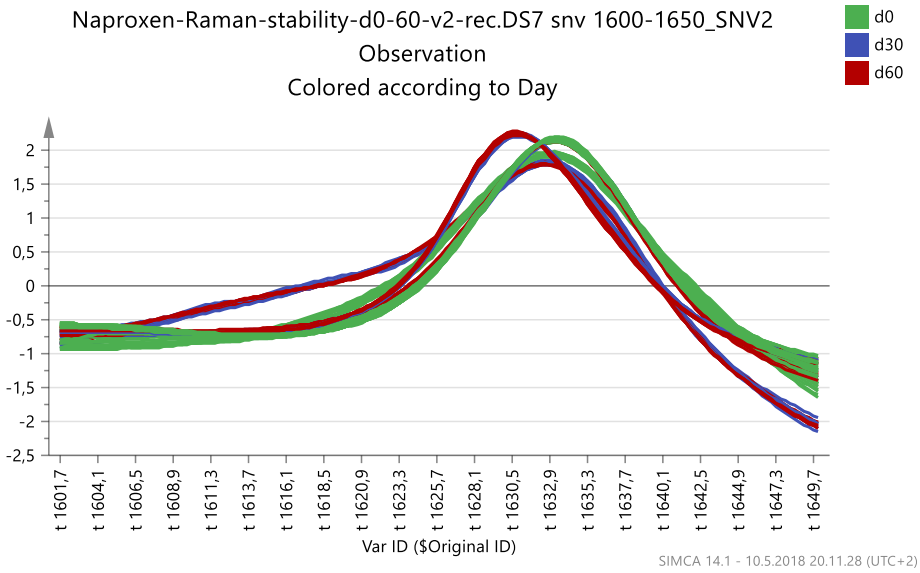

Figure 51 SNV corrected Raman spectra of NAP:Soluplus solid dispersions prepared by HME and stored at 95% relative humidity at 40°C. Coloured by storage day. Day 0 (green), day 30 (blue) and day 60 (red).

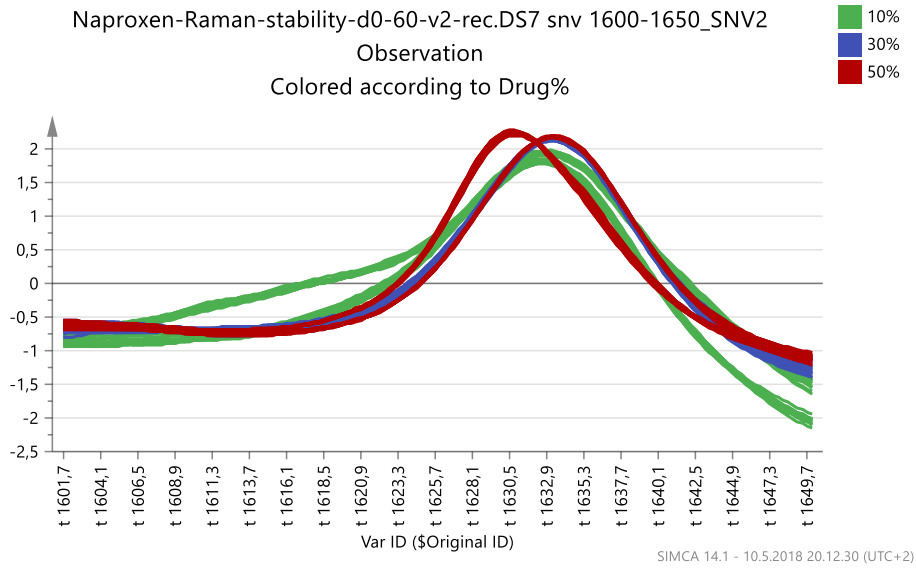

Figure 52 SNV corrected Raman spectra of NAP:Soluplus solid dispersions prepared by HME and stored at 95% relative humidity at 40ºC. Coloured by NAP content. 10% (green) 30%(blue) and 50%(red)

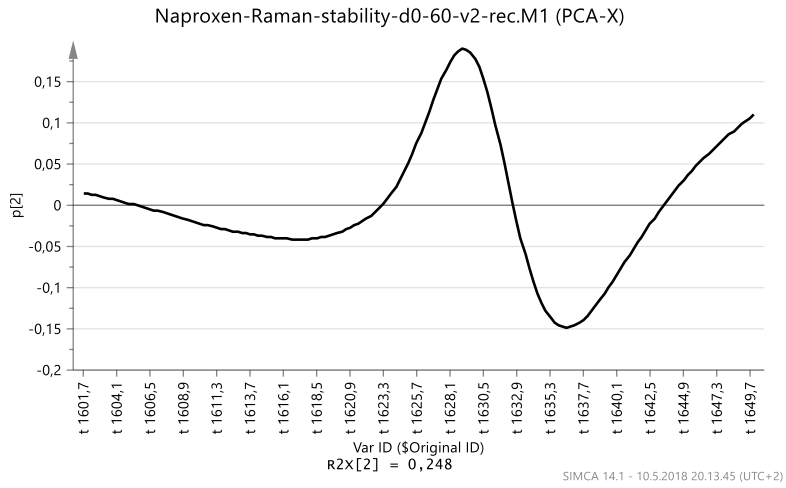

Figure 53 Loadings plot of the second component (PC-2) 24,8% explained variance

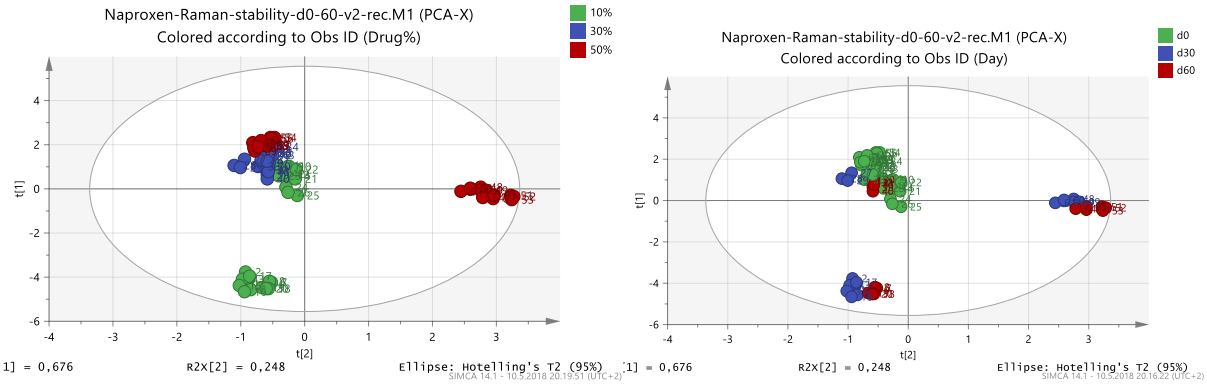

Figure 54 PCA of NAP:Soluplus extrudates during storage. Coloured by drug content (left) and storage time (right)

The results are to some extent supported by the polarized light microscopy. For 10% NAP no crystals are observed at day 0. However, at day 30 and day 60 some possible crystals can be observed (Fig 55) Due to the nature of the extrudates it is difficult to determine if this is only on the surface of the strands that are in direct contact with the moisture in the desiccator. The Raman still indicates that the 10% NAP samples are mainly amorphous. It can also be discussed if the results can be due to sampling error. Raman uses a narrow laser light that only samples a very small portion of the sample, while PLM can be moved over large areas using visual examination. The signal to noise ratio on the Raman data was also low and had to be heavily pre-processed using SNV to obtain the spectra.

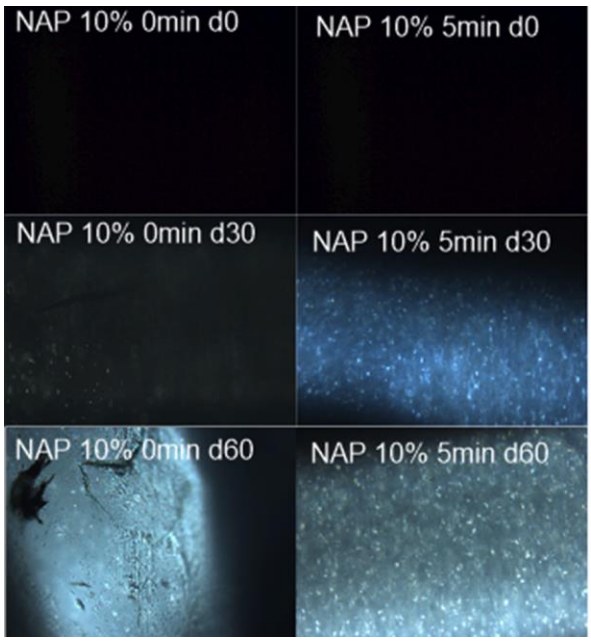

Figure 55 PLM of 10% NAP prepared by HME without recirculation (left) and with a 5-minute recirculation (right) during storage.

For 30% NAP extrudates only a few possible crystals were observed using PLM (Fig 56). The extrudates are also aligned more towards the negative side in the PCA compared to 10% indicating that it is possible the 30% NAP samples were more stable than the 10% and maintained their amorphous state.

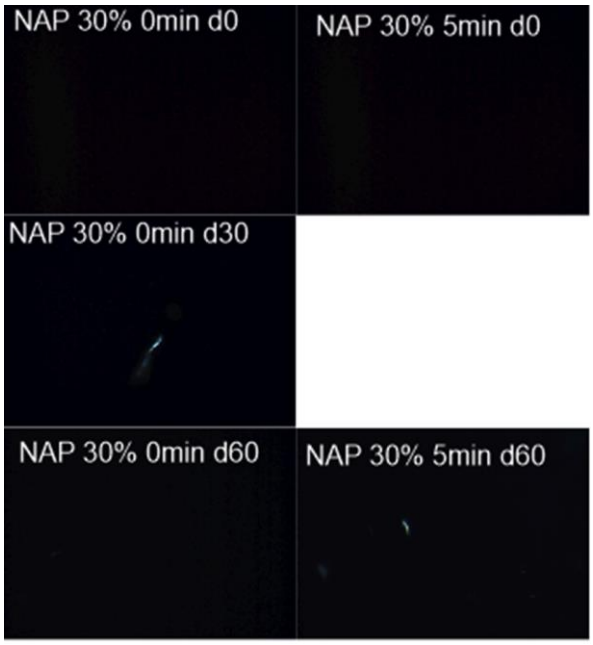

Figure 56 PLM of 30% NAP prepared by HME without recirculation (left) and with a 5-minute recirculation (right) during storage.

The 50% NAP samples show thick, white crystalline structure from day 30 and day 60 for both strands extruded continuously as well as with 5-minute recirculation in the extruder (Fig 57). At day 0 some crystals could be observed in both samples but the samples appeared to be mainly amorphous. At d30 and d60 the PLM picture is take from the edge of the sample in order to get

enough light to get a picture of the thick crystalline structure supporting the Raman data indicating crystallinity for 50% NAP after 30 days of storage.

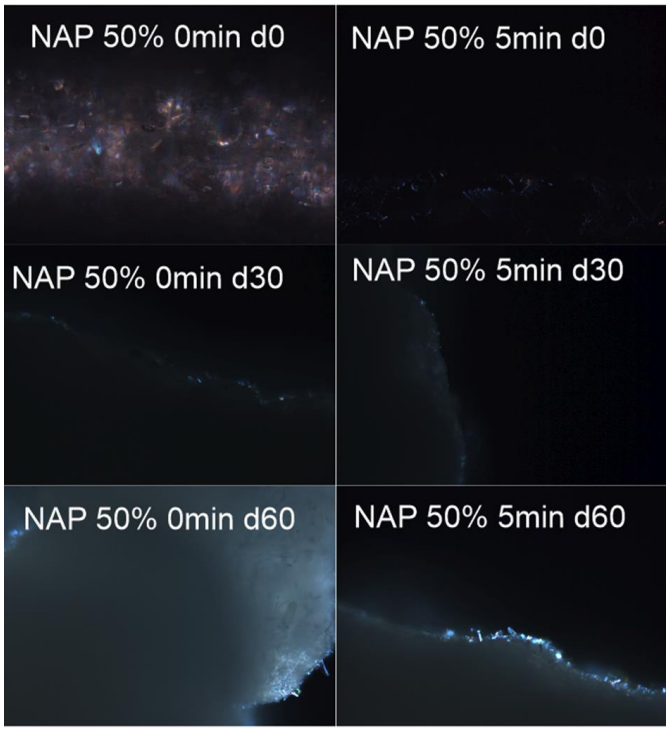

Figure 57 PLM of 50% NAP prepared by HME without recirculation (left) and with a 5-minute recirculation (right) during storage.

6.7.2 Celecoxib

For the extrudates containing CCX the Raman spectra indicates that all samples are in the amorphous state and appear to stay amorphous during the whole storage period of 60 days. (Fig 58).

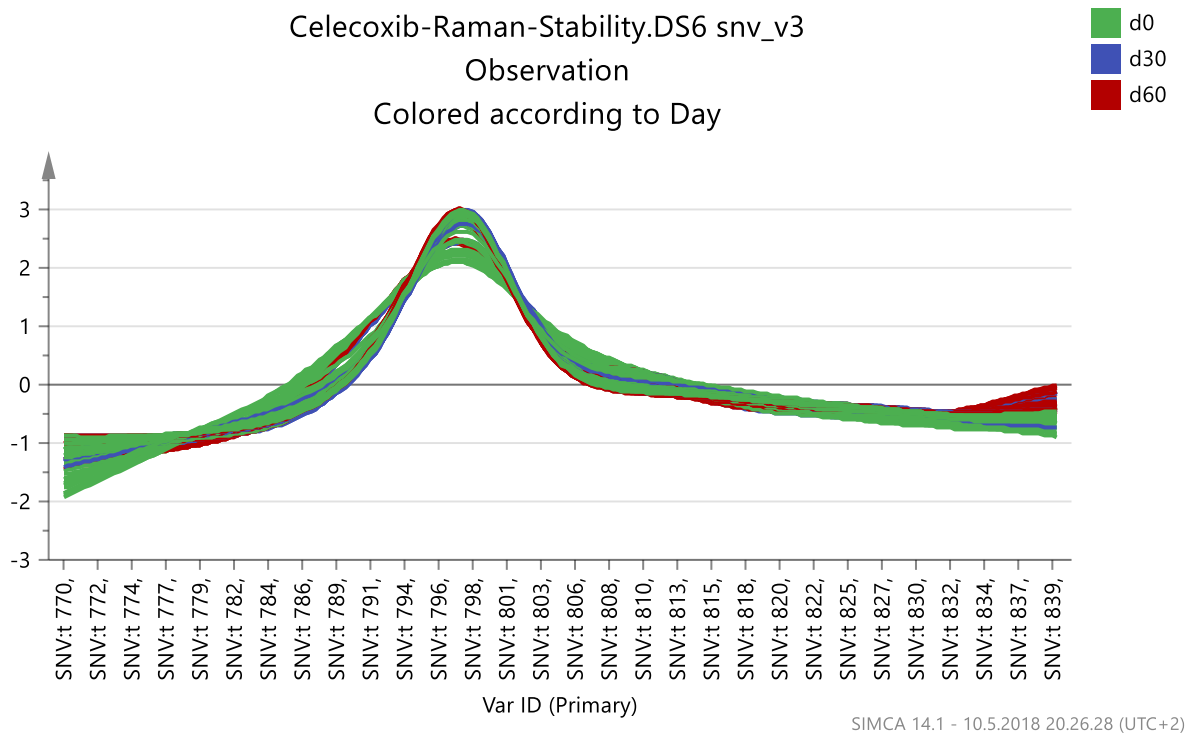

Figure 58 SNV corrected Raman spectra of CCX:Soluplus extrudates during storage

When comparing with the PLM pictures however, some crystals can be observed. The 10% CCX samples only show a few crystals possibly only on the surface of the extruded strands (Fig 59). It is also possible that the crystals are residual dust from grinded extrudates or some other impurities on top of the samples.

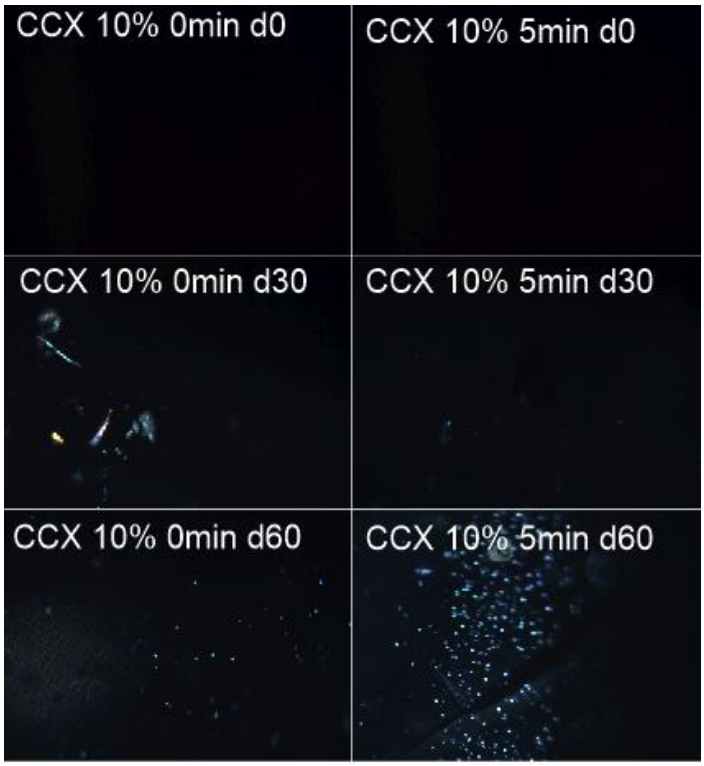

Figure 59 PLM of 10% CCX prepared by HME without recirculation (left) and with a 5-minute recirculation (right) during storage.

The 30% CCX samples indicate more crystals when visually comparing the PLM pictures with the 10% CCX (Fig 60). At day 0 the recirculated sample did not show any crystals while the continuously manufactured (0min) extrudate showed a few crystals. At d 30 more crystals could be observed on the 0min sample. The recirculated sample also showed some that appeared to be crystals within the extrudate. At d60 no visual increase of crystals could not be confirmed.

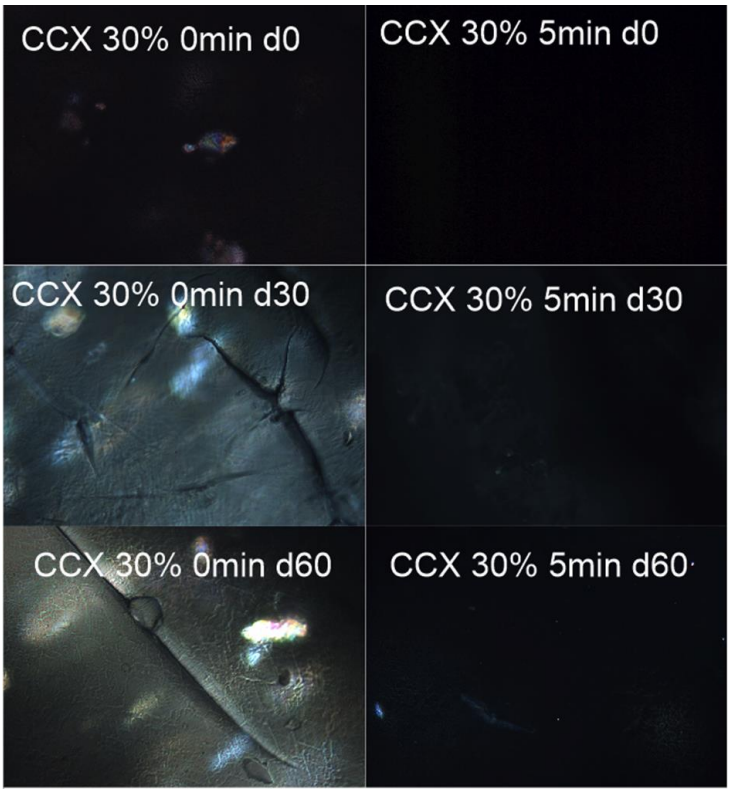

Figure 60 PLM of 30% CCX prepared by HME without recirculation (left) and with a 5-minute recirculation (right) during storage.

For extrudates containing 50% CCX some crystals could be observed from d0 (Fig 61). At d30 a visual increase could be observed. The non-reciculated samples did not properly let the light penetrate the sample due to the opaque nature of the strand. However, some light can be observed indicating possible thick layer of crystals. However, the Raman does not observe crystals in any of the samples. The 5min samples however clearly show some crystals on the PLM. It is difficult to quantify the crystallinity of the samples using PLM and more supporting data is required. It can be discussed whether Raman is a suitable method for CCX:Soluplus extrudates. It would be desirable to combine Raman with other analytical methods such as X-ray powder diffraction and infrared spectroscopy.

A test extrusion of 50% CCX at 130ºC was also done and kept at the same storage conditions. The Raman data of the samples also show amorphous content. By comparing the PLM pictures with the 50% CCX at 120ºC you can still see crystals in the pictures. Whether there are more or less crystalline CCX in the extrudates at different temperatures is difficult to determine due to lack of scaling and microscope settings. It would indicate though that a 5 minute recirculation of the API-polymer melt would increase the amount of amorphous CCX in the samples. As

with the extrudates containing NAP it would be desirable to have more analytical methods available such as XRPD and IR-spectroscopy. These methods were unfortunately not available during this research.

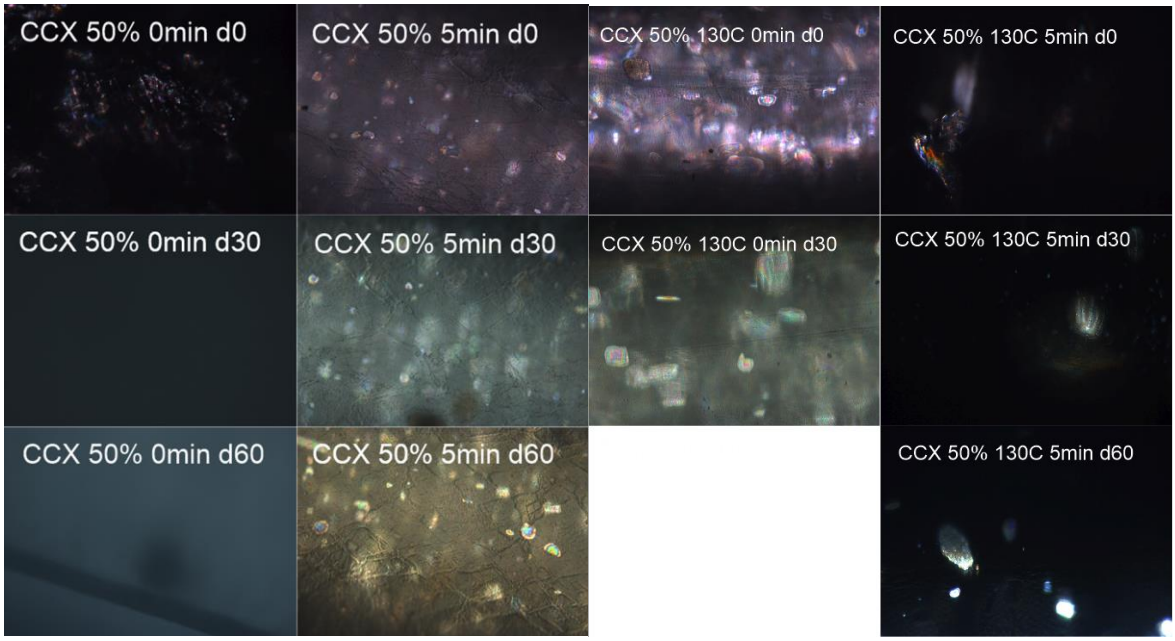

Figure 61 PLM of 50% CCX prepared by HME without recirculation and with a 5-minute recirculation during storage. Process temperature 120°C (two left columns) and 130°C (two right columns)

By comparing the solid dispersions prepared by either HME VCM significant differences can be seen when comparing rheological properties. Especially at higher API contents the VCM fails to produce amorphous API in the same extent as HME. This could be expected due to the lack of mixing and of shear forces in the VCM. The pressure inside the VCM helps to form compact API-polymer disks with little to no air entrapment, however the disks tend to be non-homogenous with drug rich compartments of crystalline API. This was apparent at when using the same process temperature for both methods. When heating the VCM above the melting temperature of the API, a significant increase in amorphisation could be observed. These high process temperatures are not possible in the extruder for the selected API-polymer mixtures due to risk of degradation of the API and the very low viscosity of the melt at higher temperatures due to the nature of Soluplus.

7 Discussion

The solubility determinations using Flory-Huggins correlate with the extrudates produced by HME. The solubility at 120°C was lower for CCX compared with NAP. This can be observed as the extrudates containing CCX are opaque indicating possible crystalline CCX within the polymer matrix. When increasing the extrusion temperature, the extrudate became clearer, indicating that more of the CCX had dissolved into the polymer. The Flory-Huggins data gives a good estimation of solubility and can be used to estimate initial drug load. Choosing parameters within the solubility limits can help in producing stable ASD's. Due to the mixing within the extruder the solubility can be higher compared to the estimation by Flory-Huggins. For VCM the solubility of the API seems to be lower compared to HME which can be explained by the lack of mixing and shear forces in the VCM-tool.

By visually examining the extrudates using PLM, some crystals can be observed in all the prepared VCM disks. Crystals were also observed in all disks prepared from extrudates produced initially by HME. The results are summarized in Table 7. Due to lack of permanent settings and magnification on the PLM, a crude quantification was chosen. The PLM data was categorised as no crystals, some crystals or crystals. The PLM data was compared with Raman data categorized as crystalline or amorphous. For NAP the difference in crystallinity between the HME and VCM is not evident. At 50% NAP content the Raman data shifts somewhat towards crystalline but no conclusive data can be obtained. For CCX a clear difference can be observed already at 10% CCX content where the VCM fails to amorphise CCX in the same extent as HME. The Raman data supports the PLM by indicating crystalline content in both 30% and 50% CCX samples prepared by VCM while all the samples prepared by HME shifts towards amorphous.

Table 7 Summary of PLM and Raman data. Crystallinity of PLM categorised into no crystals – some crystals – crystals. Raman data categorised as amorphous - Crystalline

Sample	PLM	Raman
HME NAP 10% 0min	some crystals	Amorphous
HME NAP 10% 5min	some crystals	Amorphous
MP NAP 10%	some crystals	Amorphous
HME NAP 30% 0min	some crystals	Amorphous
HME NAP 30% 5min	some crystals	Amorphous
MP NAP 30%	crystals	Amorphous
HME NAP 50% 0min	crystals	Amorphous
HME NAP 50% 5min	crystals	Amorphous
MP NAP 50%	crystals	Amorphous/Crystalline
HME CCX 10% 0min	some crystals	Amorphous
HME CCX 10% 5min	no crystals/some crystals	Amorphous
MP CCX 10%	crystals	Amorphous
HME CCX 30% 0min	some crystals	Amorphous
HME CCX 30% 5min	some crystals	Amorphous
MP CCX 30%	crystals	Crystalline
HME CCX 50% 0min	crystals	Amorphous
HME CCX 50% 5min	crystals	Amorphous
MP CCX 50%	crystals	Crystalline

When comparing the PLM and Raman results of the HME extrudates turned into VCM (HME+VCM) disks with the data obtained from the extruded strands during the stability study (Table 8), it would appear as the strands containing either NAP or CCX would have a lower crystalline content comparing with the HME+VCM disks. It can be discussed whether this is due to sampling error and PLM settings, or if some recrystallization of the extrudates occur during the disk preparation using VCM. The flat surface of the disks compared with the round shape of the extrudates can affect both the PLM and Raman data obscuring some of the crystalline content inside the extrudates.

Table 8 Summary of PLM and Raman data for extrudates during stability study. Crystallinity of PLM categorised into no crystals – some crystals – crystals. Raman data categorised as amorphous - Crystalline

	Day 0	Day 0	Day 30	Day 30	Day 60	Day 60
Sample	**PLM**	**Raman**	**PLM**	**Raman**	**PLM**	**Raman**
HME NAP 10% 0min	no crystals	Amorphous	some crystals	Amorphous	some crystals	Amorphous
HME NAP 10% 5min	no crystals	Amorphous	some crystals	Amorphous	some crystals	Amorphous
HME NAP 30% 0min	no crystals	Amorphous	some crystals	Amorphous	no crystals	Amorphous
HME NAP 30% 5min	no crystals	Amorphous	-	Amorphous	some crystals	Amorphous
HME NAP 50% 0min	some crystals	Amorphous	crystals	Crystalline	crystals	Crystalline
HME NAP 50% 5min	some crystals	Amorphous	crystals	Crystalline	crystals	Crystalline
HME CCX 10% 0min	no crystals	Amorphous	some crystals	Amorphous	some crystals	Amorphous
HME CCX 10% 5min	no crystals	Amorphous	some crystals	Amorphous	some crystals	Amorphous
HME CCX 30% 0min	some crystals	Amorphous	crystals	Amorphous	crystals	Amorphous
HME CCX 30% 5min	no crystals	Amorphous	some crystals	Amorphous	some crystals	Amorphous
HME CCX 50% 0min	some crystals	Amorphous	crystals	Amorphous	crystals	Amorphous
HME CCX 50% 5min	some crystals	Amorphous	crystals	Amorphous	crystals	Amorphous
HME CCX 50% 130C 0min	crystals	Amorphous	crystals	Amorphous		Amorphous
HME CCX 50% 130C 5min	some crystals	Amorphous	some crystals	Amorphous	some crystals	Amorphous

From both the PLM and Raman data it would appear that CCX has a lower ability to form ASD's with Soluplus when compared to NAP. The rheological and DSC data also show an increased plasticization and decrease in T_g with increased NAP content even at 50%. The Flory-Huggins estimation also suggest that over 50% of NAP should be able to solubilise in Soluplus.

The rheological and DSC data for CCX does not show the same magnitude of T_g reduction. Especially at higher CCX content, the viscosity and T_g of the melt increases. This can be due to residual CCX crystals increasing the viscosity of the melt

The results support the Flory-Huggins model, suggesting that solubility determination can be used as a first screening method for optimal drug content for the chosen polymer. It can also be used to find the optimal polymer for the chosen API by preparing DSC samples containing different polymers. VCM and rheology can give further information of the melt properties of the API-polymer melt, assisting in choosing optimal process parameters such as temperature. It is worth nothing that VCM, due to lack of shear force and mixing does not have the same amorphising ability as HME. VCM still offers a rapid, cost-effective sample preparation as an initial screening tool before moving towards small scale extrusions.

PLM due to its offline and time-consuming nature is not an optimal analytical tool for continuous manufacturing processes such as HME. PLM still offers great supporting data with a low limit of detection for crystalline residue as the PLM detected crystals when the Raman did not. Still, when optimised Raman can be used as a in-line analytical tool due to its rapid, non-destructive nature. For Raman optimal software containing data-processing is required. Raman. Raman can also be supported by further analytical methods such as X-ray powder diffraction and infrared spectroscopy to give a better understanding of the drug-polymer melts and the interaction of the materials within.

This thesis has investigated the use of VCM as a screening tool for HME. Even though VCM appears to have a lower ability to form ASD's compared to HME, especially at higher drug contents, it can still be a viable tool in initial assessment of melt properties. Based on the data obtained a flow chart was made depicting the process from raw materials to downstream processing (Fig. 62). After chosen API and polymer a solubility determination should be done to determine solubility of the API in the chosen polymer. Based on the results test formulations can be produced using VCM and rheological analysis. The resulting solid dispersions can be analysed for confirming amorphisity. After narrowing down to a few possible formulations, small scale extrusions can be made using lab-scale extrusions to save material costs and time. The required raw materials are small for the initial screening before upscaling, making them economically viable.

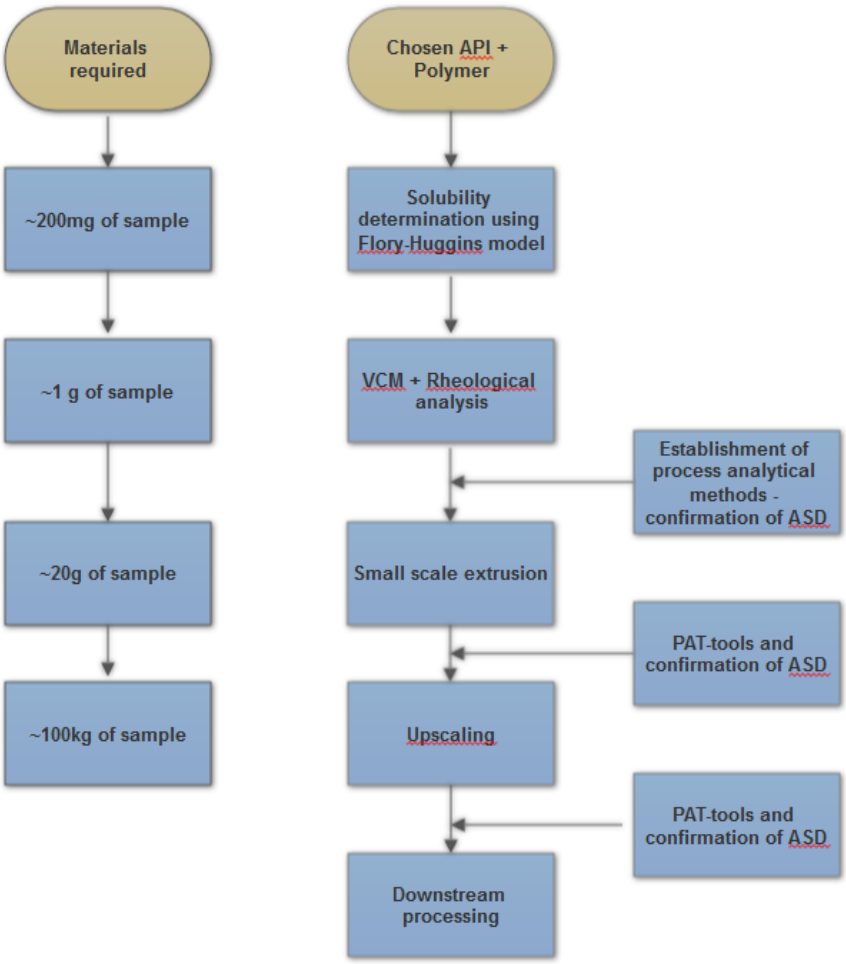

Figure 62 Flow chart containing a suggestion for screening of ASD melt processability and formulation for HME

PAT-tools and offline analytical methods can be used to confirm amorphisity and evaluate processability of the formulation. HME enables relatively easy upscaling and with modulated extruders there is room for customisation. After screening and determination of optimal formulation and process conditions HME can be used to continuously produce ASD's ready for downstream processing for optimal drug formulations.

8 Conclusions

As amorphous solid dispersions can increase the solubility and thus bioavailability of poorly soluble drug, preparation of solid dispersions is an interesting prospect in the pharmaceutical field requiring further research. Hot-melt extrusion appears to be a viable method for preparation of solid dispersions and can produce continuously reducing time and cost of production. Vacuum compression moulding due to its efficient sample preparation can be used as a screening tool for HME formulations. Combined with rheological analysis and solubility estimation an understanding of the drug-polymer melt can be obtained before moving to small-scale extrusions and final formulation optimisation, saving both time and resources. VCM should still be used with consideration when predicting melt properties of melt extrudates, especially at higher drug loads due to the lack of mixing and shear forces having a lower ability to form ASD's compared with HME.

However, with limited analytical methods available, it was difficult to determine the actual crystalline content in the samples. By adding methods such as X-ray powder diffraction and infrared spectroscopy a better understanding of the drug-polymer melts can be made. Solubility estimation using the Flory-Huggins model is also a cost-effective tool for assessing the solubility of the drug in the chosen polymer, as oversaturation can increase the risk of recrystallization within the polymer matrix.

Polarized light microscopy revealed crystals in samples that were determined amorphous by Raman spectroscopy. The limit of detection and optimal analytical tools for process control of ASD's needs to be ensured.

Overall, both solubility estimation and VCM combined with rheological analysis can provide efficient tools when screening for optimal formulation and process parameters for Hot-melt extrusion

8.1 Future perspectives

In this study the extrudates were characterized by a range of analytical techniques. Incorporation of process analytical technology in the manufacturing process would enable for continuous characterization of extrudates in-line produced by continuous manufacturing. Addition of analytical methods such as X-ray powder diffraction and infrared spectroscopy as

supplement to Raman and PLM, could give a further understanding of the characteristics of solid dispersions. An optimal tool with a low limit of detection for crystalline content should be optimized for the desired drug-polymer melts and if possible incorporated in the continuous manufacturing line as a process analytical technology tool.

The effect of process temperature was only briefly touched in this thesis and should be studied more. The appearance of the extrudates of celecoxib changed from opaque to clear by a 10ºC increase of extrusion temperature and should be investigated further. Also, other process parameters including screw speed and melt pressure can influence the extrudates and should be evaluated. PLM indicated that some residual crystals could be found in most of the samples.

Most of the sample extrudates also showed some crystallinity in polarized light microscopy and thus an evaluation of increased recirculation time would be of interest. By looking at the solubility predictions of the model compound naproxen in Soluplus, a higher solubility can be observed than the used ratios in this study. However especially the high drug content extrudates showed some crystallinity initially and already after 30 days of storage at 95% relative humidity seemed to have recrystallized significantly. It would be interesting to see how increase of time in the extruder at elevated temperature and shear forces would affect the extrudates. Liquid chromatography could be used to assess degradation of the materials.

Rheology is utilized a lot in the food industry but has not found widespread interest in the pharmaceutical industry. By using standardized rheological testing methods, it can be possible to predict the processability of compounds and polymers. The use of rheology as a screening tool should further be investigated and further optimization should be done. The many benefits of rheology have been investigated and discussed in literature and should be incorporated more into the pharmaceutical industry.

This thesis has focused on producing solid dispersions and evaluating the melt processability of the drug-polymer melts in order to produce oral dosage forms with increased bioavailability. To ensure improved dissolution and bioavailability, dissolution testing and release studies should be done on the produced extrudates.

For commercial solid dispersions it is of crucial importance that the produced solid dispersions are completely amorphous and no residual crystals of API can be found. For this, reliable analytical tools should be evaluated. The possibility of continuous manufacturing requires continuous analytical tools both in-line and off-line to ensure product quality. Once a suitable

production method for an amorphous solid dispersion has been found, the product and process should be validated and all the important parameters be investigated i.e. temperature, drug content, process speed and settings. This is of course routine for all types of drug manufacturing and is regulated by appropriate authorities.

Works cited

Abdi, H., & Williams, L. J. (2010). Principal component analysis. *Wiley interdisciplinary reviews: computational statistics, 2*(4), 433-459.

Aho, J. (2011). Rheological characterization of polymer melts in shear and extension: measurement reliability and data for practical processing. *Tampere University of Technology*.

Aho, J., Boetker, J. P., Baldursdottir, S., & Rantanen, J. (2015). Rheology as a tool for evaluation of melt processability of innovative dosage forms. *International journal of pharmaceutics, 494*(2), 623-642.

Aho, J., Edinger, M., Botker, J., Baldursdottir, S., & Rantanen, J. (2016). Oscillatory shear rheology in examining the drug-polymer interactions relevant in hot melt extrusion. *Journal of pharmaceutical sciences, 105*(1), 160-167.

Aho, J., Hvidt, S., & Baldursdottir, S. (2016). Rheology in Pharmaceutical Sciences *Analytical Techniques in the Pharmaceutical Sciences* (pp. 719-750): Springer.

Ali, S., Langley, N., Djuric, D., & Kolter, K. (2015). Eye on excipients.

Allesø, M., Chieng, N., Rehder, S., Rantanen, J., Rades, T., & Aaltonen, J. (2009). Enhanced dissolution rate and synchronized release of drugs in binary systems through formulation: Amorphous naproxen–cimetidine mixtures prepared by mechanical activation. *Journal of Controlled Release, 136*(1), 45-53.

Amidon, G. L., Lennernäs, H., Shah, V. P., & Crison, J. R. (1995). A theoretical basis for a biopharmaceutic drug classification: the correlation of in vitro drug product dissolution and in vivo bioavailability. *Pharmaceutical research, 12*(3), 413-420.

Andrews, G. P., Abu‐Diak, O., Kusmanto, F., Hornsby, P., Hui, Z., & Jones, D. S. (2010). Physicochemical characterization and drug‐release properties of celecoxib hot‐melt extruded glass solutions. *Journal of Pharmacy and Pharmacology, 62*(11), 1580-1590.

Baird, J. A., Van Eerdenbrugh, B., & Taylor, L. S. (2010). A classification system to assess the crystallization tendency of organic molecules from undercooled melts. *Journal of pharmaceutical sciences, 99*(9), 3787-3806.

Barnes, H. A., Hutton, J. F., & Walters, K. (1989). *An introduction to rheology* (Vol. 3): Elsevier.

Blaabjerg, L. I., Lindenberg, E., Löbmann, K., Grohganz, H., & Rades, T. (2016). Glass forming ability of amorphous drugs investigated by continuous cooling and isothermal transformation. *Molecular pharmaceutics, 13*(9), 3318-3325.

Breitenbach, J. (2002). Melt extrusion: from process to drug delivery technology. *European Journal of Pharmaceutics and Biopharmaceutics, 54*(2), 107-117.

Brouwers, J., Brewster, M. E., & Augustijns, P. (2009). Supersaturating drug delivery systems: The answer to solubility‐limited oral bioavailability? *Journal of pharmaceutical sciences, 98*(8), 2549-2572.

Burbaum, J. J. (1998). Miniaturization technologies in HTS: how fast, how small, how soon? *Drug discovery today, 3*(7), 313-322.

Byrn, S. R., Zografi, G., & Chen, X. S. (2017). X‐ray Powder Diffraction. *Solid State Properties of Pharmaceutical Materials*, 107-123.

Carlton, R. A. (2011). Polarized light microscopy *Pharmaceutical microscopy* (pp. 7-64): Springer.

Caron, V., Hu, Y., Tajber, L., Erxleben, A., Corrigan, O. I., McArdle, P., & Healy, A. M. (2013). Amorphous solid dispersions of sulfonamide/Soluplus® and sulfonamide/PVP prepared by ball milling. *Aaps Pharmscitech, 14*(1), 464-474.

Chawla, G., Gupta, P., Thilagavathi, R., Chakraborti, A. K., & Bansal, A. K. (2003). Characterization of solid-state forms of celecoxib. *European Journal of Pharmaceutical Sciences, 20*(3), 305-317.

Chokshi, R., & Zia, H. (2010). Hot-melt extrusion technique: a review. *Iranian Journal of Pharmaceutical Research*, 3-16.

Clas, S.-D., Dalton, C. R., & Hancock, B. C. (1999). Differential scanning calorimetry: applications in drug development. *Pharmaceutical science & technology today, 2*(8), 311-320.
Coats, A., & Redfern, J. (1963). Thermogravimetric analysis. A review. *Analyst, 88*(1053), 906-924.
Crowley, M. M., Zhang, F., Koleng, J. J., & McGinity, J. W. (2002). Stability of polyethylene oxide in matrix tablets prepared by hot-melt extrusion. *Biomaterials, 23*(21), 4241-4248.
Crowley, M. M., Zhang, F., Repka, M. A., Thumma, S., Upadhye, S. B., Kumar Battu, S., . . . Martin, C. (2007). Pharmaceutical applications of hot-melt extrusion: part I. *Drug development and industrial pharmacy, 33*(9), 909-926.
Dahan, A., & Hoffman, A. (2008). Rationalizing the selection of oral lipid based drug delivery systems by an in vitro dynamic lipolysis model for improved oral bioavailability of poorly water soluble drugs. *Journal of Controlled Release, 129*(1), 1-10.
Duncan, R. (2011). Polymer therapeutics as nanomedicines: new perspectives. *Current opinion in biotechnology, 22*(4), 492-501.
Edinger, M., Knopp, M. M., Kerdoncuff, H., Rantanen, J., Rades, T., & Löbmann, K. (2018). Quantification of microwave-induced amorphization of celecoxib in PVP tablets using transmission Raman spectroscopy. *European Journal of Pharmaceutical Sciences, 117*, 62-67.
Fakes, M. G., Vakkalagadda, B. J., Qian, F., Desikan, S., Gandhi, R. B., Lai, C., . . . Brown, J. (2009). Enhancement of oral bioavailability of an HIV-attachment inhibitor by nanosizing and amorphous formulation approaches. *International journal of pharmaceutics, 370*(1-2), 167-174.
Ferry, J. D. (1980). *Viscoelastic properties of polymers*: John Wiley & Sons.
Fincher, J. H. (1968). Particle size of drugs and its relationship to absorption and activity. *Journal of pharmaceutical sciences, 57*(11), 1825-1835.
Flory, P. J. (1953). *Principles of polymer chemistry*: Cornell University Press.
Forrest, J., Dalnoki-Veress, K., Stevens, J., & Dutcher, J. (1996). Effect of free surfaces on the glass transition temperature of thin polymer films. *Physical review letters, 77*(10), 2002.
George, H. F., & Qureshi, F. (2013). Newton's Law of Viscosity, Newtonian and Non-Newtonian Fluids *Encyclopedia of Tribology* (pp. 2416-2420): Springer.
Guzman, H. R., Tawa, M., Zhang, Z., Ratanabanangkoon, P., Shaw, P., Gardner, C. R., . . . Remenar, J. F. (2007). Combined use of crystalline salt forms and precipitation inhibitors to improve oral absorption of celecoxib from solid oral formulations. *Journal of pharmaceutical sciences, 96*(10), 2686-2702.
Hancock, B. C., & Parks, M. (2000). What is the true solubility advantage for amorphous pharmaceuticals? *Pharmaceutical research, 17*(4), 397-404.
Huang, J., Wigent, R. J., Bentzley, C. M., & Schwartz, J. B. (2006). Nifedipine solid dispersion in microparticles of ammonio methacrylate copolymer and ethylcellulose binary blend for controlled drug delivery: Effect of drug loading on release kinetics. *International journal of pharmaceutics, 319*(1-2), 44-54.
Huang, Y., & Dai, W.-G. (2014). Fundamental aspects of solid dispersion technology for poorly soluble drugs. *Acta Pharmaceutica Sinica B, 4*(1), 18-25.
Jang, D.-J., Kim, S. T., Lee, K., & Oh, E. (2014). Improved bioavailability and antiasthmatic efficacy of poorly soluble curcumin-solid dispersion granules obtained using fluid bed granulation. *Bio-medical materials and engineering, 24*(1), 413-429.
Jermain, S. V., Brough, C., & Williams III, R. O. (2018). Amorphous solid dispersions and nanocrystal technologies for poorly water-soluble drug delivery–An update. *International journal of pharmaceutics, 535*(1-2), 379-392.
Junghanns, J.-U. A., & Müller, R. H. (2008). Nanocrystal technology, drug delivery and clinical applications. *International journal of nanomedicine, 3*(3), 295.
Kalaiselvan, R., Mohanta, G., Madhusudan, S., Manna, P., & Manavalan, R. (2007). Enhancement of bioavailability and anthelmintic efficacy of albendazole by solid dispersion and cyclodextrin complexation techniques. *Die Pharmazie-An International Journal of Pharmaceutical Sciences, 62*(8), 604-607.
Keck, C. M., & Müller, R. H. (2006). Drug nanocrystals of poorly soluble drugs produced by high pressure homogenisation. *European Journal of Pharmaceutics and Biopharmaceutics, 62*(1), 3-16.

Kliger, D. S., & Lewis, J. W. (2012). *Polarized light in optics and spectroscopy*: Elsevier.
Knopp, M. M., Gannon, N., Porsch, I., Rask, M. B., Olesen, N. E., Langguth, P., . . . Rades, T. (2016). A promising new method to estimate drug-polymer solubility at room temperature. *Journal of pharmaceutical sciences, 105*(9), 2621-2624.
Knopp, M. M., Tajber, L., Tian, Y., Olesen, N. E., Jones, D. S., Kozyra, A., . . . Holm, R. (2015). Comparative study of different methods for the prediction of drug–polymer solubility. *Molecular pharmaceutics, 12*(9), 3408-3419.
Kolter, K., Karl, M., Gryczke, A., & Ludwigshafen am Rhein, B. (2012). *Hot-melt extrusion with BASF pharma polymers: extrusion compendium*: BASF.
Ku, M. S. (2008). Use of the biopharmaceutical classification system in early drug development. *The AAPS journal, 10*(1), 208-212.
Larkin, P. (2017). *Infrared and Raman spectroscopy: principles and spectral interpretation*: Elsevier.
Leizea, I., Mendizabal, A., Alvarez, H., Aguinaga, I., Borro, D., & Sanchez, E. (2017). Real-Time Visual Tracking of Deformable Objects in Robot-Assisted Surgery. *IEEE computer graphics and applications, 37*(1), 56-68.
Leuner, C., & Dressman, J. (2000). Improving drug solubility for oral delivery using solid dispersions. *European Journal of Pharmaceutics and Biopharmaceutics, 50*(1), 47-60.
Liu, X., Zhou, L., & Zhang, F. (2017). Reactive melt extrusion to improve the dissolution performance and physical stability of naproxen amorphous solid dispersions. *Molecular pharmaceutics, 14*(3), 658-673.
Loftsson, T., & Brewster, M. E. (1996). Pharmaceutical applications of cyclodextrins. 1. Drug solubilization and stabilization. *Journal of pharmaceutical sciences, 85*(10), 1017-1025.
Loftsson, T., & Duchêne, D. (2007). Cyclodextrins and their pharmaceutical applications. *International journal of pharmaceutics, 329*(1-2), 1-11.
Löbenberg, R., & Amidon, G. L. (2000). Modern bioavailability, bioequivalence and biopharmaceutics classification system. New scientific approaches to international regulatory standards. *European Journal of Pharmaceutics and Biopharmaceutics, 50*(1), 3-12.
May, C. J., & Henderson, K. O. (2013). Rheological Measurement Methods and Equipment *Encyclopedia of Tribology* (pp. 2777-2787): Springer.
Mayr, L. M., & Bojanic, D. (2009). Novel trends in high-throughput screening. *Current opinion in pharmacology, 9*(5), 580-588.
Miller, J. M., Beig, A., Carr, R. A., Spence, J. K., & Dahan, A. (2012). A win–win solution in oral delivery of lipophilic drugs: supersaturation via amorphous solid dispersions increases apparent solubility without sacrifice of intestinal membrane permeability. *Molecular pharmaceutics, 9*(7), 2009-2016.
Newman, A., Knipp, G., & Zografi, G. (2012). Assessing the performance of amorphous solid dispersions. *Journal of pharmaceutical sciences, 101*(4), 1355-1377.
Noyes, A. A., & Whitney, W. R. (1897). The rate of solution of solid substances in their own solutions. *Journal of the American Chemical Society, 19*(12), 930-934.
Patil, H., Tiwari, R. V., & Repka, M. A. (2016). Hot-melt extrusion: from theory to application in pharmaceutical formulation. *Aaps Pharmscitech, 17*(1), 20-42.
Paudel, A., Worku, Z. A., Meeus, J., Guns, S., & Van den Mooter, G. (2013). Manufacturing of solid dispersions of poorly water soluble drugs by spray drying: formulation and process considerations. *International journal of pharmaceutics, 453*(1), 253-284.
Paulson, S. K., Vaughn, M. B., Jessen, S. M., Lawal, Y., Gresk, C. J., Yan, B., . . . Karim, A. (2001). Pharmacokinetics of celecoxib after oral administration in dogs and humans: effect of food and site of absorption. *Journal of Pharmacology and Experimental Therapeutics, 297*(2), 638-645.
Repka, M. A., Gerding, T. G., Repka, S. L., & McGinity, J. W. (1999). Influence of plasticizers and drugs on the physical-mechanical properties of hydroxypropylcellulose films prepared by hot melt extrusion. *Drug development and industrial pharmacy, 25*(5), 625-633.
Rudin, A. (1998). *Elements of Polymer Science & Engineering: An Introductory Text and Reference for Engineers and Chemists*: Elsevier.
Ruiz-Garcia, A., Bermejo, M., Moss, A., & Casabo, V. G. (2008). Pharmacokinetics in drug discovery. *Journal of pharmaceutical sciences, 97*(2), 654-690.

Saerens, L., Dierickx, L., Lenain, B., Vervaet, C., Remon, J. P., & De Beer, T. (2011). Raman spectroscopy for the in-line polymer–drug quantification and solid state characterization during a pharmaceutical hot-melt extrusion process. *European journal of Pharmaceutics and Biopharmaceutics, 77*(1), 158-163.
Satchi-Fainaro, R., & Duncan, R. (2006). *Polymer therapeutics I: polymers as drugs, conjugates and gene delivery systems* (Vol. 192): Springer Science & Business Media.
Schaber, S. D., Gerogiorgis, D. I., Ramachandran, R., Evans, J. M., Barton, P. I., & Trout, B. L. (2011). Economic analysis of integrated continuous and batch pharmaceutical manufacturing: a case study. *Industrial & Engineering Chemistry Research, 50*(17), 10083-10092.
Shaji, J., & Patole, V. (2008). Protein and peptide drug delivery: oral approaches. *Indian journal of pharmaceutical sciences, 70*(3), 269.
Singh, A., & Van den Mooter, G. (2016). Spray drying formulation of amorphous solid dispersions. *Advanced drug delivery reviews, 100*, 27-50.
Singh, A., Worku, Z. A., & Van den Mooter, G. (2011). Oral formulation strategies to improve solubility of poorly water-soluble drugs. *Expert opinion on drug delivery, 8*(10), 1361-1378.
Smith, E., & Dent, G. (2013). *Modern Raman spectroscopy: a practical approach*: John Wiley & Sons.
Ta, L. E., & Dionne, R. A. (2004). Treatment of painful temporomandibular joints with a cyclooxygenase-2 inhibitor: a randomized placebo-controlled comparison of celecoxib to naproxen. *Pain, 111*(1-2), 13-21.
Takagi, T., Ramachandran, C., Bermejo, M., Yamashita, S., Yu, L. X., & Amidon, G. L. (2006). A provisional biopharmaceutical classification of the top 200 oral drug products in the United States, Great Britain, Spain, and Japan. *Molecular pharmaceutics, 3*(6), 631-643.
Treffer, D., Troiss, A., & Khinast, J. (2015). A novel tool to standardize rheology testing of molten polymers for pharmaceutical applications. *International journal of pharmaceutics, 495*(1), 474-481.
Tsinman, O., Tsinman, K., & Shaukat, A. (2015). Excipient update-Soluplus®: An understanding of supersaturation from amorphous solid dispersions. *Drug Dev. Deliv*.
Tung, N. T., Park, C. W., Oh, T. o., Kim, J. Y., Ha, J. M., Rhee, Y. S., & Park, E. S. (2011). Formulation of solid dispersion of rebamipide evaluated in a rat model for improved bioavailability and efficacy. *Journal of Pharmacy and Pharmacology, 63*(12), 1539-1547.
Wahl, P. R., Treffer, D., Mohr, S., Roblegg, E., Koscher, G., & Khinast, J. G. (2013). Inline monitoring and a PAT strategy for pharmaceutical hot melt extrusion. *International journal of pharmaceutics, 455*(1-2), 159-168.
Vasanthavada, M., Tong, W.-Q. T., Joshi, Y., & Kislalioglu, M. S. (2005). Phase behavior of amorphous molecular dispersions II: Role of hydrogen bonding in solid solubility and phase separation kinetics. *Pharmaceutical research, 22*(3), 440-448.
Vasconcelos, T., Sarmento, B., & Costa, P. (2007). Solid dispersions as strategy to improve oral bioavailability of poor water soluble drugs. *Drug discovery today, 12*(23), 1068-1075.
Wilson, M., Williams, M. A., Jones, D. S., & Andrews, G. P. (2012). Hot-melt extrusion technology and pharmaceutical application. *Therapeutic delivery, 3*(6), 787-797.
Wolman, M., & Kasten, F. (1986). Polarized light microscopy in the study of the molecular structure of collagen and reticulin. *Histochemistry, 85*(1), 41-49.
Yoshioka, M., Hancock, B. C., & Zografi, G. (1995). Inhibition of indomethacin crystallization in poly (vinylpyrrolidone) coprecipitates. *Journal of pharmaceutical sciences, 84*(8), 983-986.
Yu, L. (2001). Amorphous pharmaceutical solids: preparation, characterization and stabilization. *Advanced drug delivery reviews, 48*(1), 27-42.

Appendix

A.1 TGA

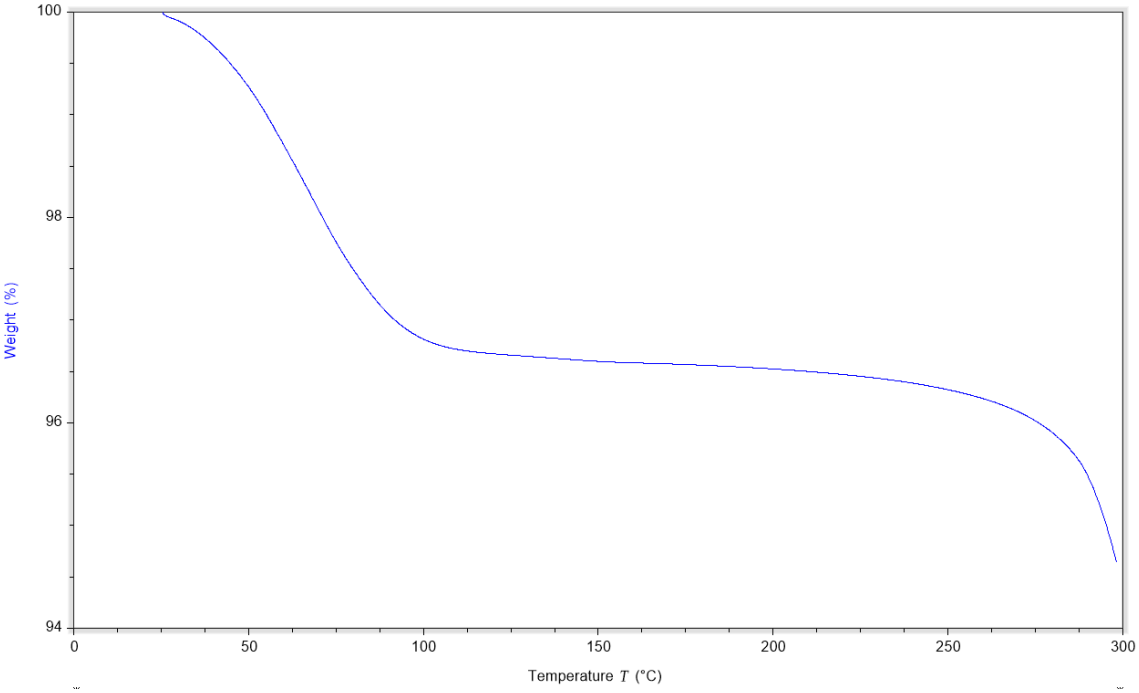

Figure 63 TGA Soluplus

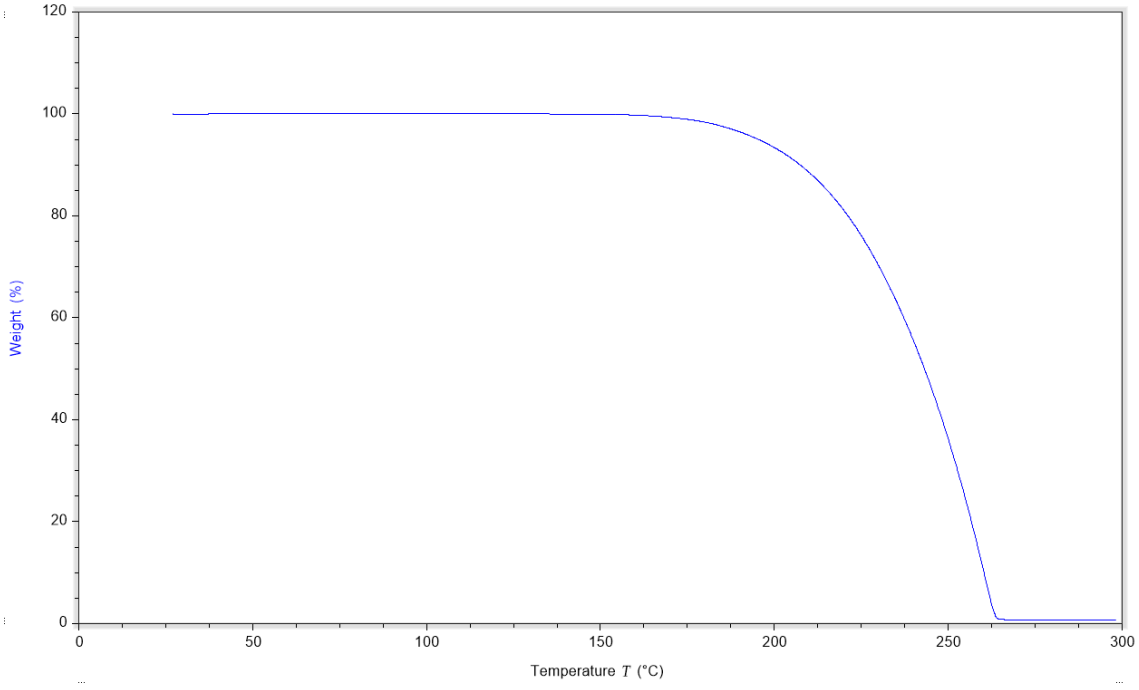

Figure 64 TGA NAP

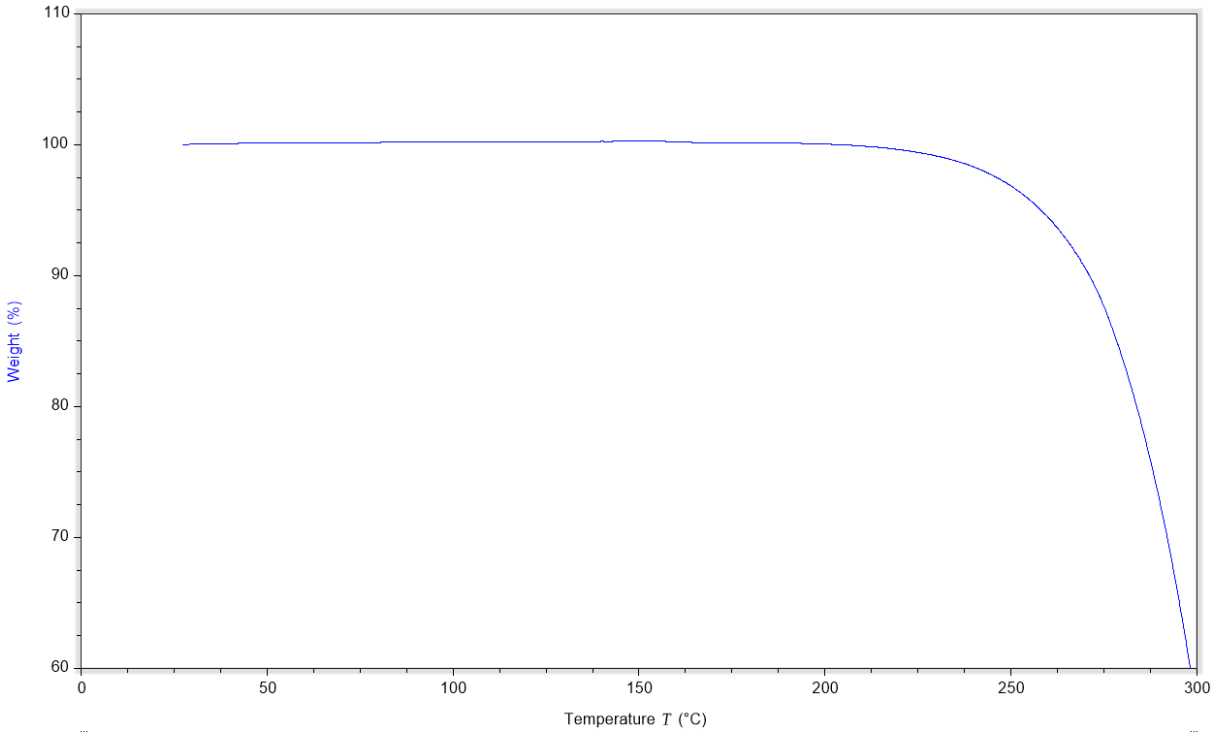

Figure 65 TGA CCX

A.2 DSC

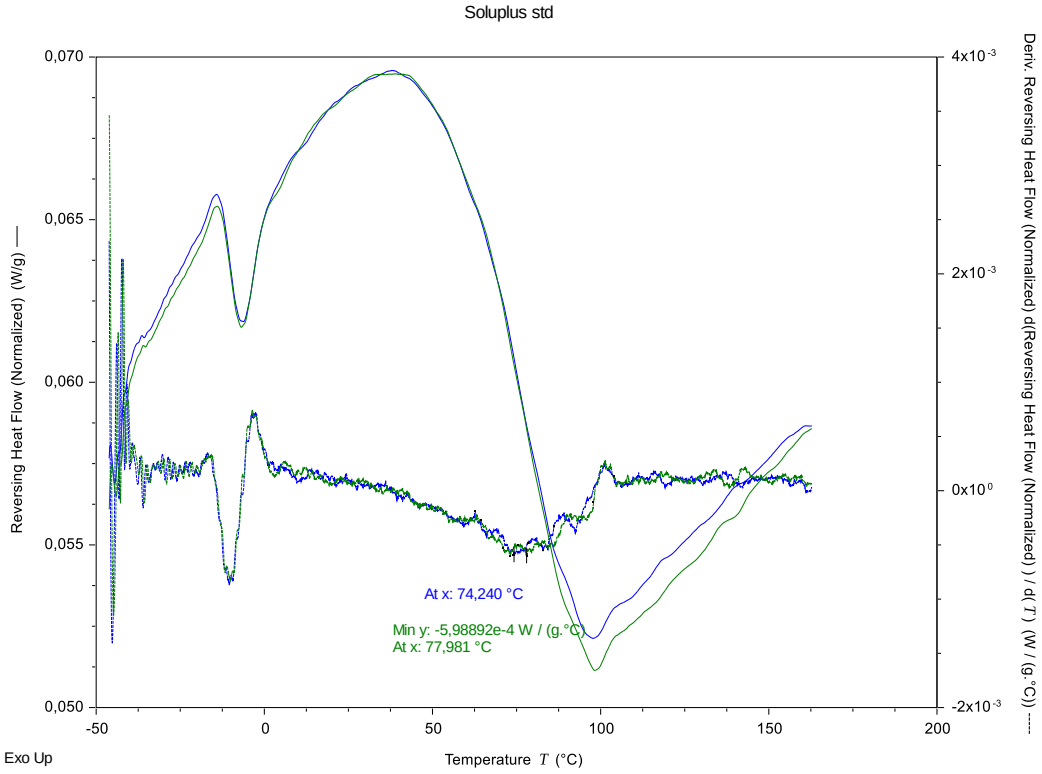

Figure 66 Reversing heat flow of Ramp 2 (blue) & Ramp 3 (green) with corresponding derrivatives and Tg inflection point. Soluplus standard

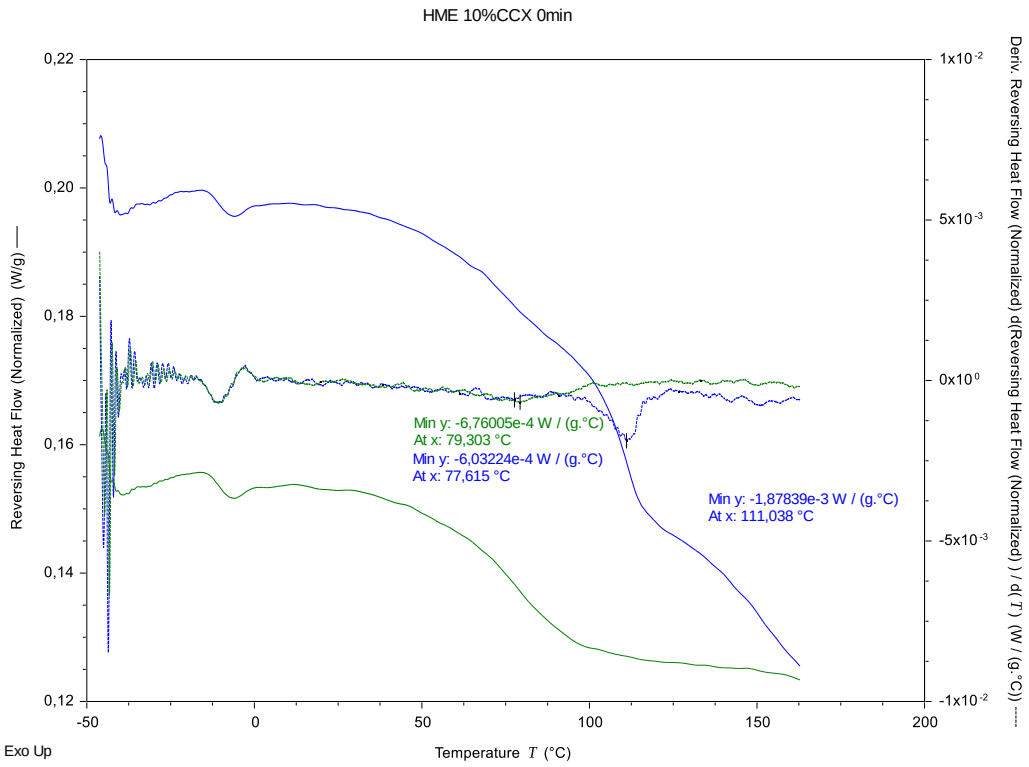

Figure 67 Reversing heat flow of Ramp 2 (blue) & Ramp 3 (green) with corresponding derrivatives and Tg inflection point. HME CCX:Soluplus 10:90 0min recirculation

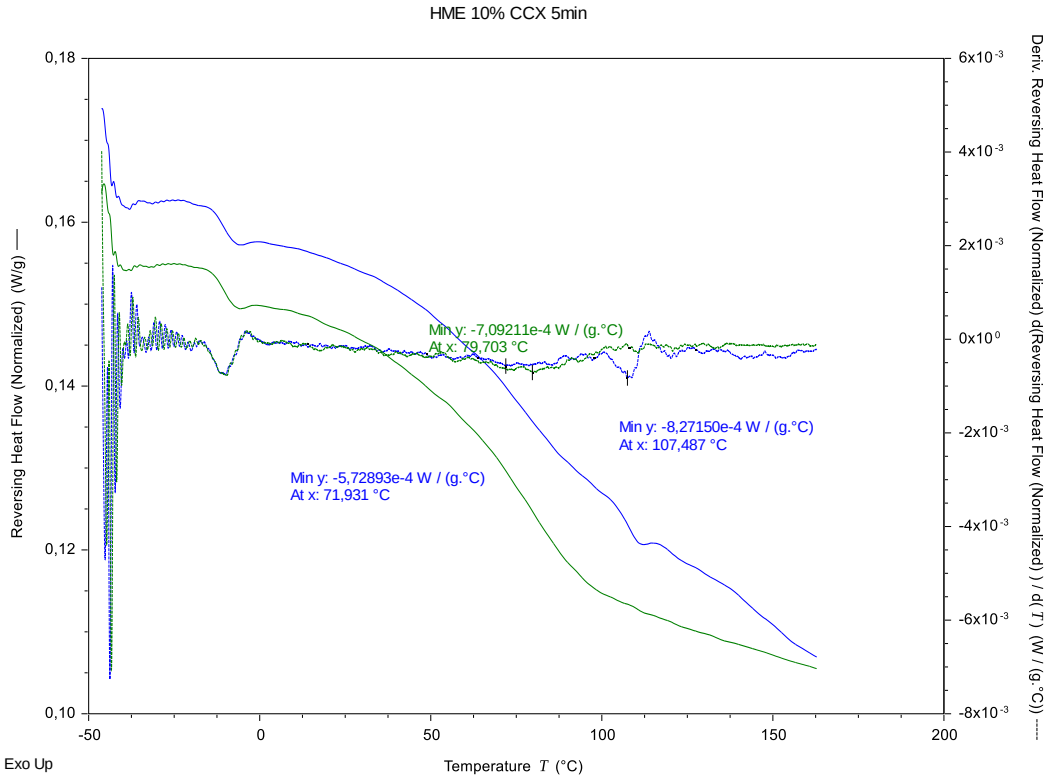

Figure 68 Reversing heat flow of Ramp 2 (blue) & Ramp 3 (green) with corresponding derrivatives and Tg inflection point. HME CCX:Soluplus 10:90 5min recirculation

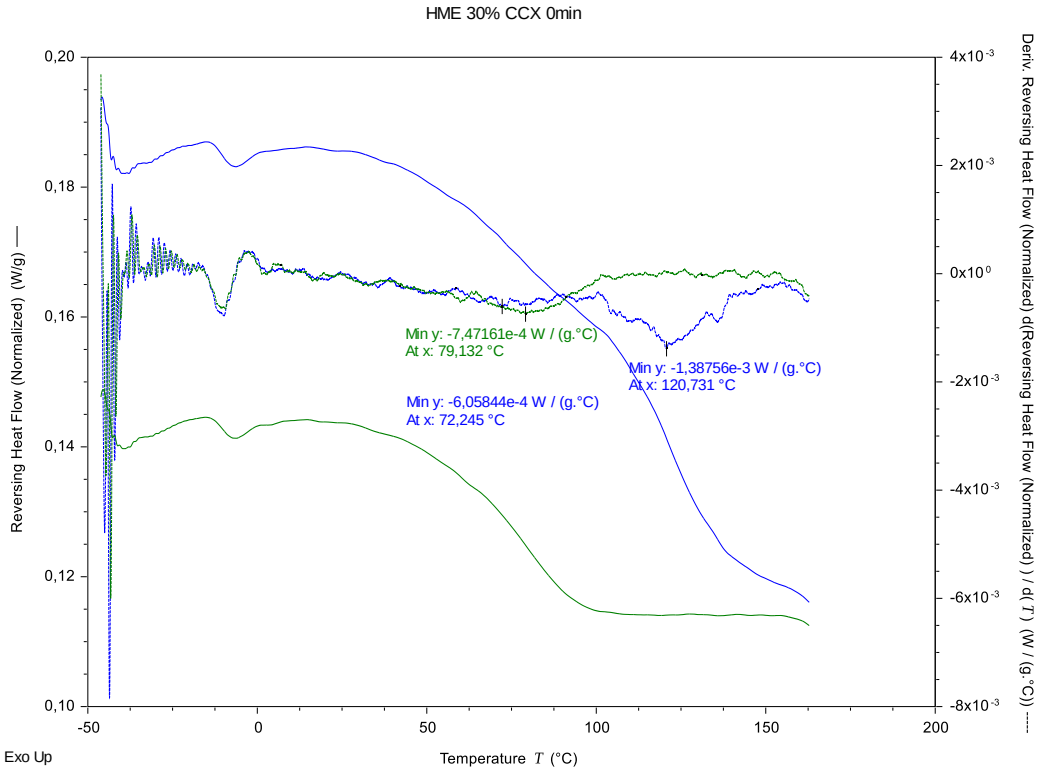

Figure 69 Reversing heat flow of Ramp 2 (blue) & Ramp 3 (green) with corresponding derrivatives and Tg inflection point. HME CCX:Soluplus 30:70 0min recirculation

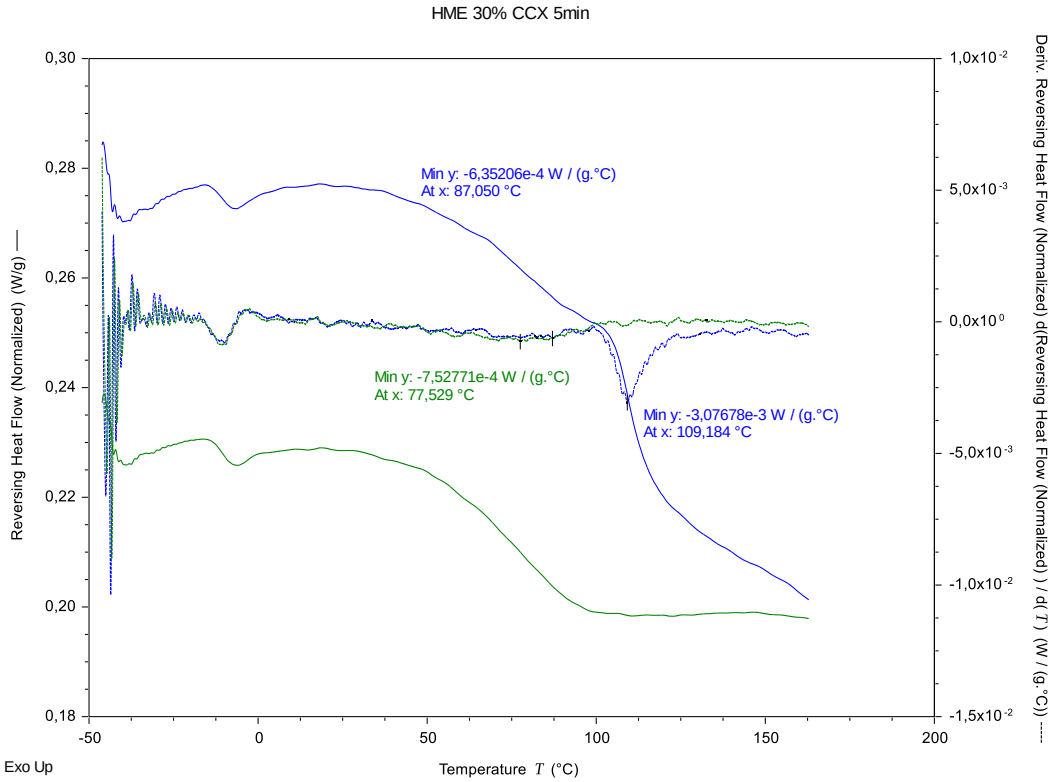

Figure 70 Reversing heat flow of Ramp 2 (blue) & Ramp 3 (green) with corresponding derrivatives and Tg inflection point. HME CCX:Soluplus 30:70 5min recirculation

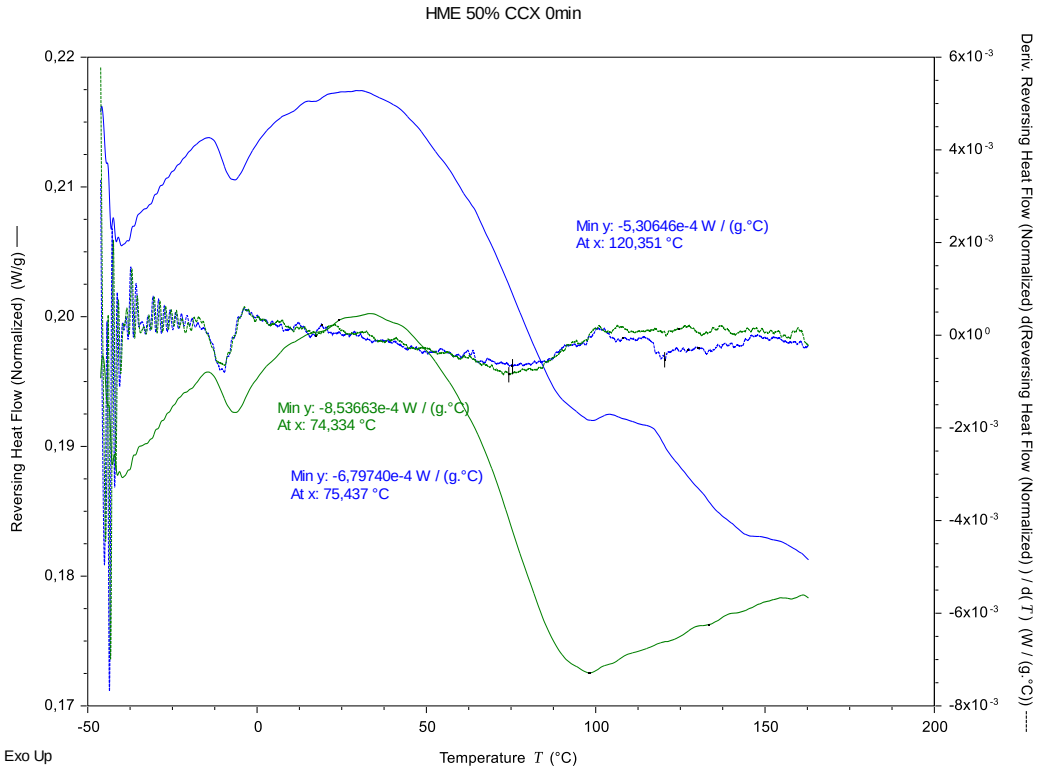

Figure 71 Reversing heat flow of Ramp 2 (blue) & Ramp 3 (green) with corresponding derrivatives and Tg inflection point. HME CCX:Soluplus 50:50 0min recirculation

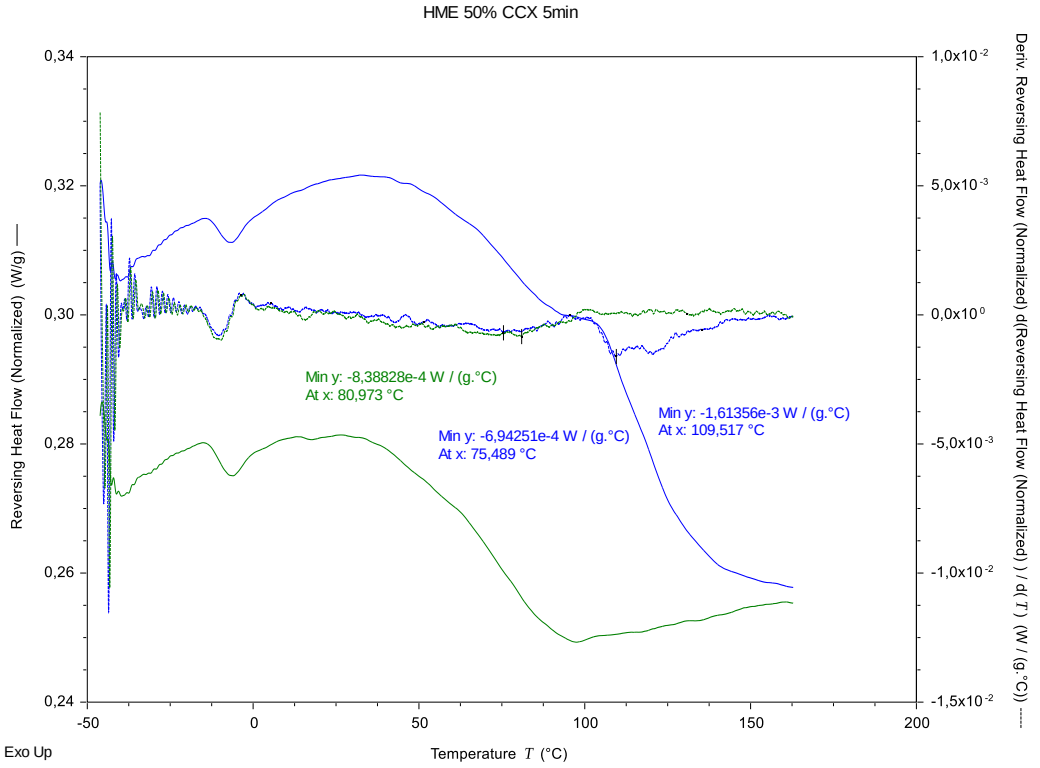

Figure 72 Reversing heat flow of Ramp 2 (blue) & Ramp 3 (green) with corresponding derrivatives and Tg inflection point. HME CCX:Soluplus 50:50 5min recirculation

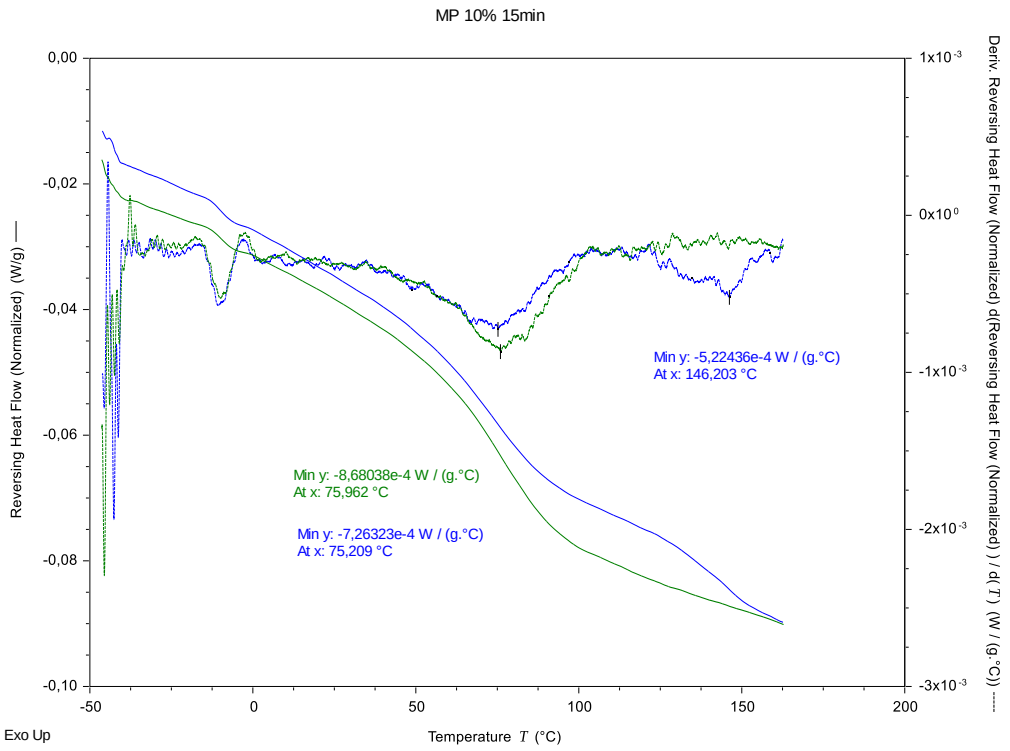

Figure 73 Reversing heat flow of Ramp 2 (blue) & Ramp 3 (green) with corresponding derrivatives and Tg inflection point. MeltPrep CCX:Soluplus 10:90 15min recirculation

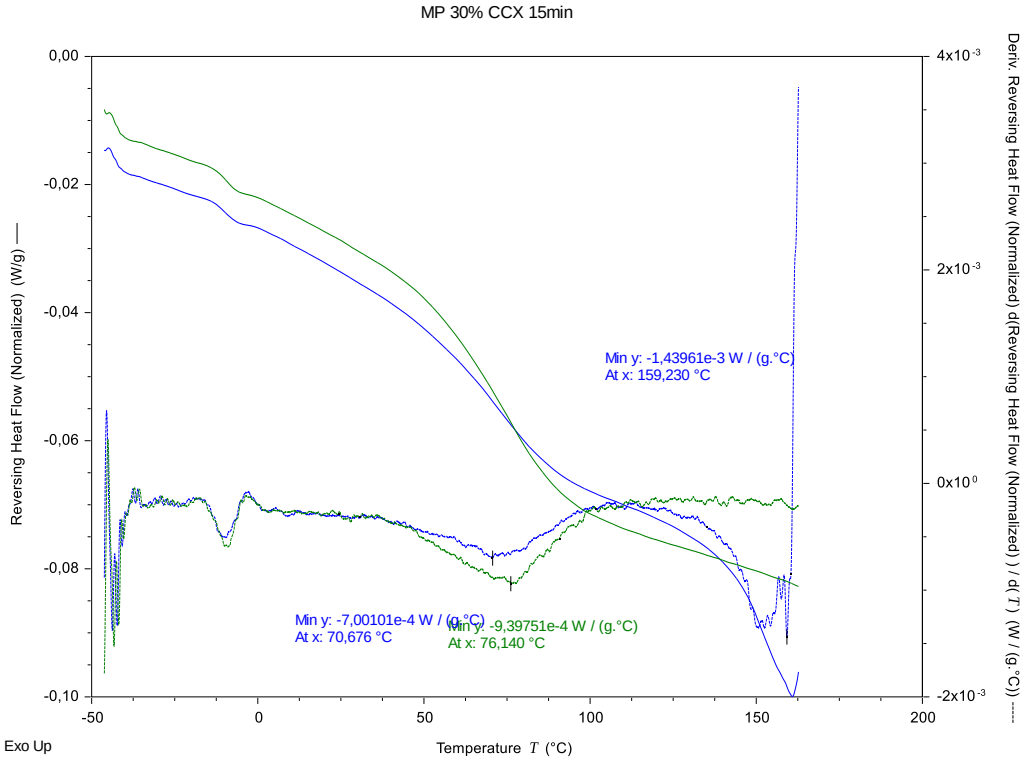

Figure 74 Reversing heat flow of Ramp 2 (blue) & Ramp 3 (green) with corresponding derrivatives and Tg inflection point. MeltPrep CCX:Soluplus 30:70 15min recirculation

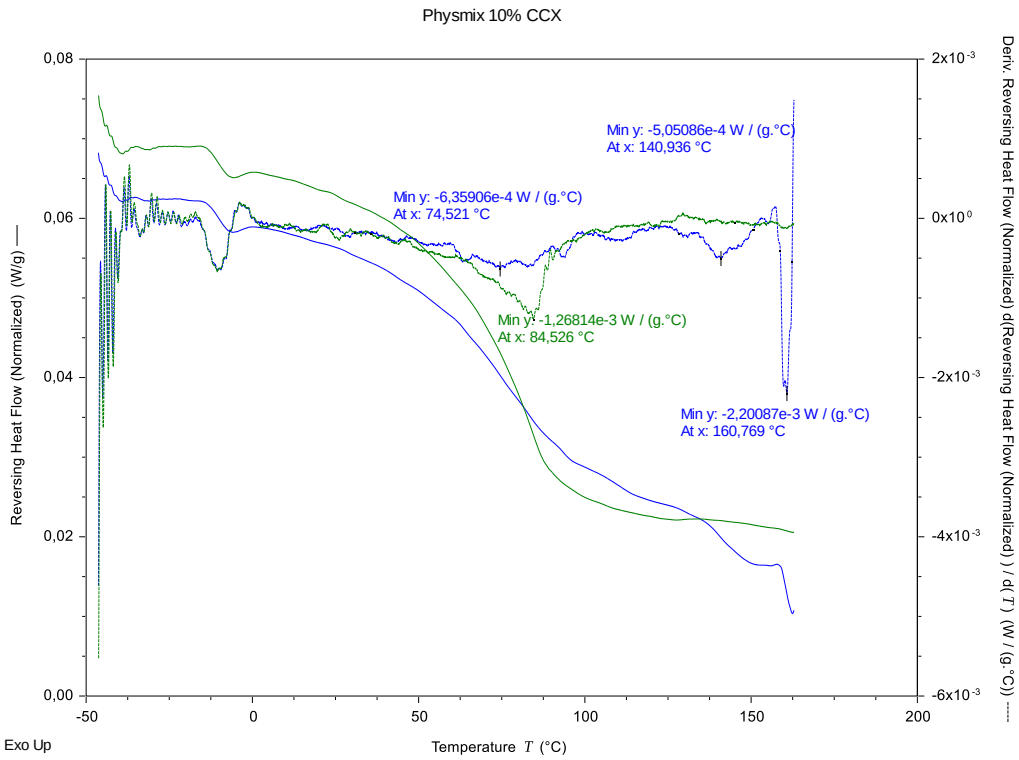

Figure 75 Reversing heat flow of Ramp 2 (blue) & Ramp 3 (green) with corresponding derrivatives and Tg inflection point. Physical mixture of raw materials CCX:Soluplus 10:90

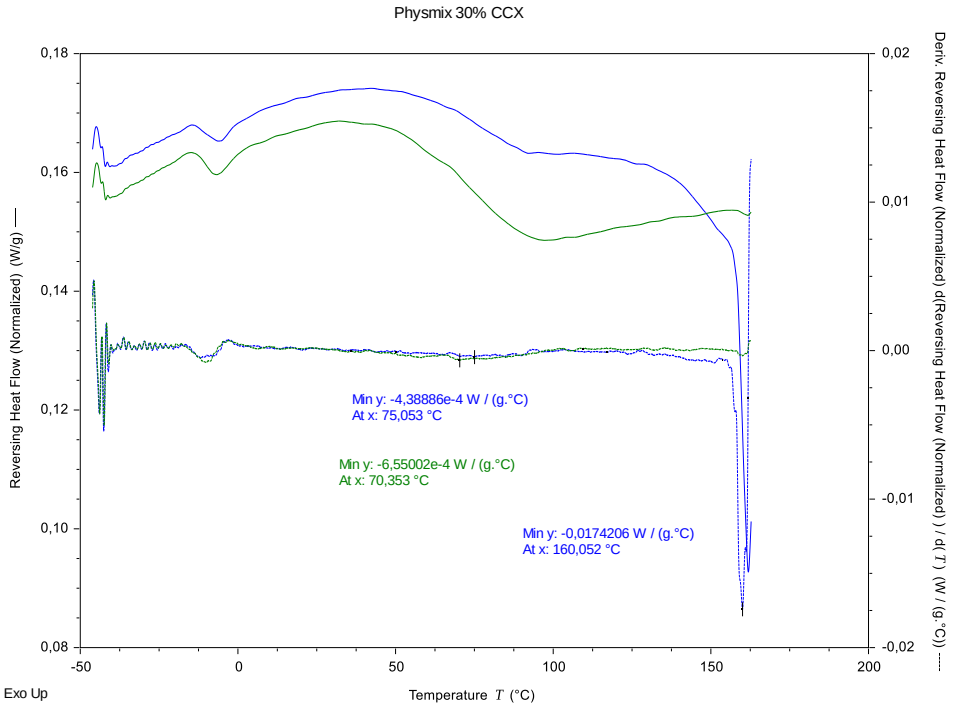

Figure 76 Reversing heat flow of Ramp 2 (blue) & Ramp 3 (green) with corresponding derrivatives and Tg inflection point. Physical mixture of raw materials CCX:Soluplus 30:70

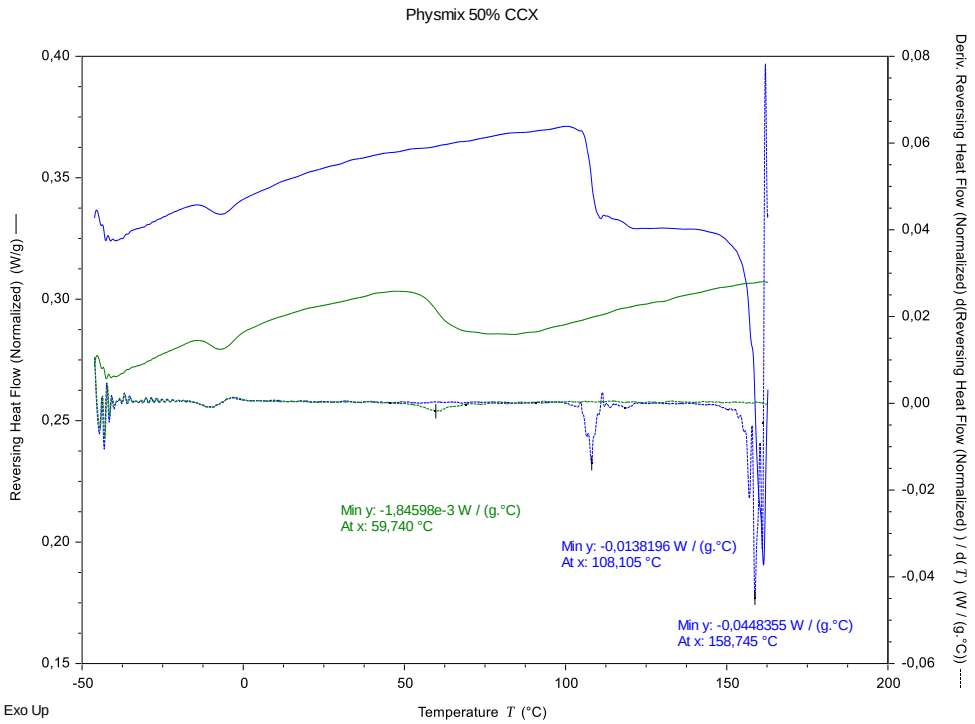

Figure 77 Reversing heat flow of Ramp 2 (blue) & Ramp 3 (green) with corresponding derrivatives and Tg inflection point. Physical mixture of raw materials CCX:Soluplus 50:50

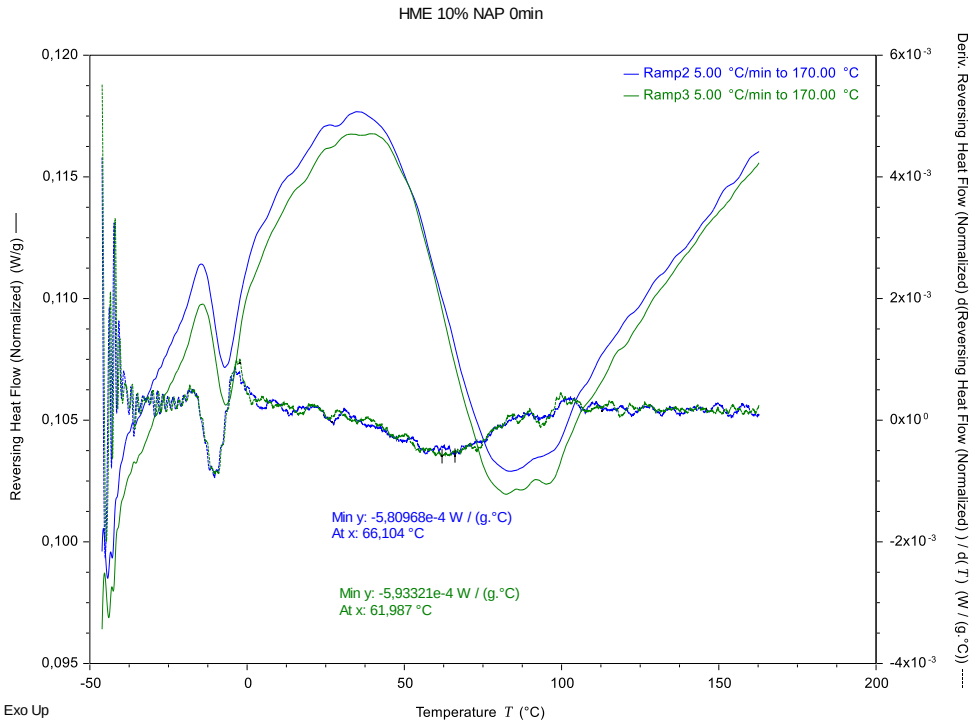

Figure 78 Reversing heat flow of Ramp 2 (blue) & Ramp 3 (green) with corresponding derrivatives and Tg inflection point. HME NAP:Soluplus 10:90 0min recirculation

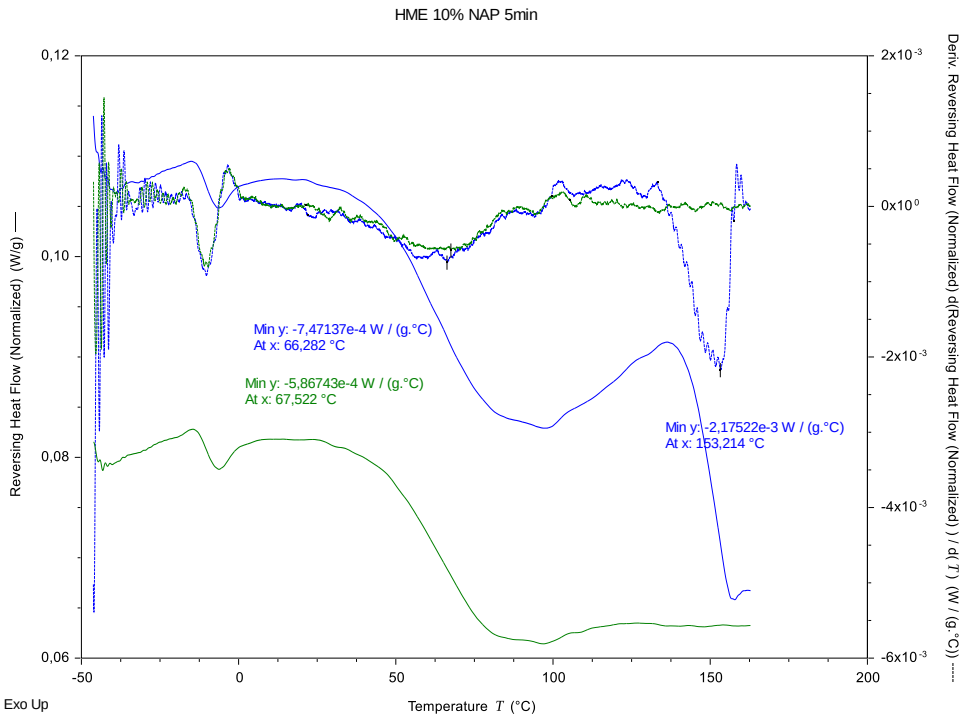

Figure 79 Reversing heat flow of Ramp 2 (blue) & Ramp 3 (green) with corresponding derrivatives and Tg inflection point. HME NAP:Soluplus 10:90 5min recirculation

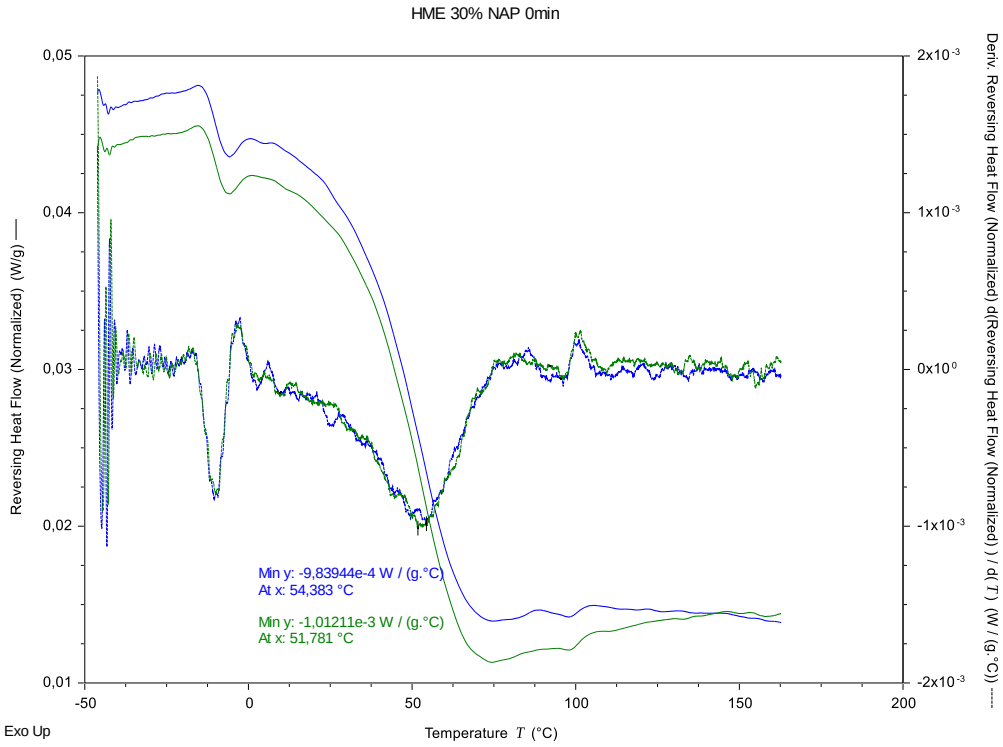

Figure 80 Reversing heat flow of Ramp 2 (blue) & Ramp 3 (green) with corresponding derrivatives and Tg inflection point. HME NAP:Soluplus 30:70 0min recirculation

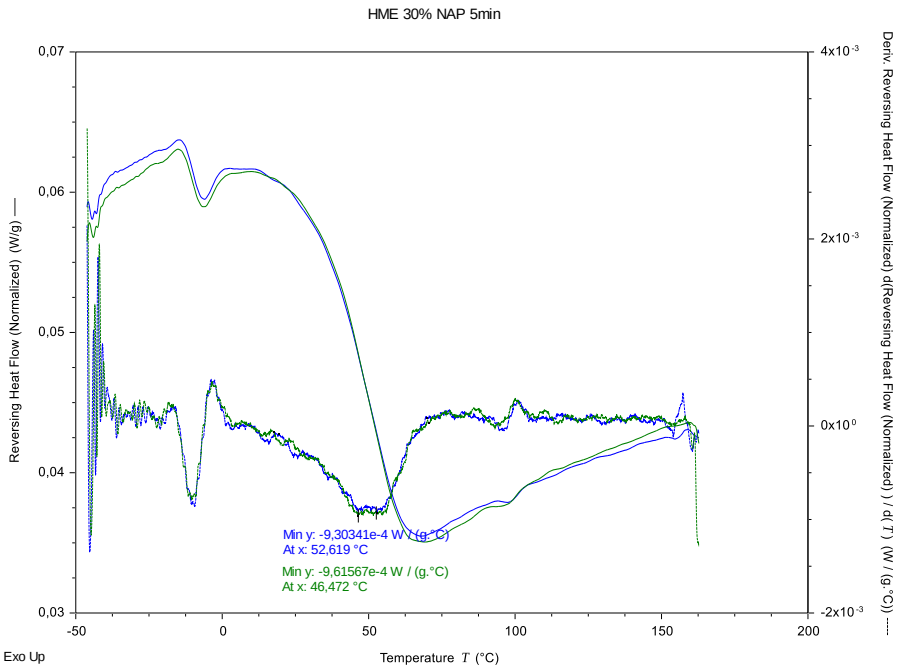

Figure 81 Reversing heat flow of Ramp 2 (blue) & Ramp 3 (green) with corresponding derrivatives and Tg inflection point. HME NAP:Soluplus 30:70 5min recirculation

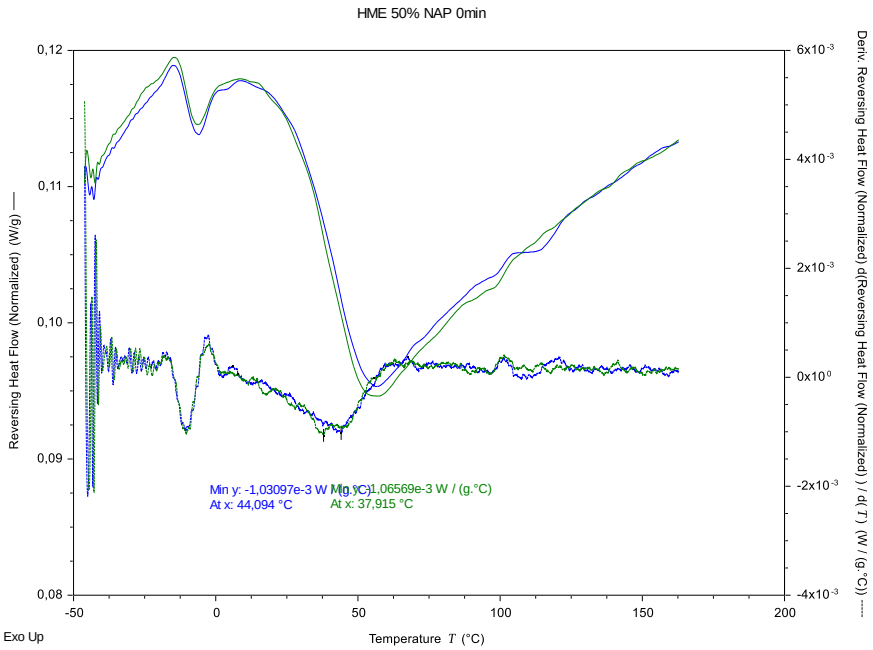

Figure 82 Reversing heat flow of Ramp 2 (blue) & Ramp 3 (green) with corresponding derrivatives and Tg inflection point. HME NAP:Soluplus 50:50 0min recirculation

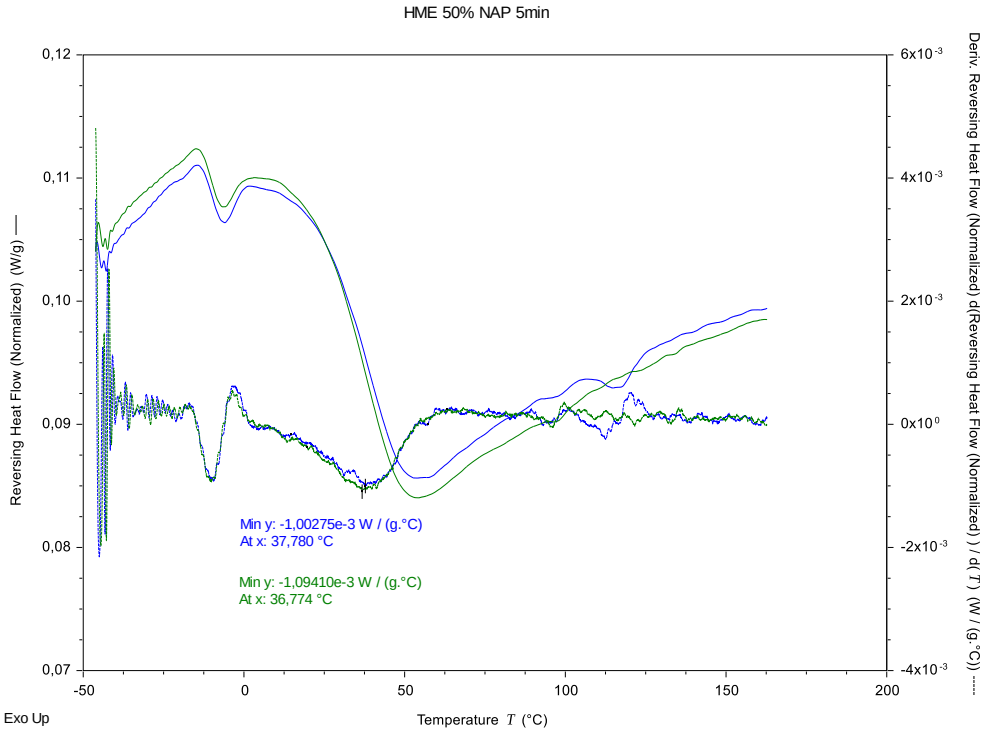

Figure 83 Reversing heat flow of Ramp 2 (blue) & Ramp 3 (green) with corresponding derrivatives and Tg inflection point. HME NAP:Soluplus 50:50 5min recirculation

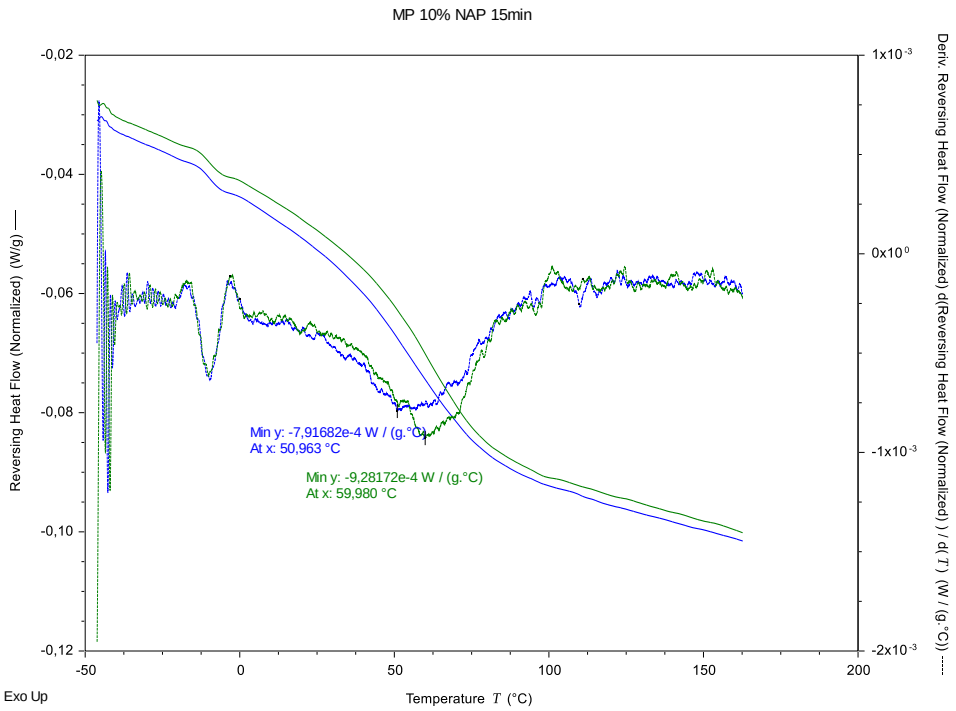

Figure 84 Reversing heat flow of Ramp 2 (blue) & Ramp 3 (green) with corresponding derrivatives and Tg inflection point. MeltPrep NAP:Soluplus 10:90 15min

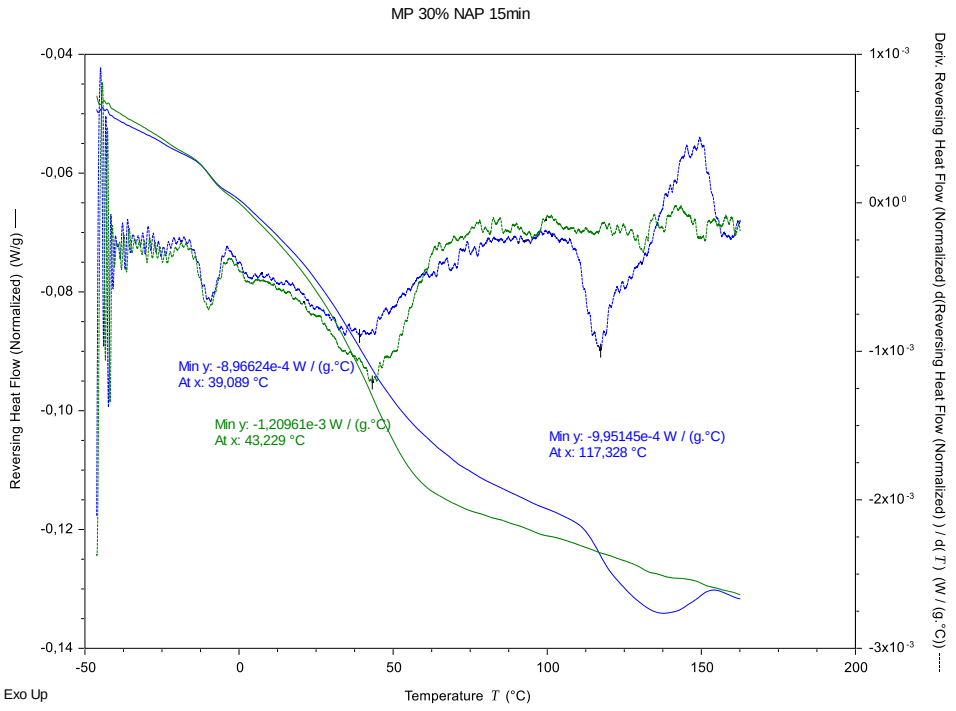

Figure 85 Reversing heat flow of Ramp 2 (blue) & Ramp 3 (green) with corresponding derrivatives and Tg inflection point. MeltPrep NAP:Soluplus 30:70 15min

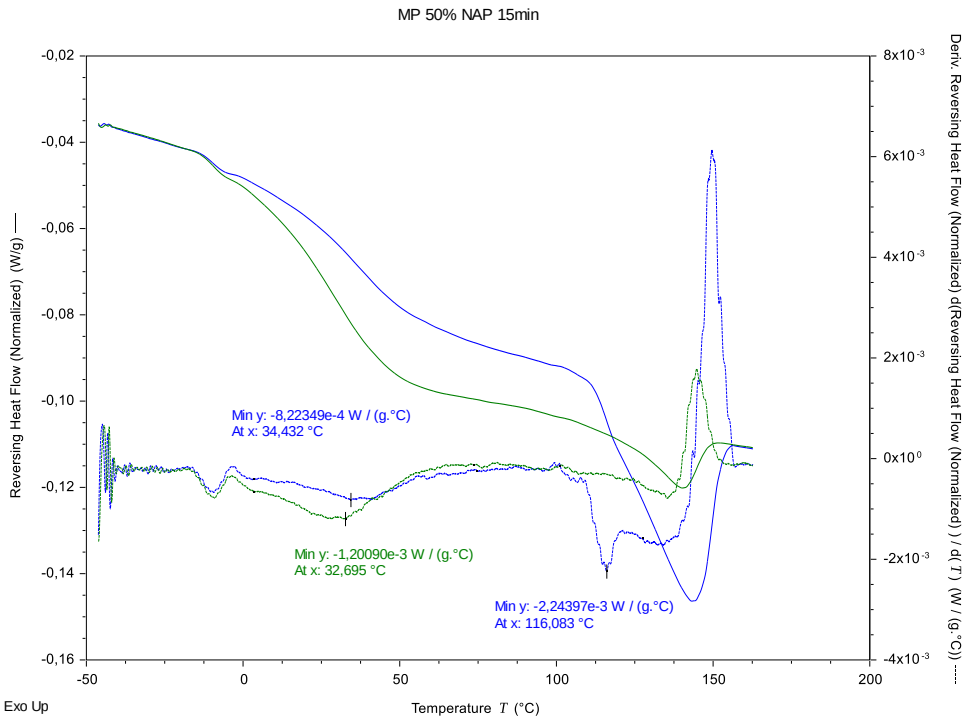

Figure 86 Reversing heat flow of Ramp 2 (blue) & Ramp 3 (green) with corresponding derrivatives and Tg inflection point. MeltPrep NAP:Soluplus 50:50 15min

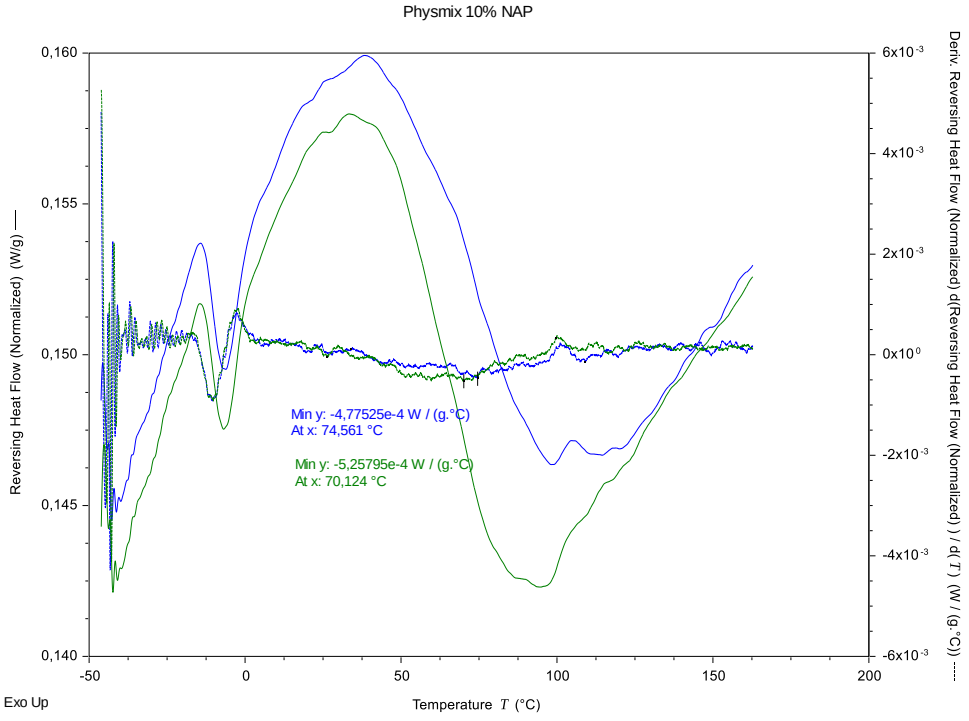

Figure 87 Reversing heat flow of Ramp 2 (blue) & Ramp 3 (green) with corresponding derrivatives and Tg inflection point. Physical mixture of raw materials NAP:Soluplus 10:90

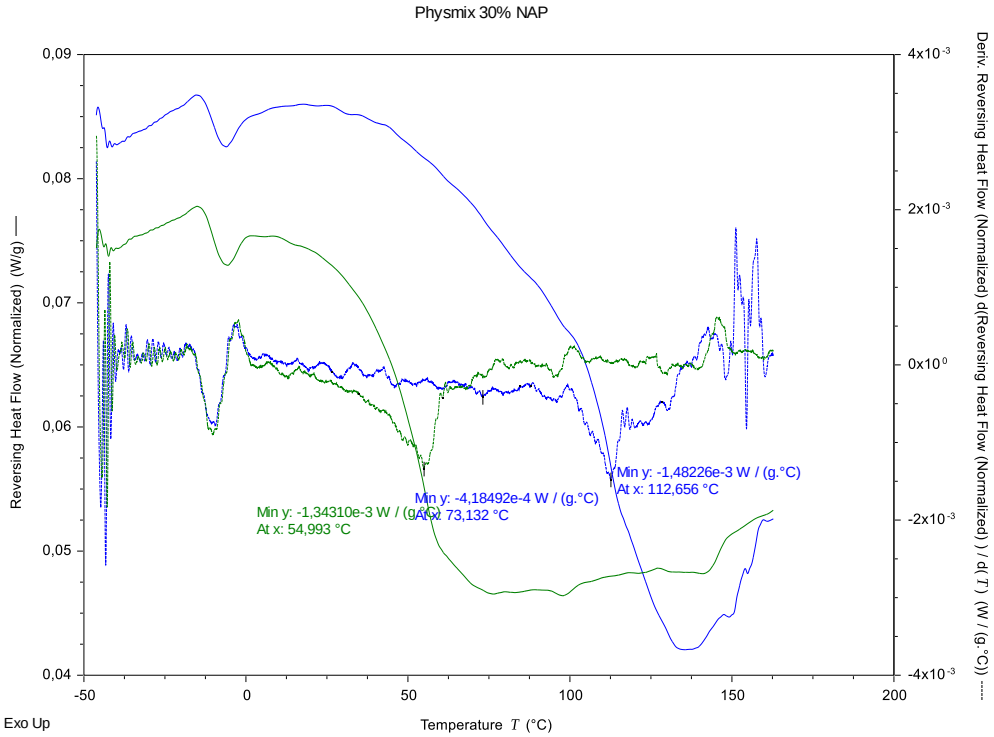

Figure 88 Reversing heat flow of Ramp 2 (blue) & Ramp 3 (green) with corresponding derrivatives and Tg inflection point. Physical mixture of raw materials NAP:Soluplus 30:70

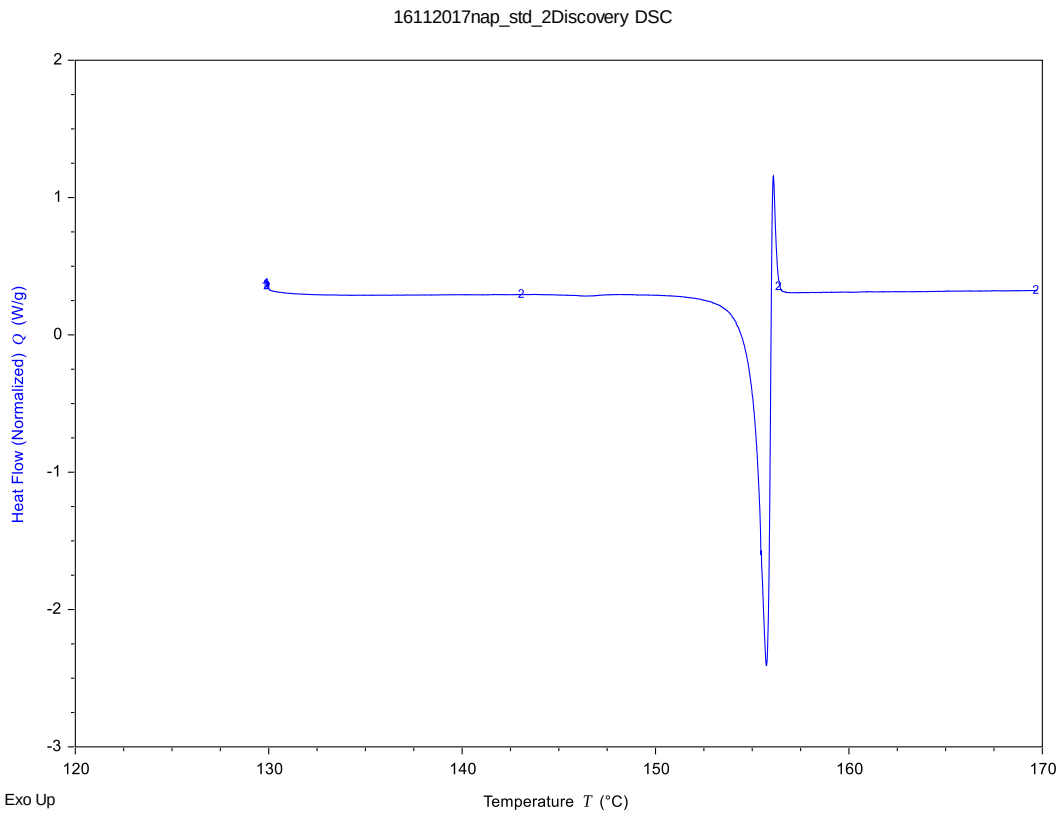

Figure 89 Melting point determination of NAP

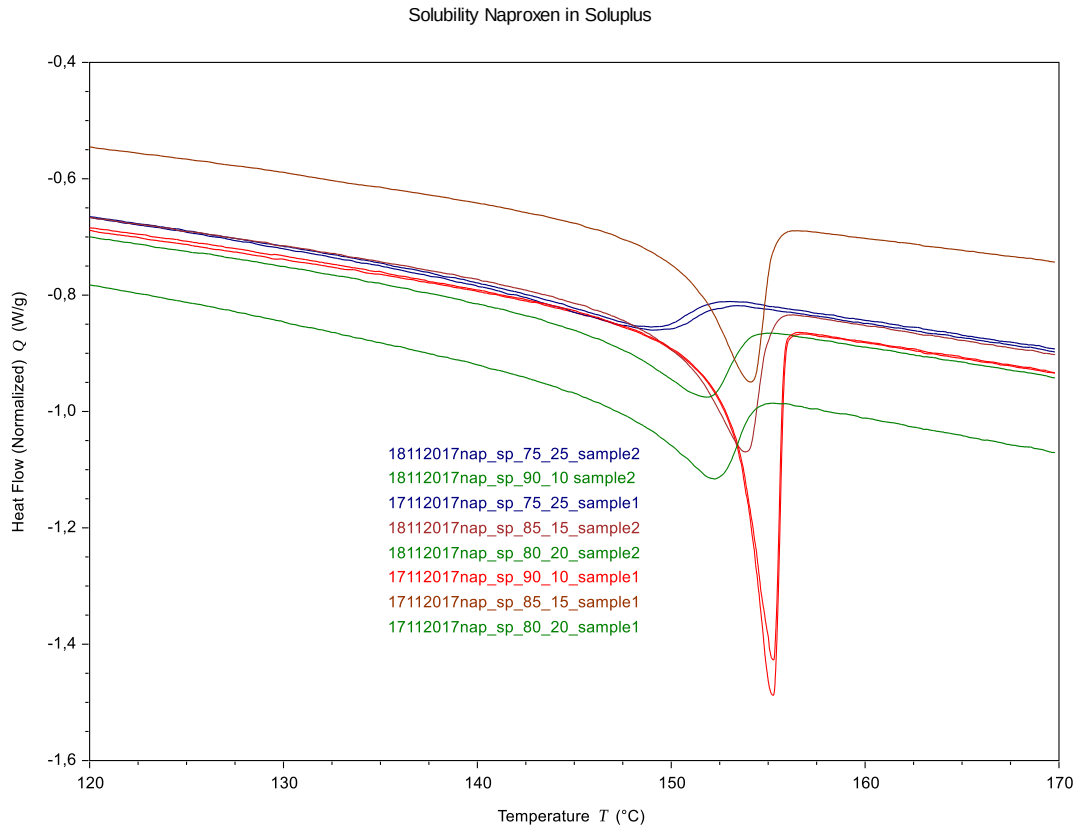

Figure 90 Melting point depression of NAP:Soluplus mixtures

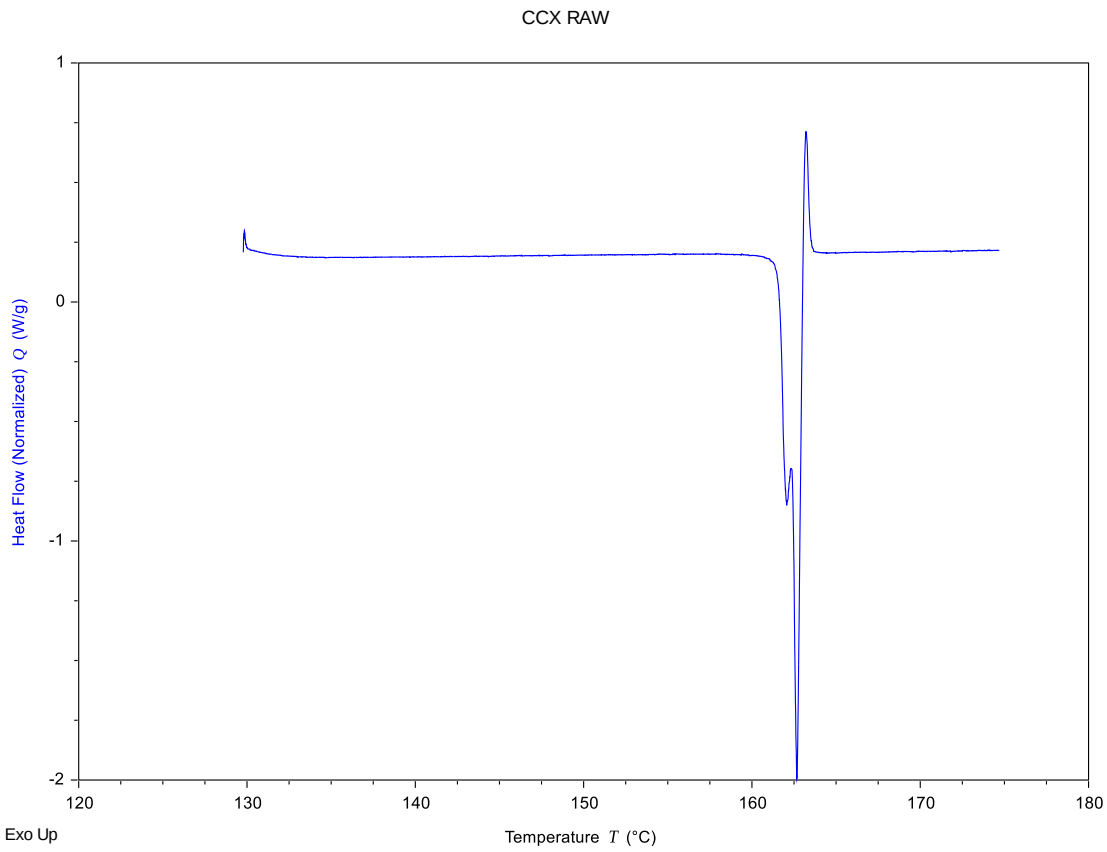

Figure 91 Melting point determination of CCX

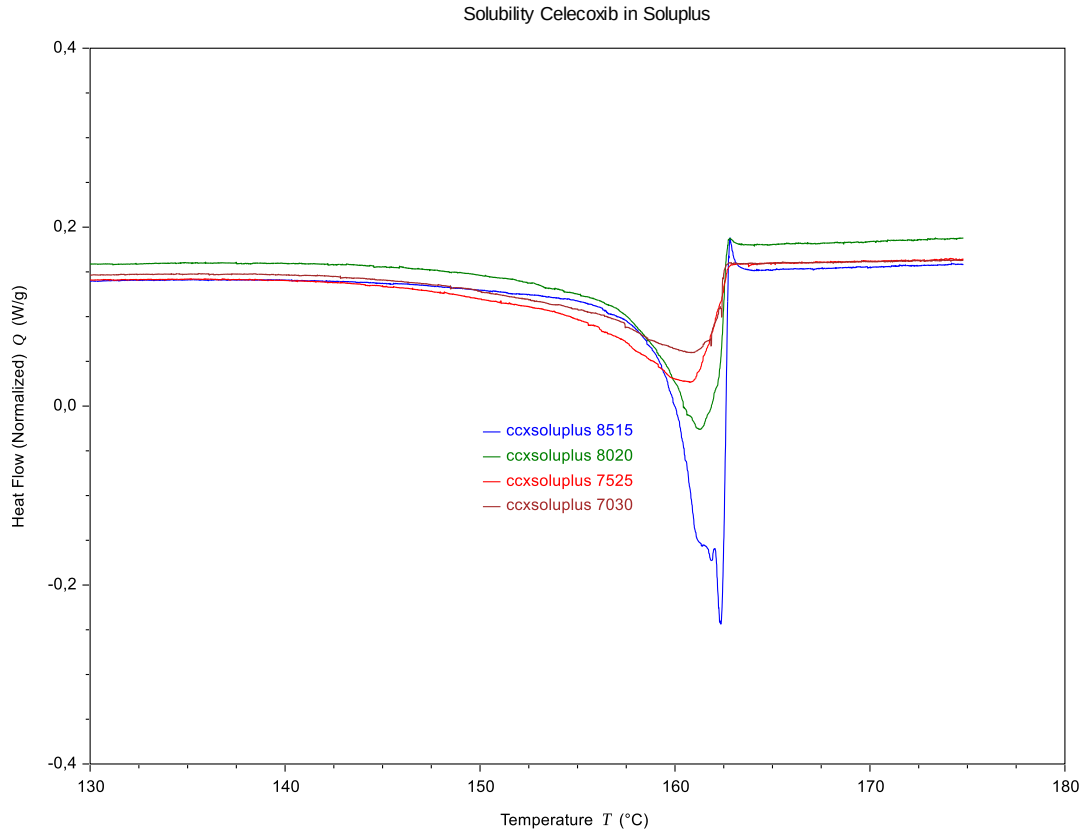

Figure 92 Melting point depression of CCX:Soluplus mixtures

The calculation sheet for the solubility determination using the Flory-Huggins model can be requested by email: nek000@post.uit.no

A.3 Rheology

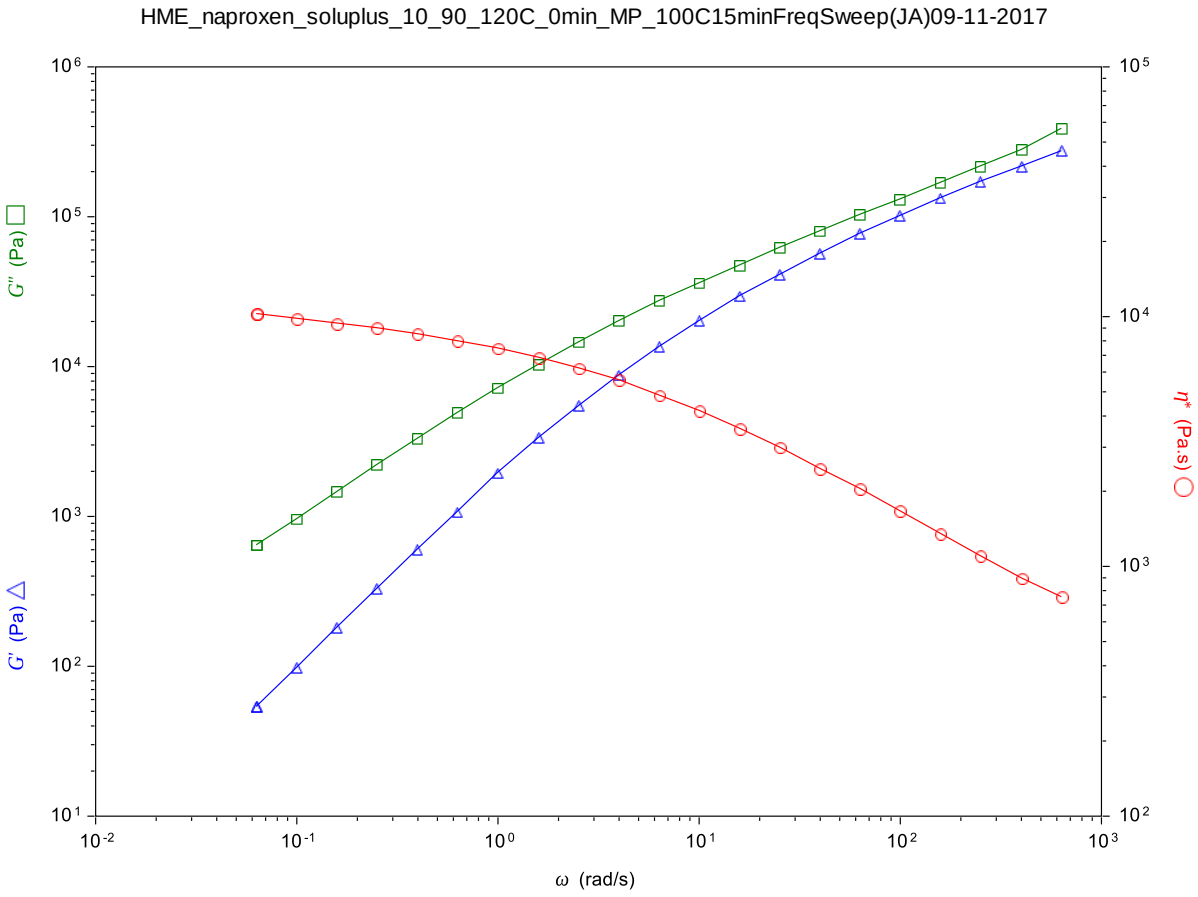

Figure 93 Frequency sweep 10% NAP HME 0min

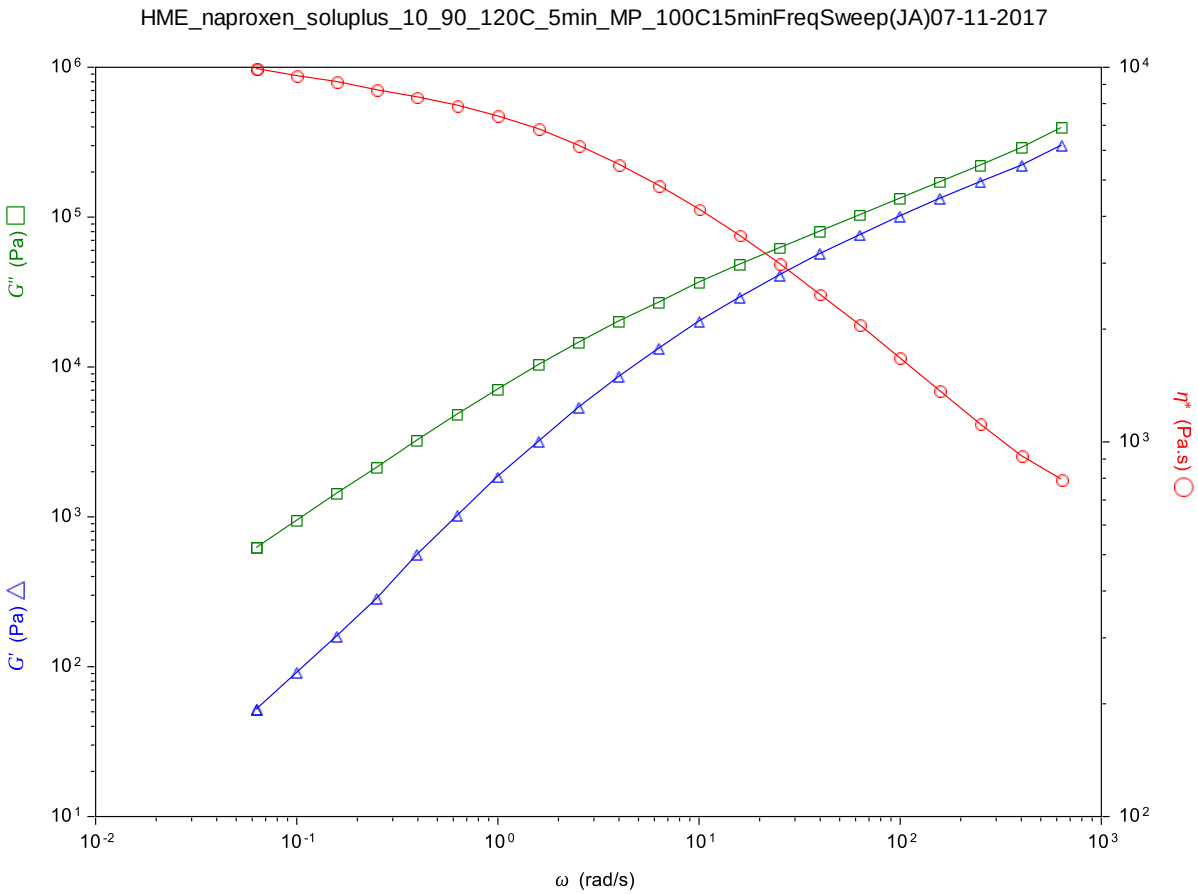

Figure 94 Frequency sweep 10% NAP HME 5min

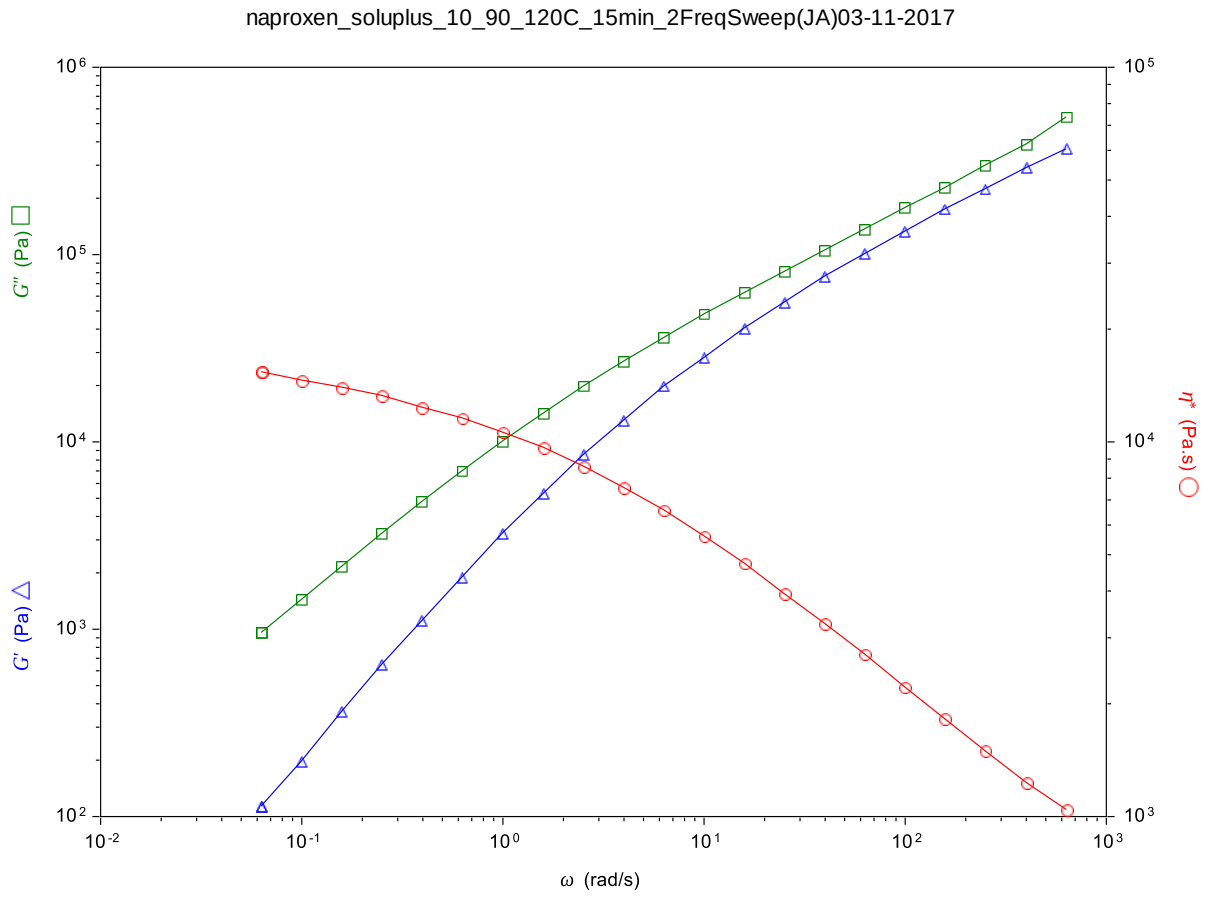

Figure 95 Frequency sweep 10% NAP VCM 15min

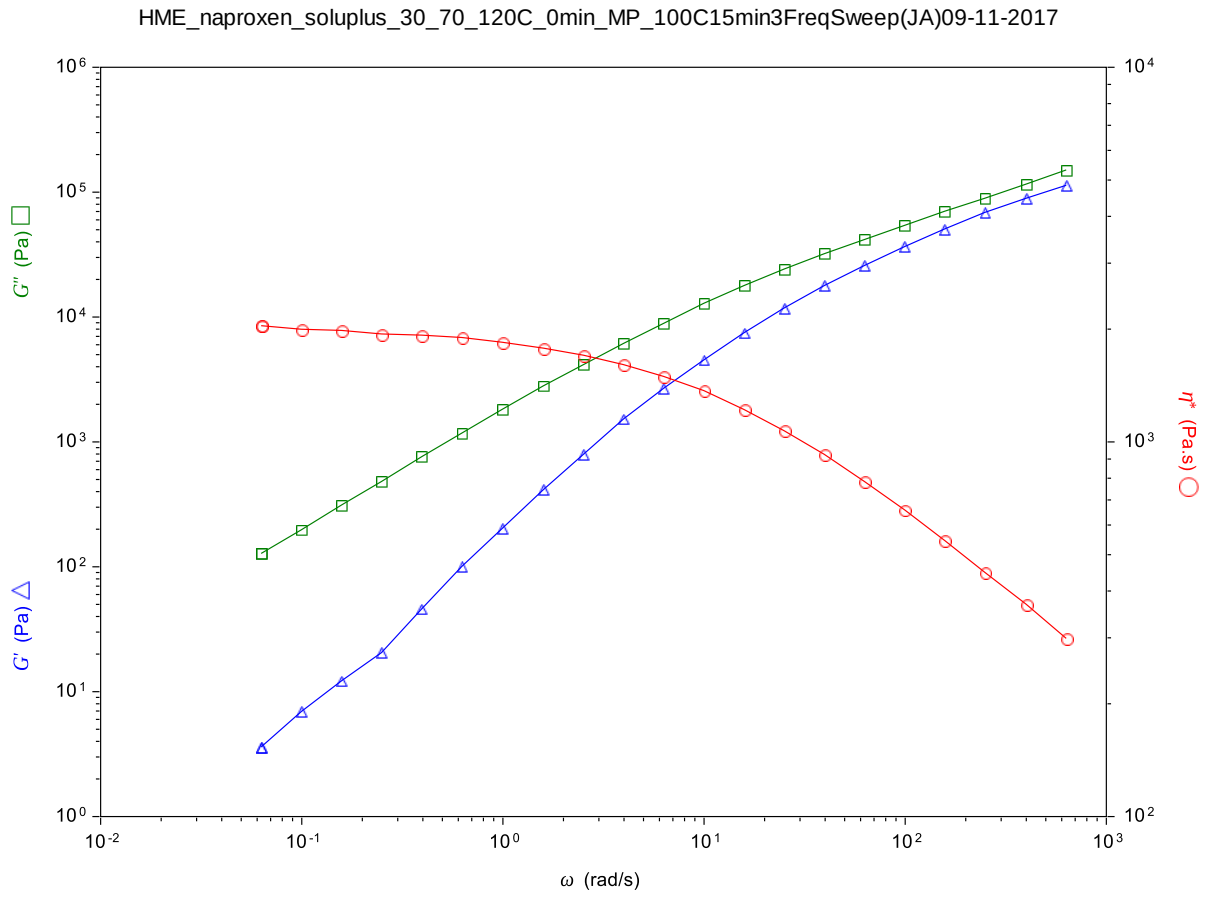

Figure 96 Frequency sweep 30% NAP HME 0min

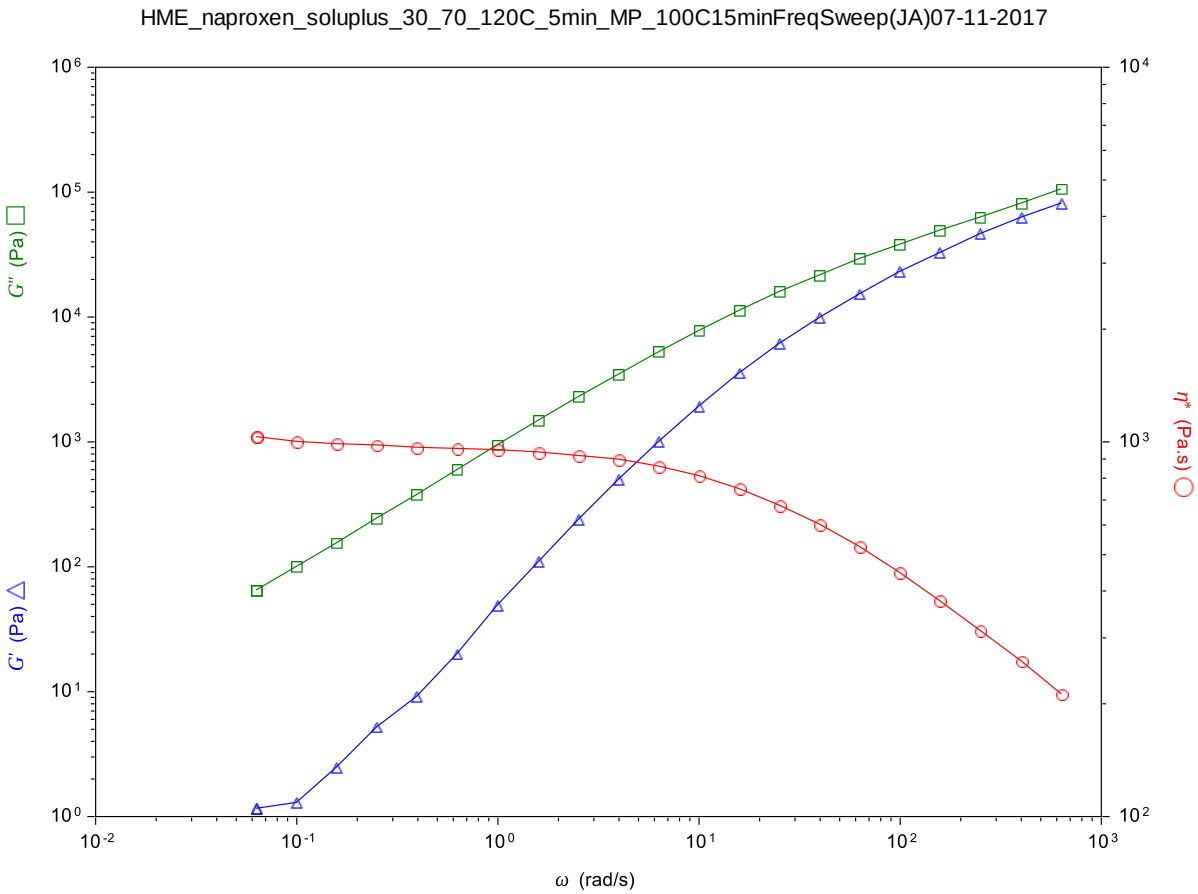

Figure 97 Frequency sweep 30% NAP HME 5min

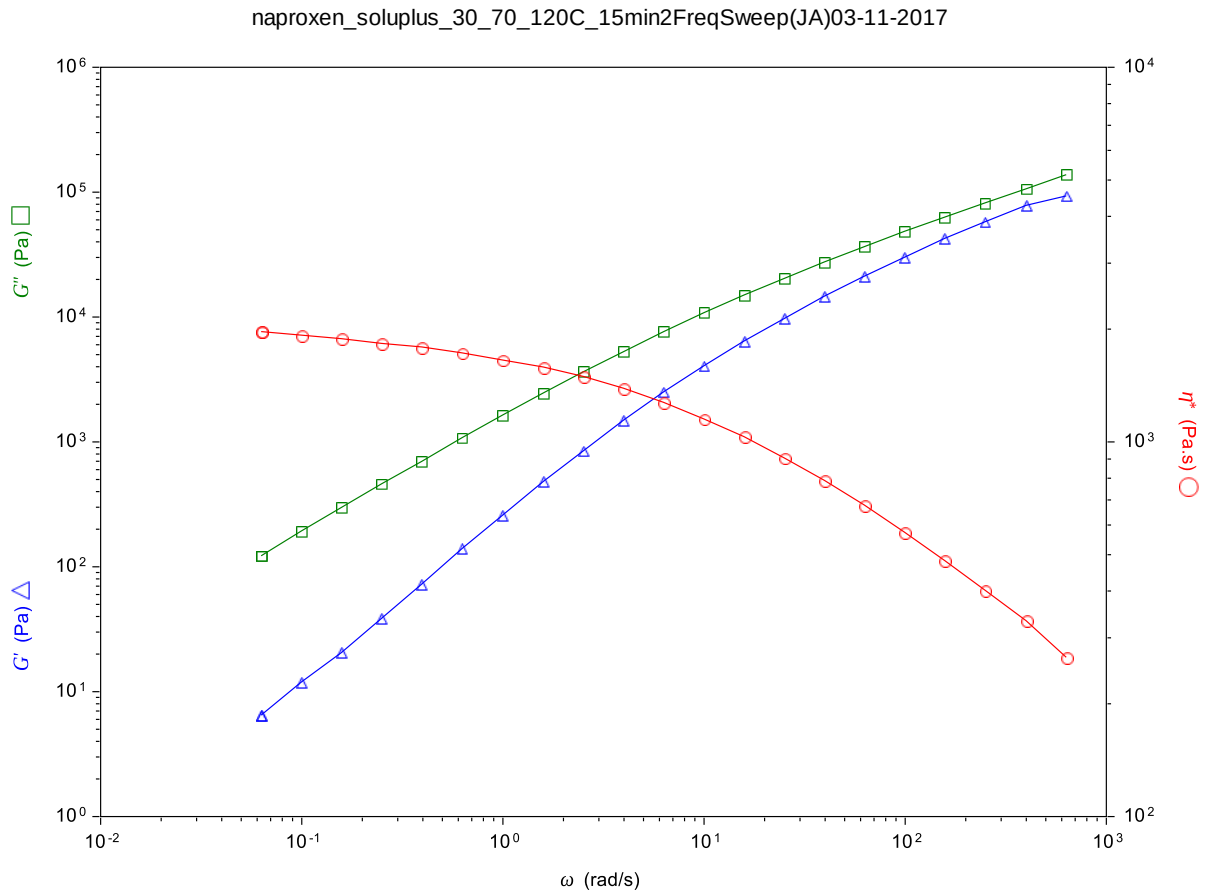

Figure 98 Frequency sweep 30% NAP VCM 15min

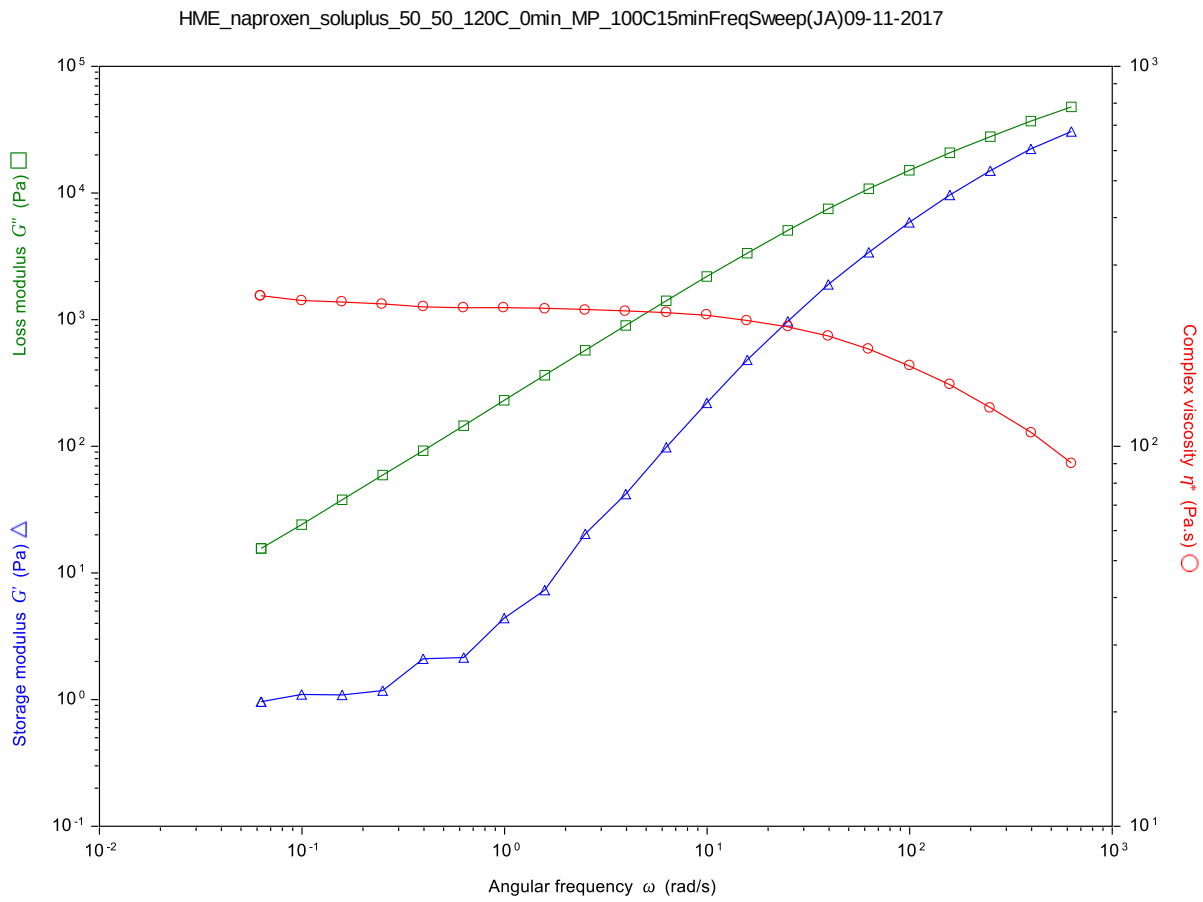

Figure 99 Frequency sweep 50% NAP HME 0 min

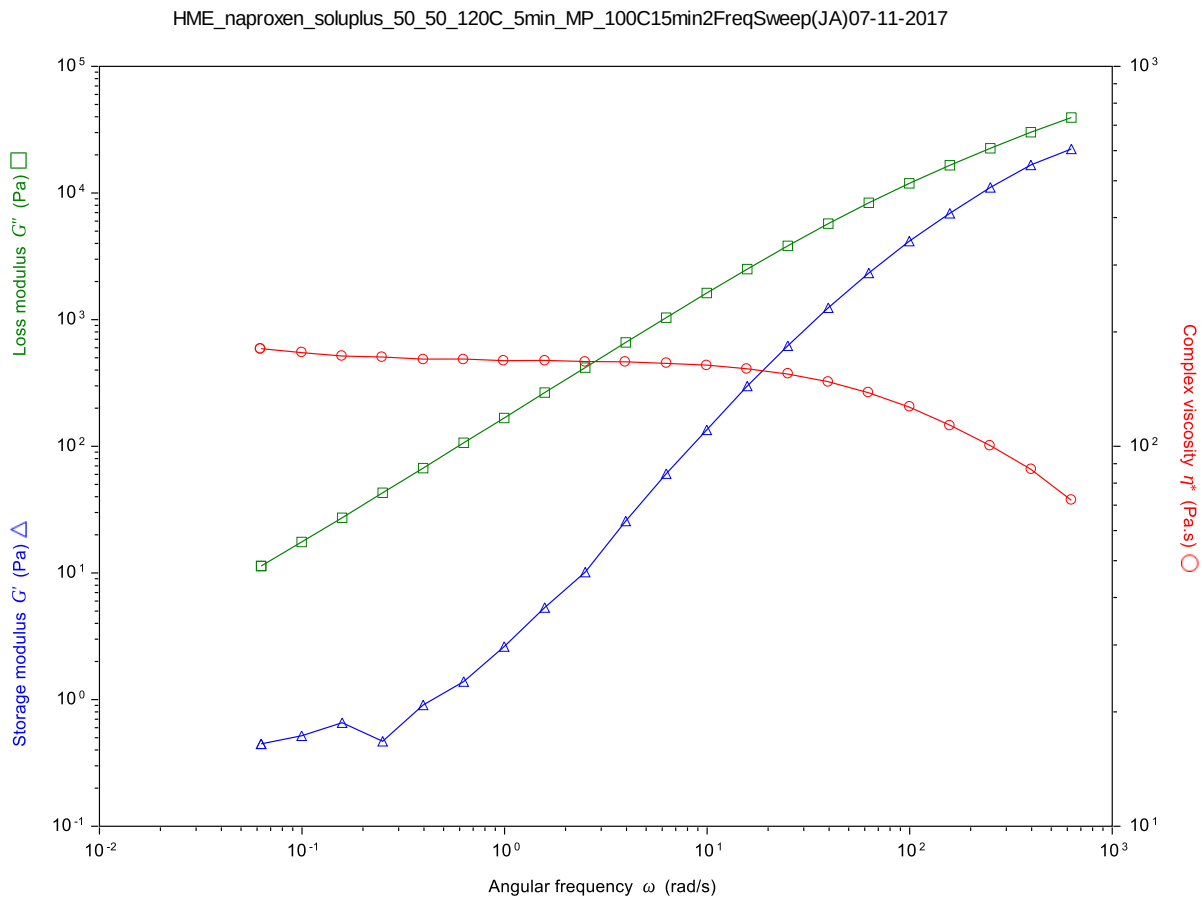

Figure 100 Frequency sweep 50% NAP HME 5 min

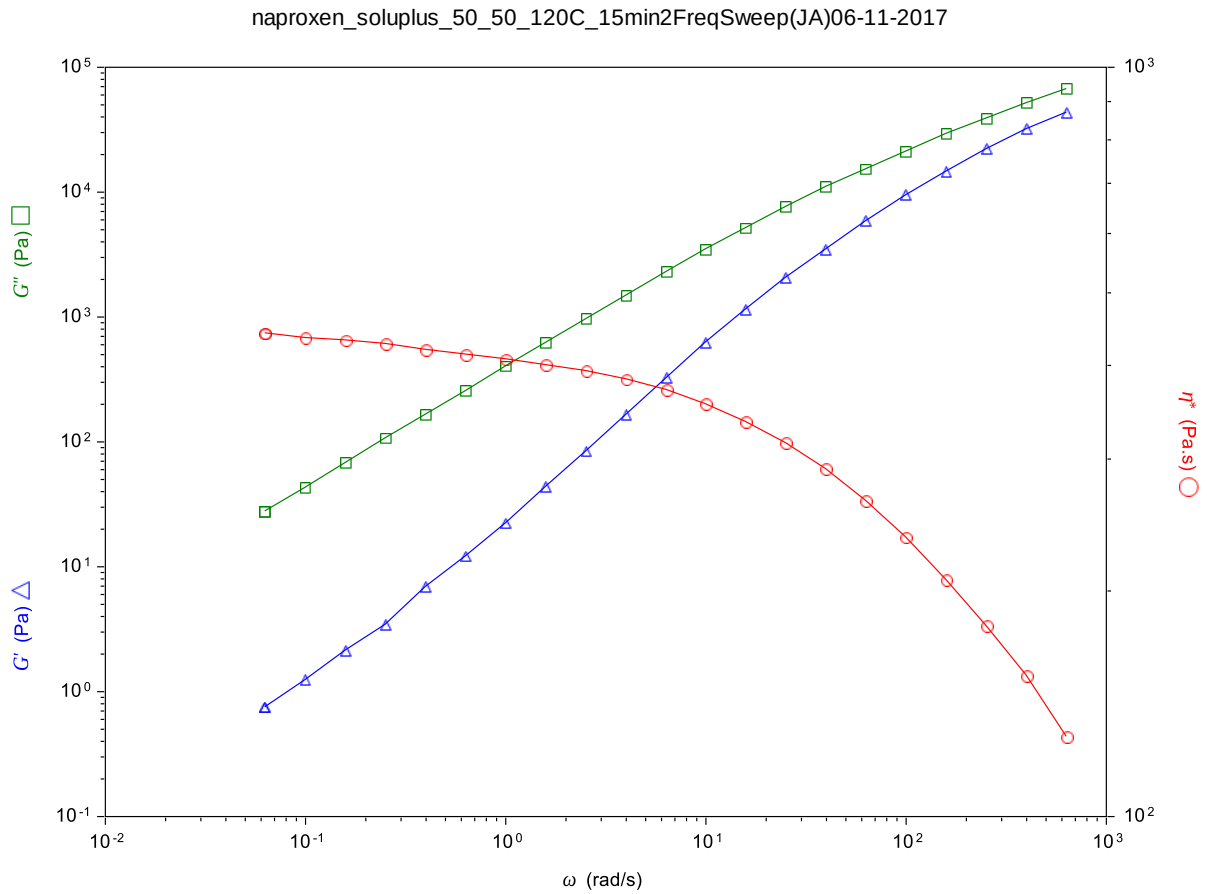

Figure 101 Frequency sweep 50% NAP VCM 15min

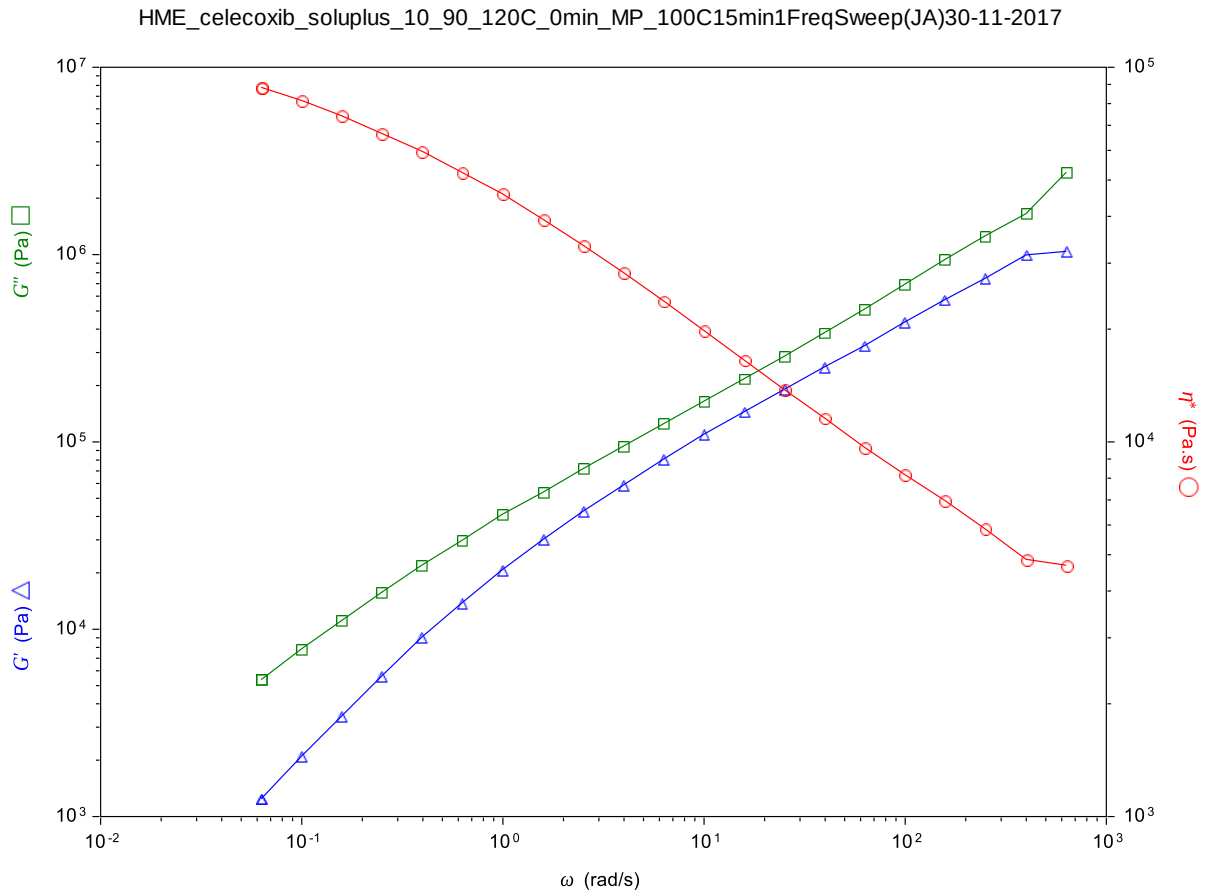

Figure 102 Frequency sweep 10% CCX HME 0 min

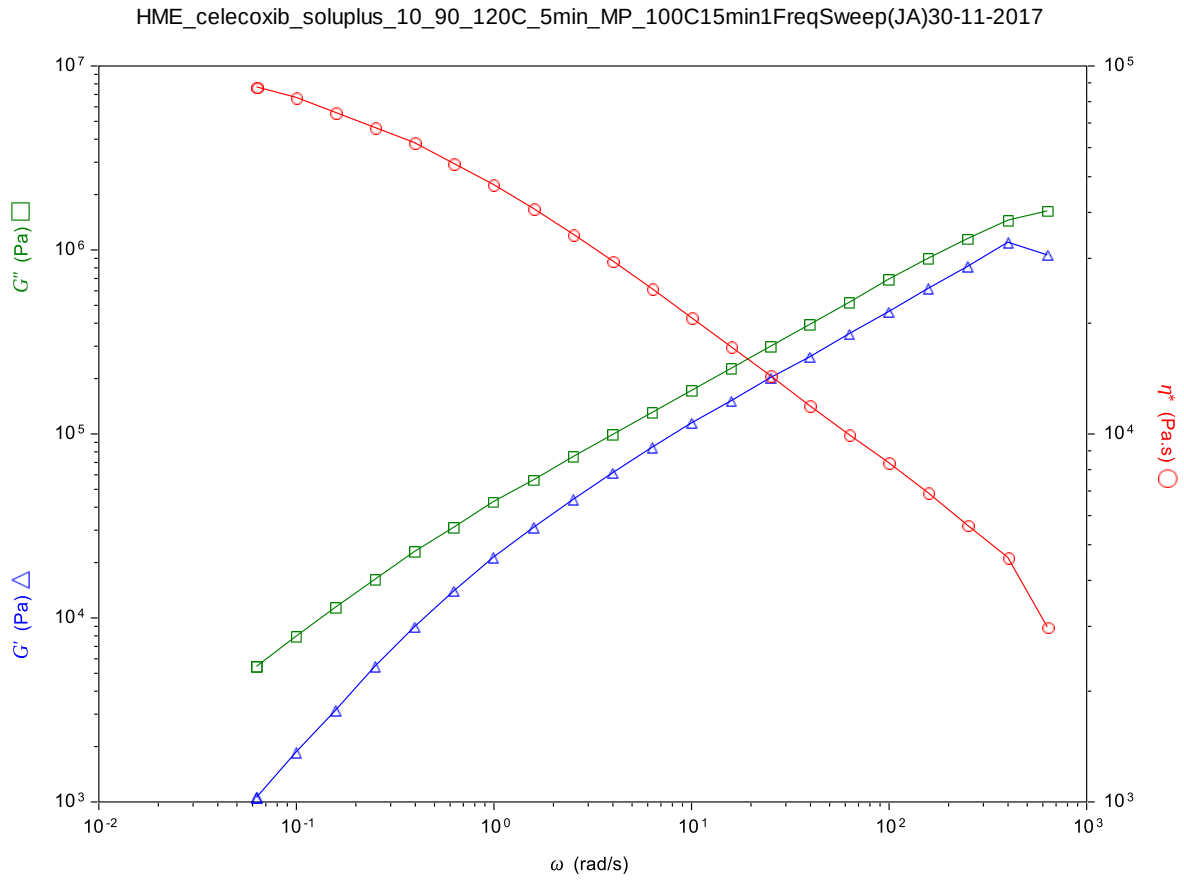

Figure 103 Frequency sweep 10% CCX HME 5 min

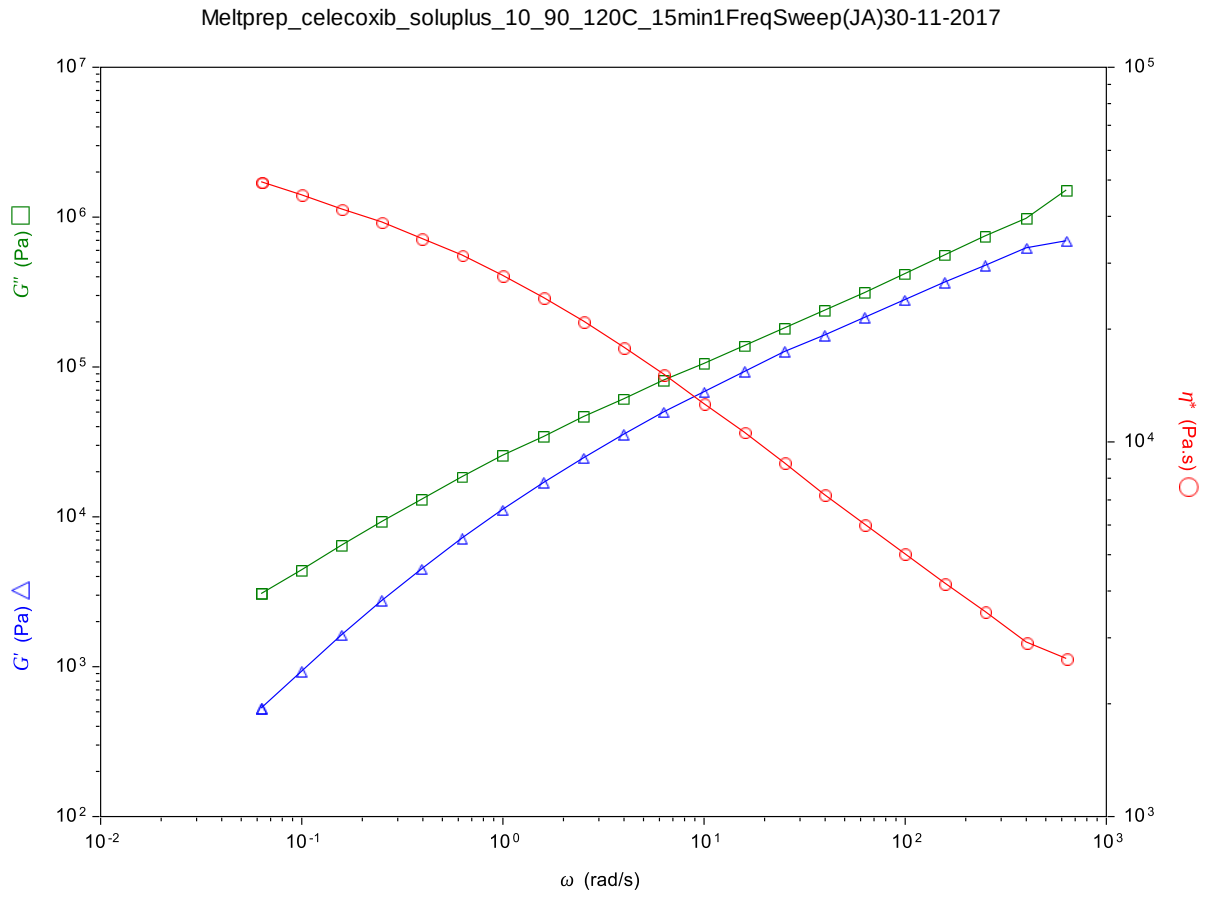

Figure 104 Frequency sweep 10% CCX VCM 15min

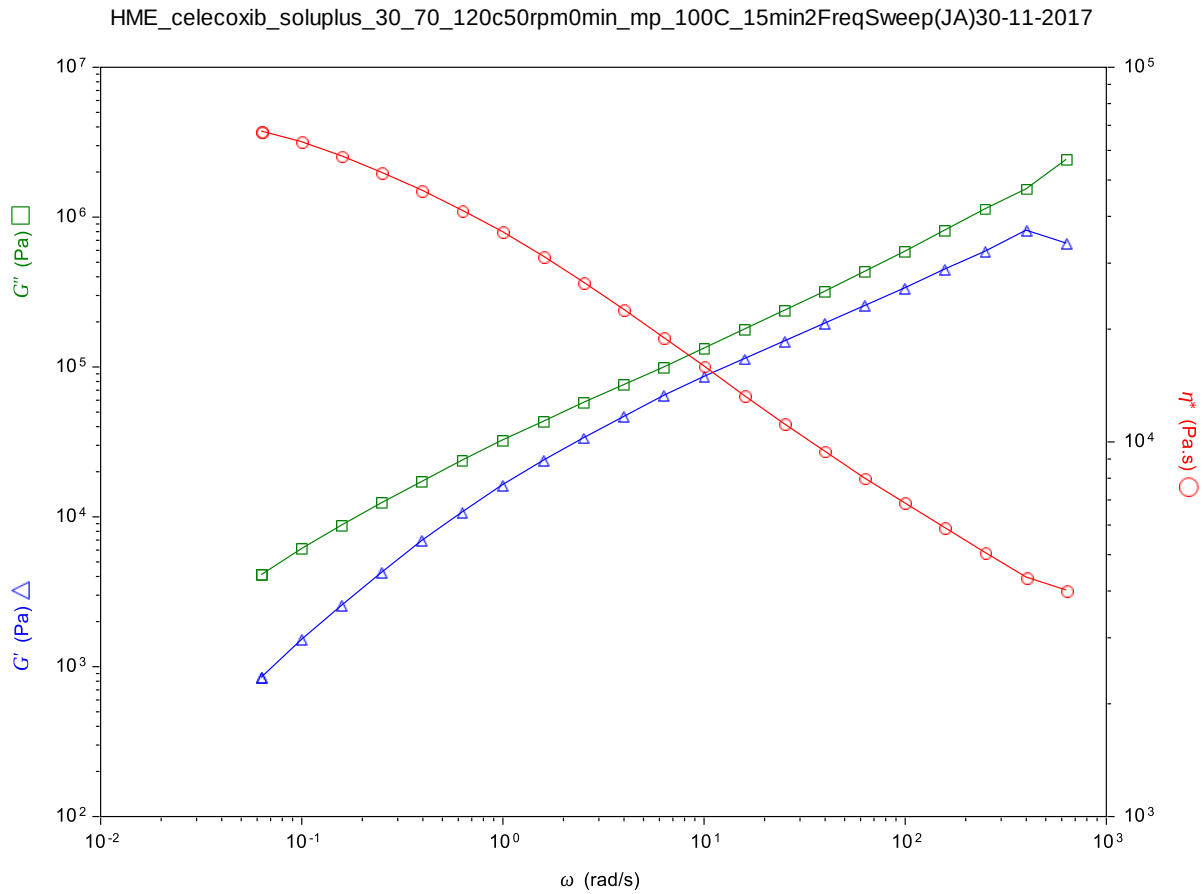

Figure 105 Frequency sweep 30% CCX HME 0 min

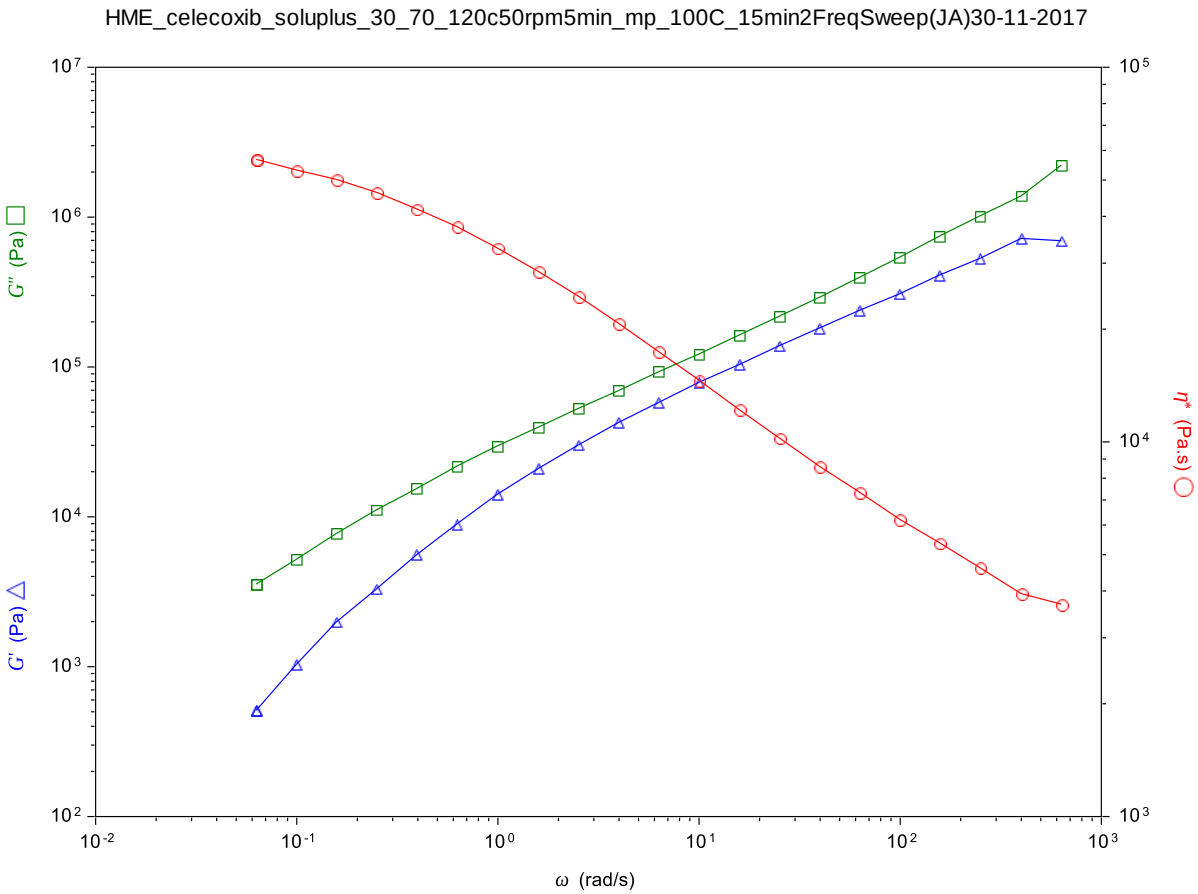

Figure 106 Frequency sweep 30% CCX HME 5 min

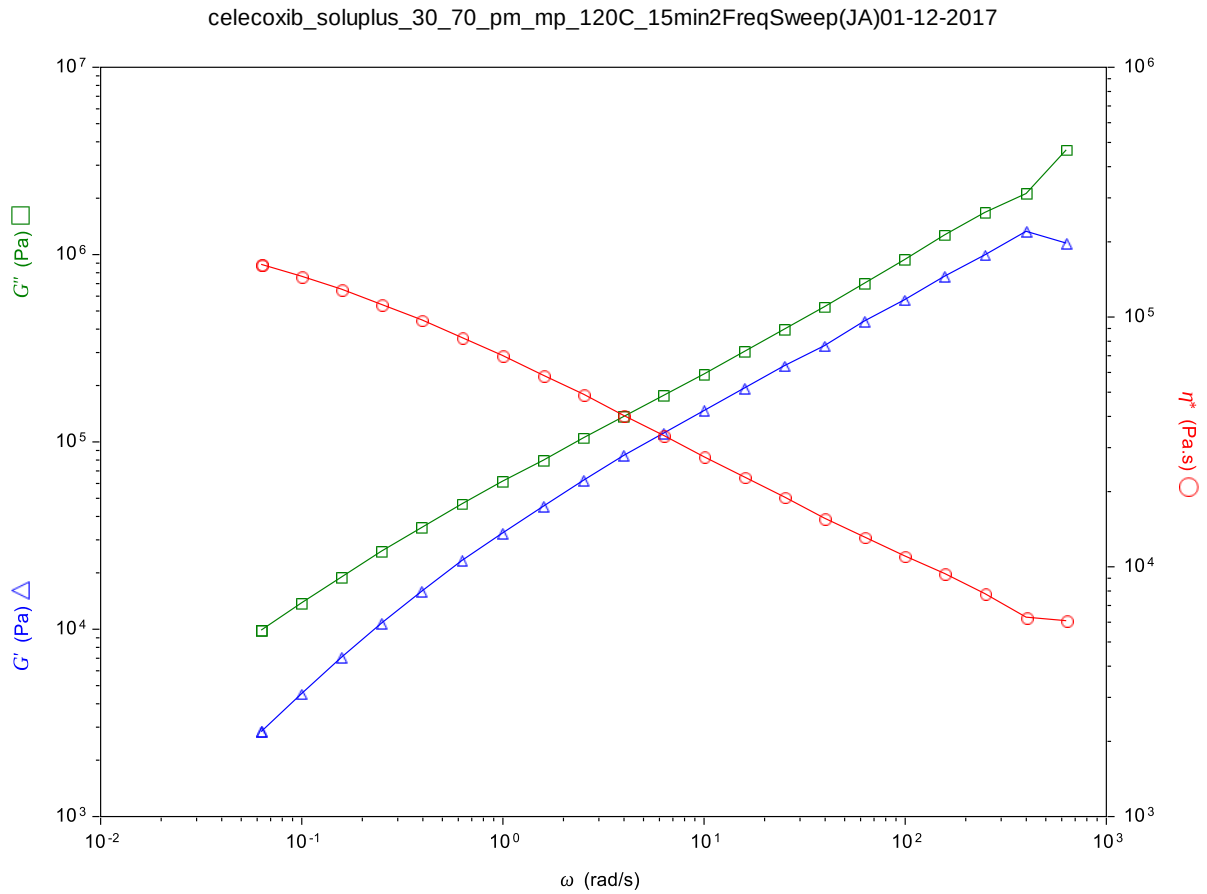

Figure 107 Frequency sweep 30% CCX VCM 15min

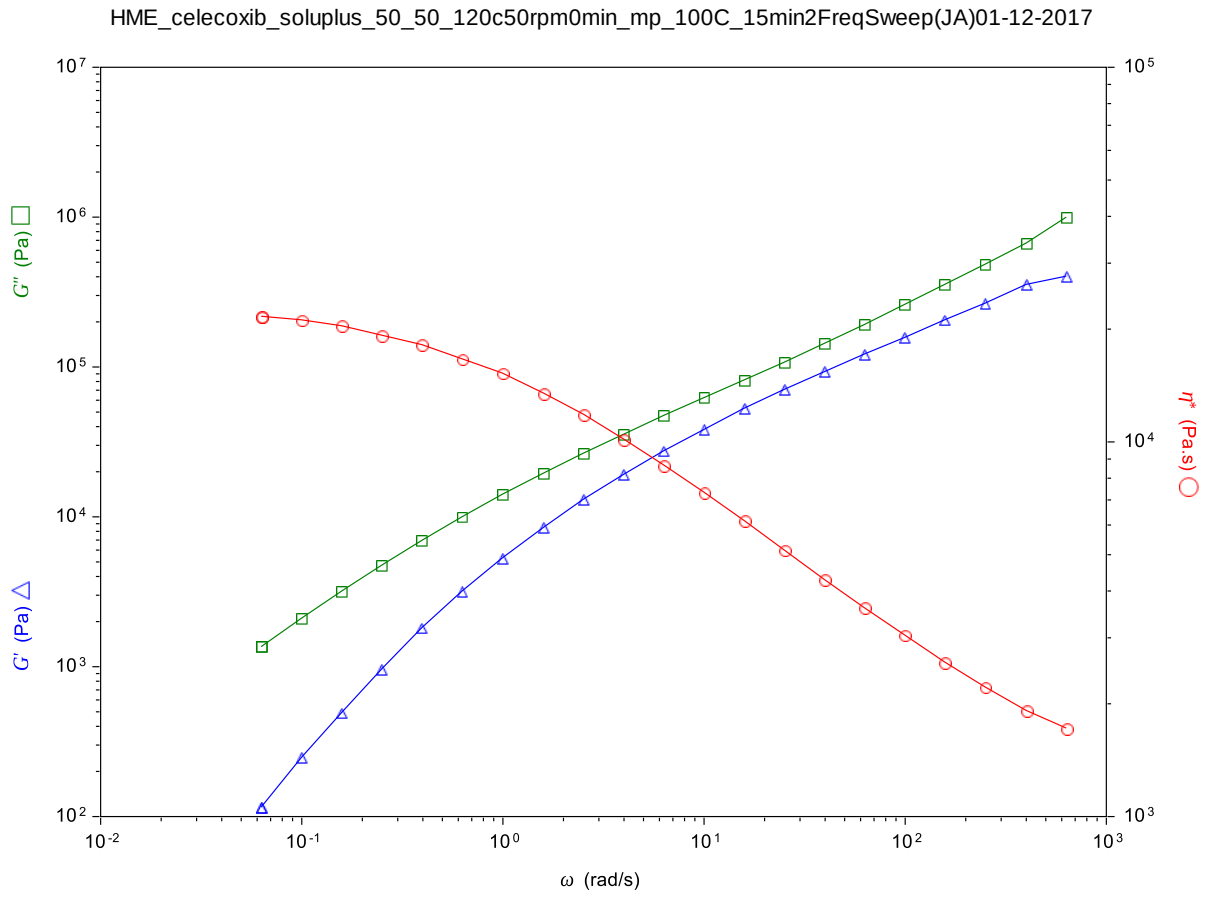

Figure 108 Frequency sweep 50% CCX HME 0 min

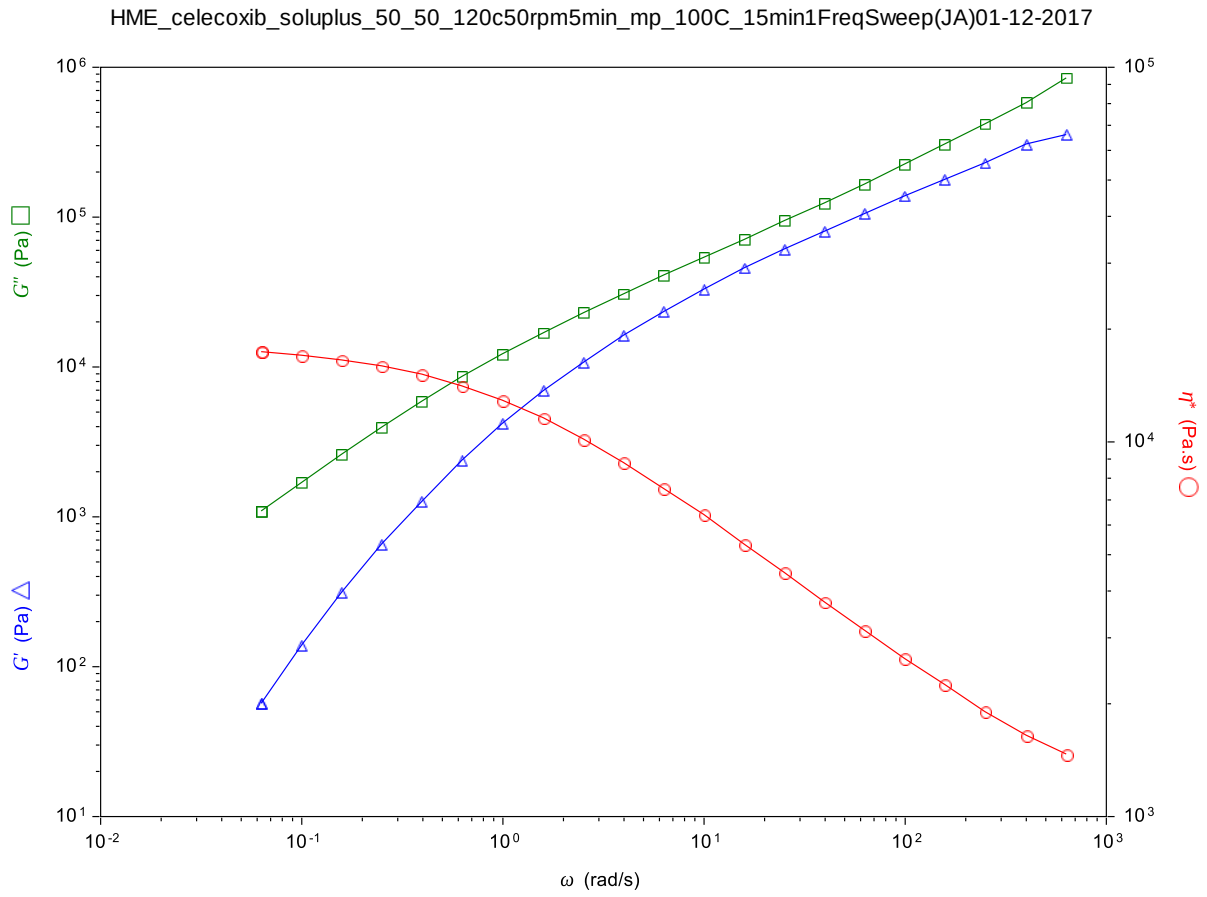

Figure 109 Frequency sweep 50% CCX HME 5 min

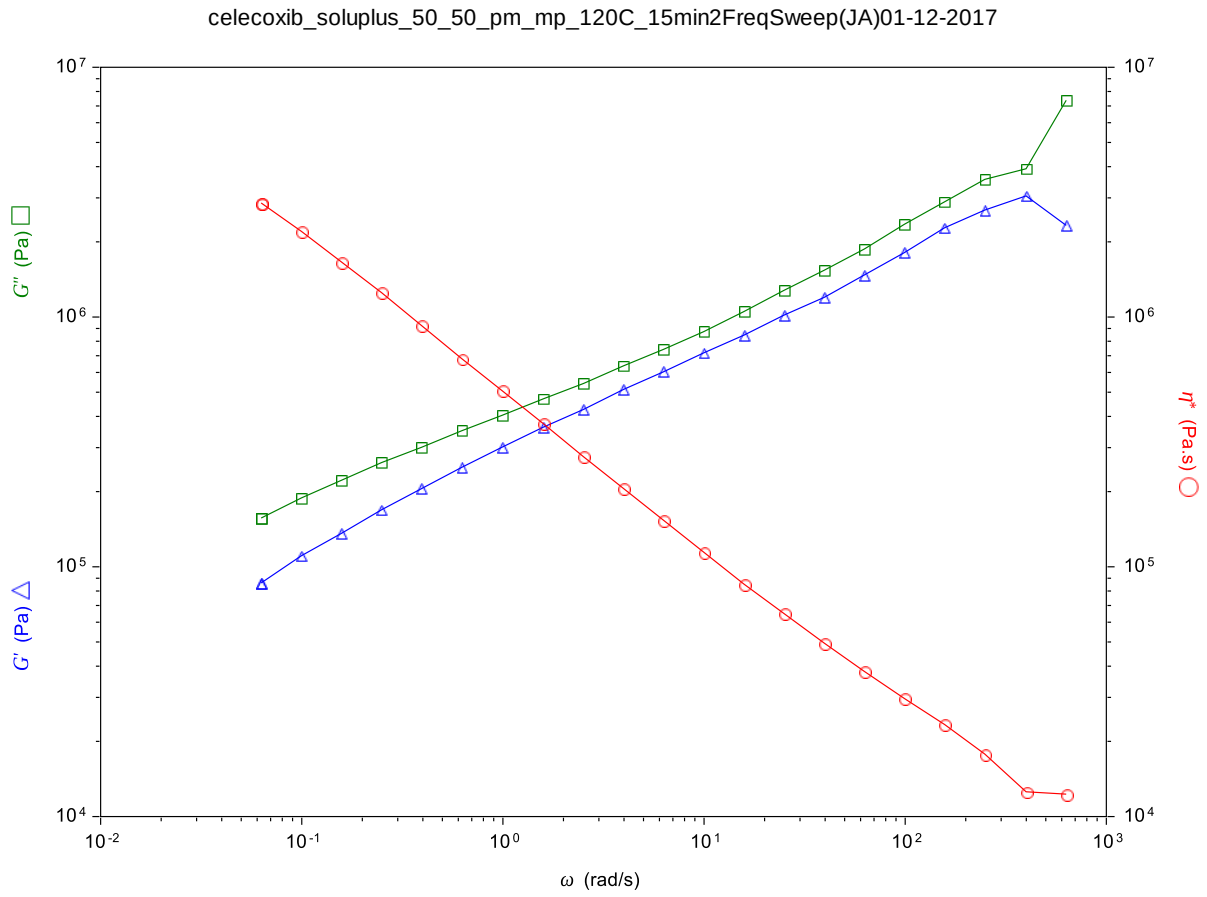

Figure 110 Frequency sweep 50% CCX VCM 15min

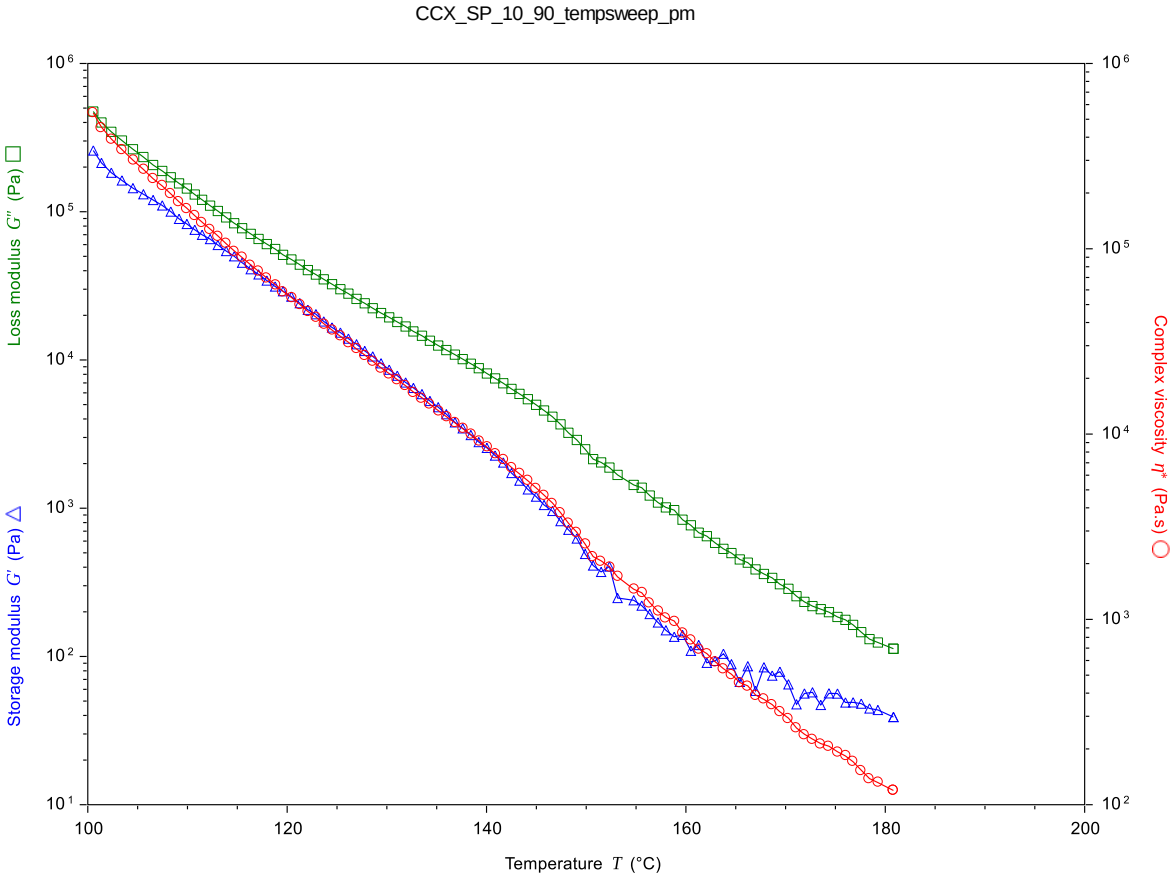

Figure 111 Temperature sweep CCX 10%

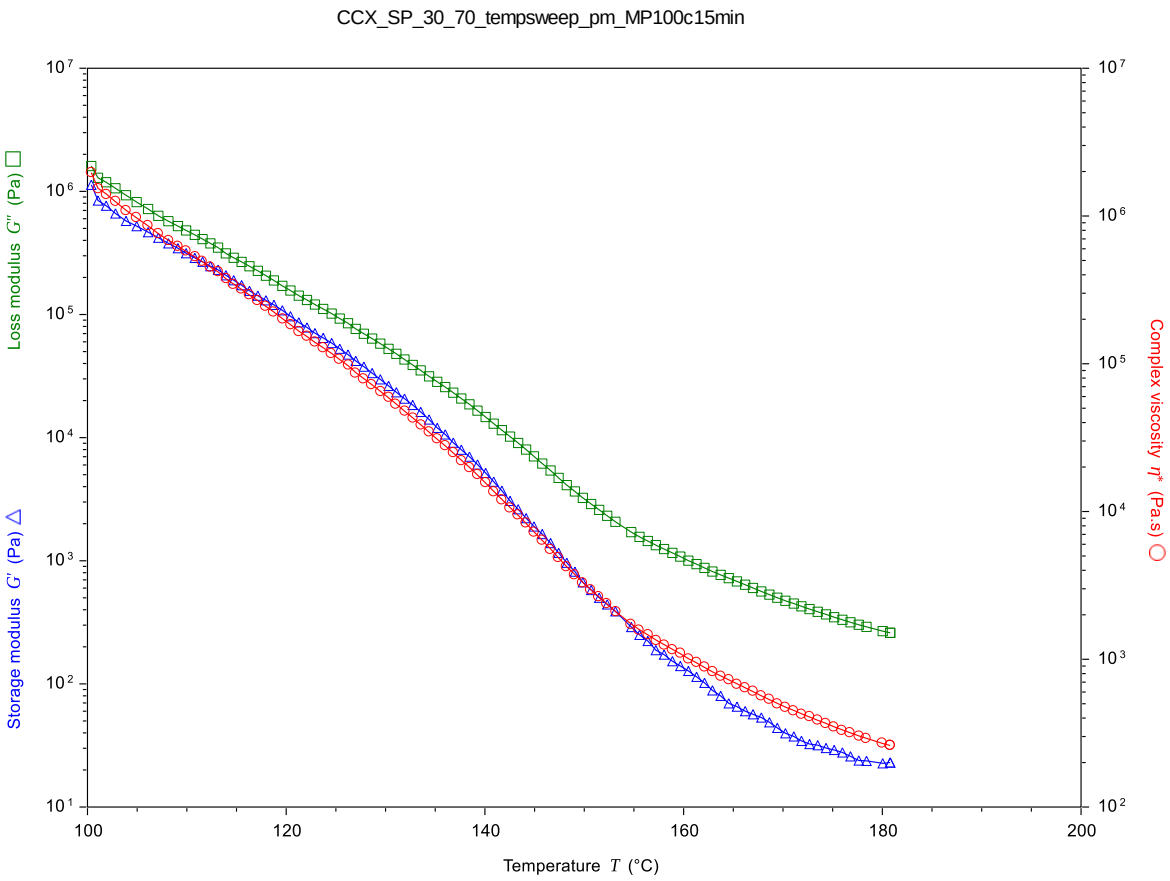

Figure 112Temperature sweep CCX 30%

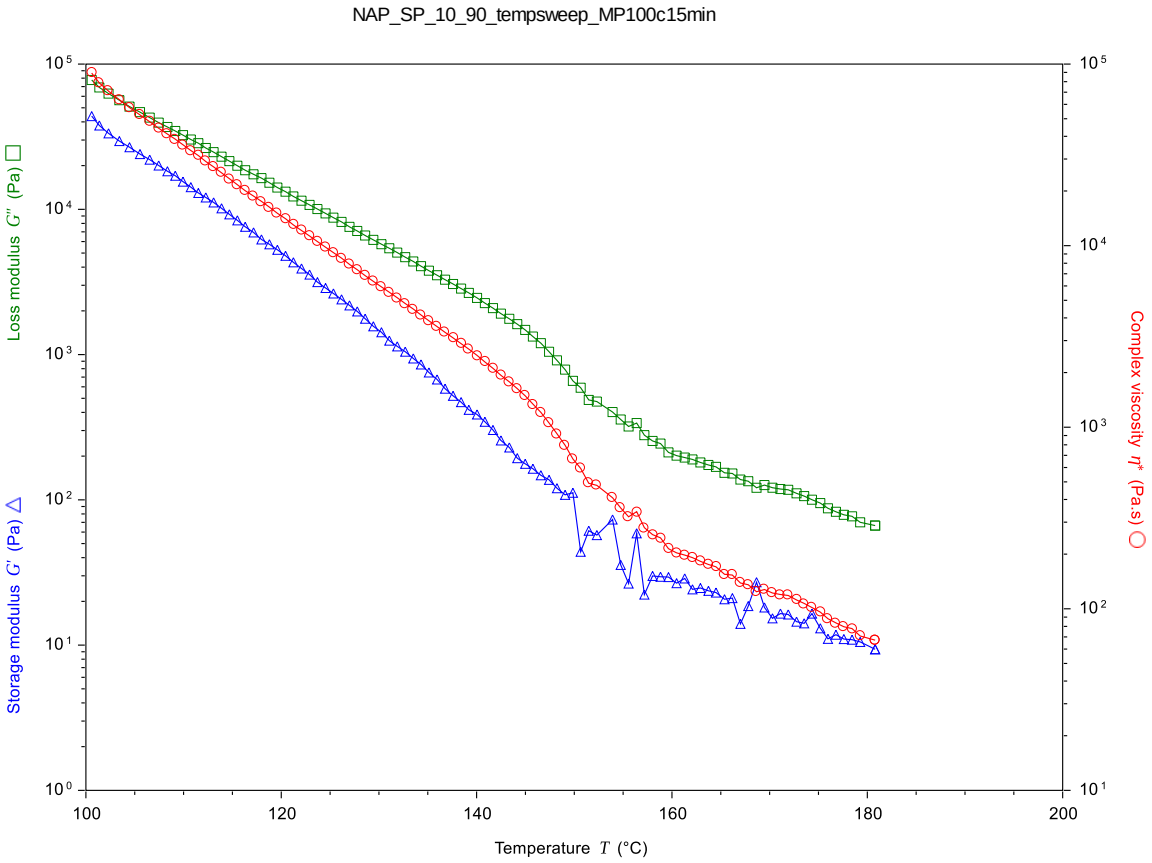

Figure 113 Temperature sweep NAP 10%

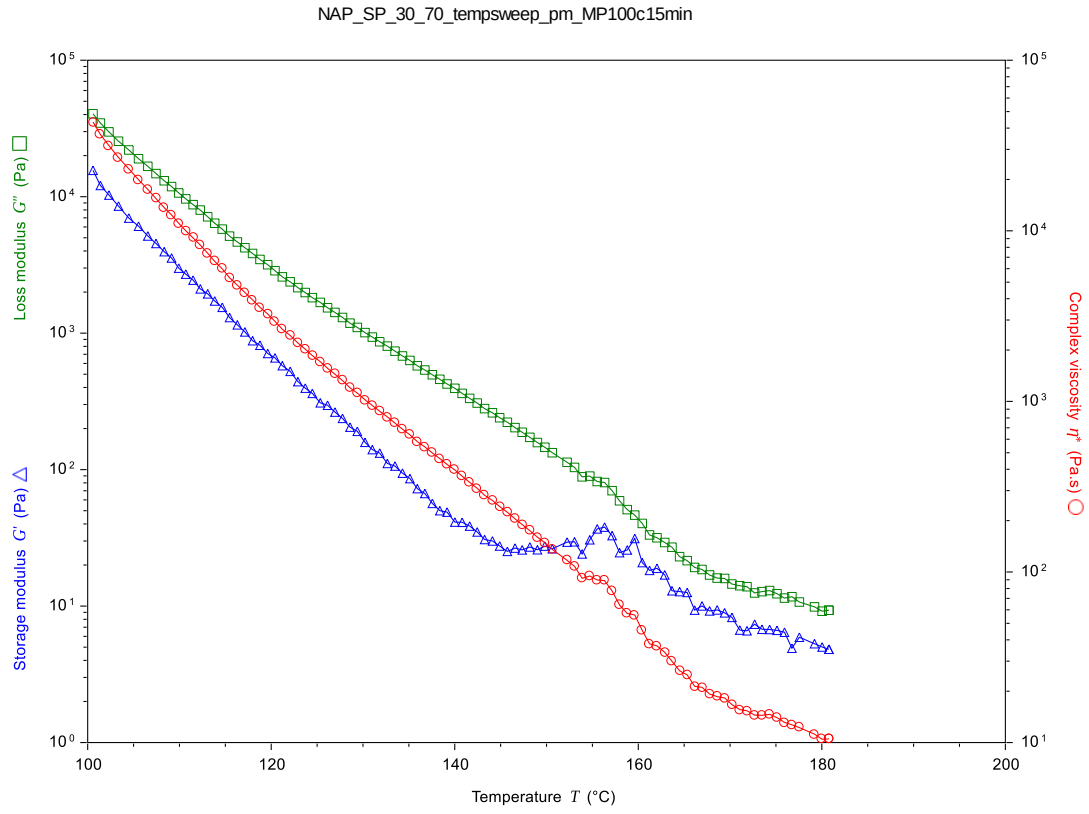

Figure 114 Temperature sweep NAP 30%

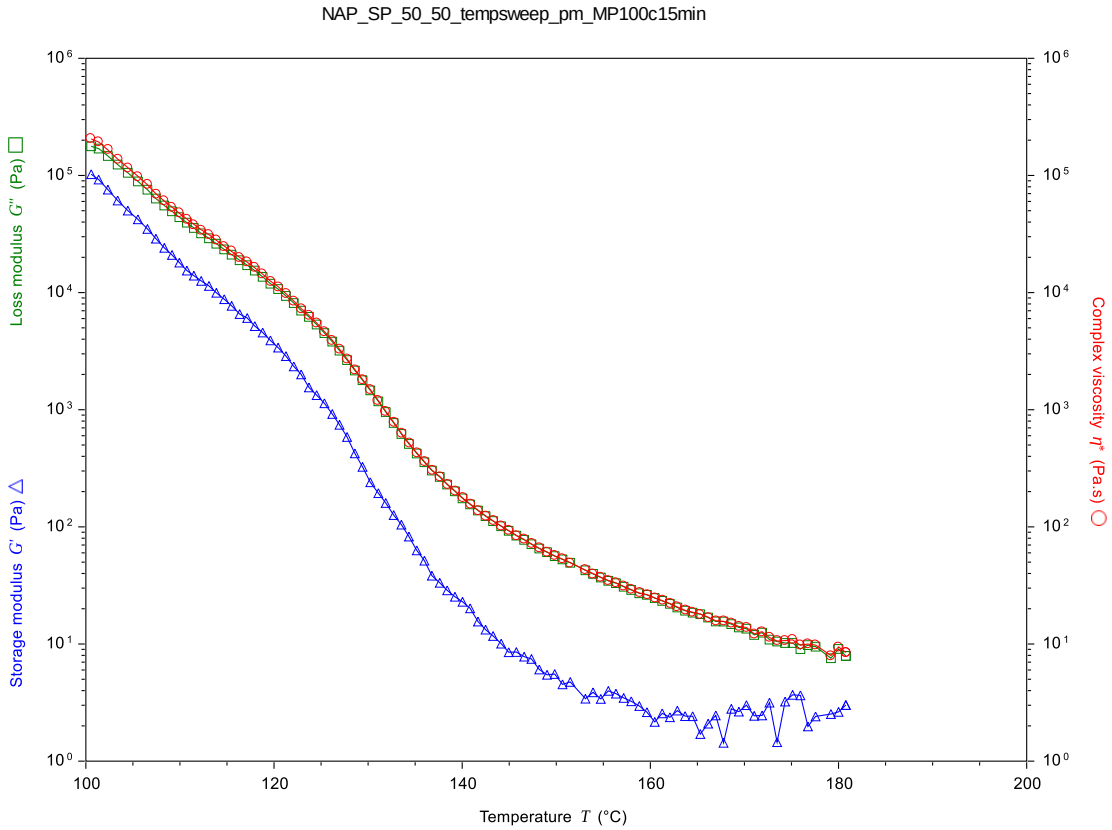

Figure 115 Temperature sweep NAP 50%

A.4 Raman

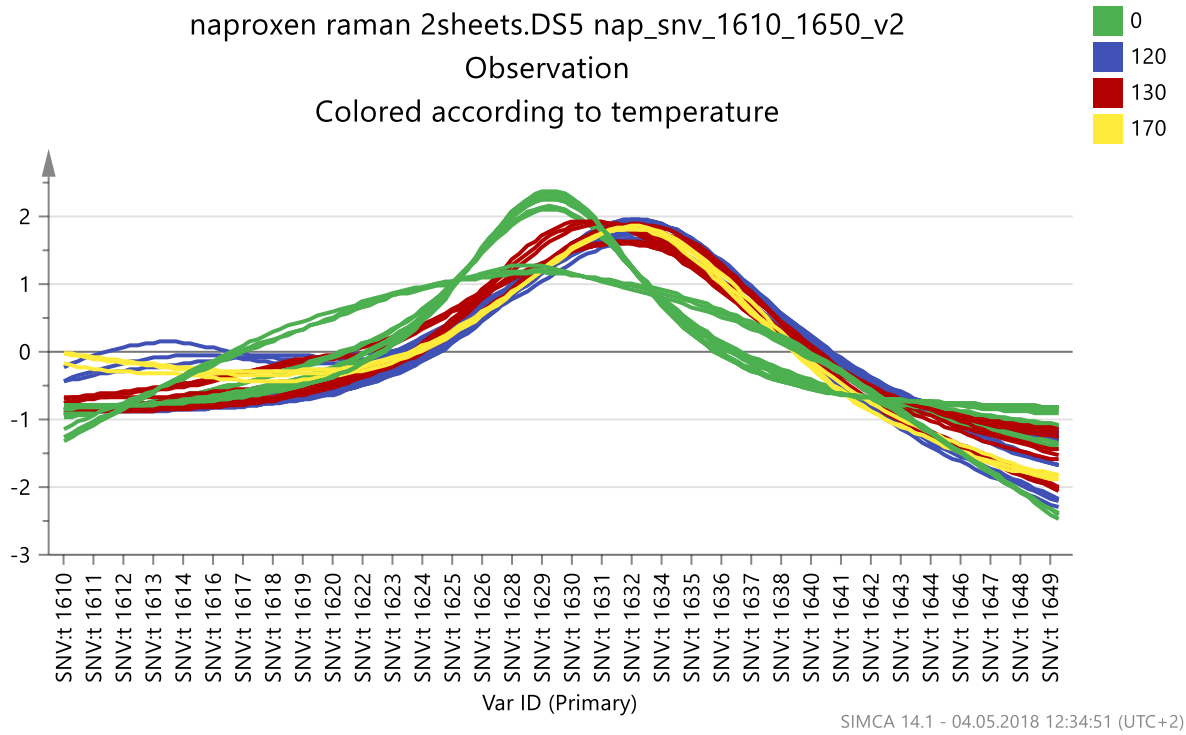

Figure 116 SNV corrected Raman spectra of NAP:Soluplus solid dispersions. Coloured according to process temperature. 120°C (blue) 130°C (red) and 170°C (yellow). Physical mixtures for reference(green)

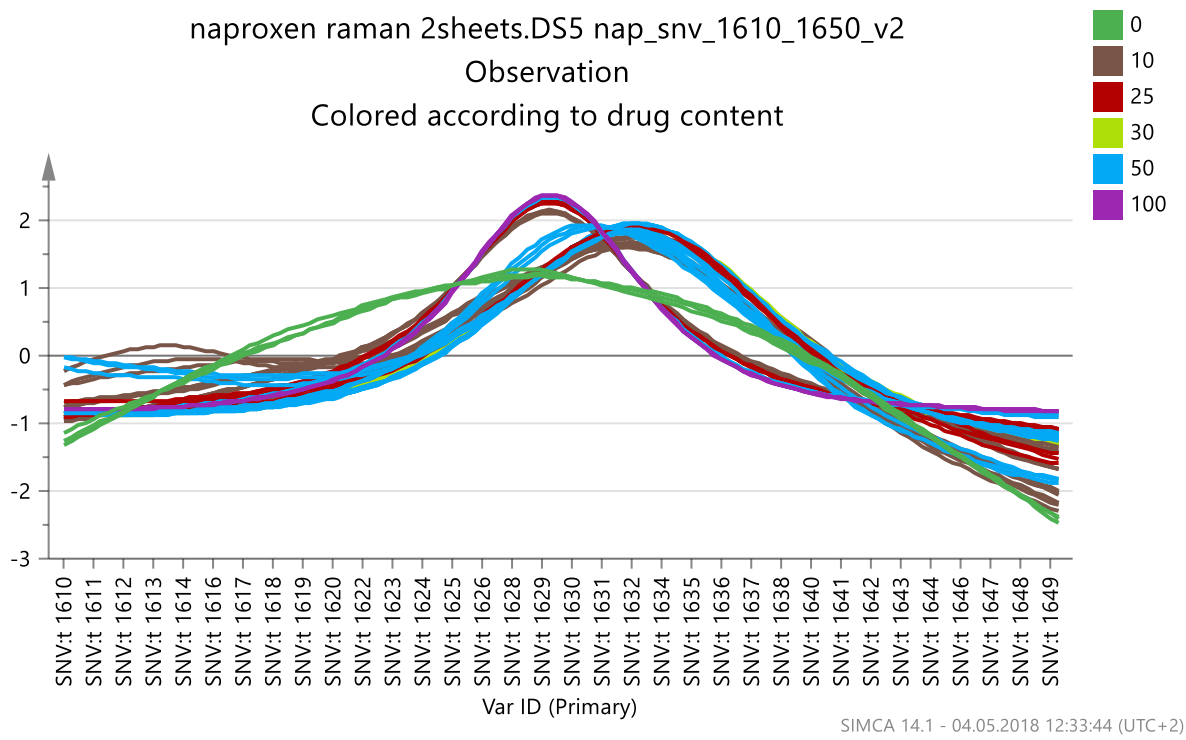

Figure 117 SNV corrected Raman spectra of NAP:Soluplus solid dispersions. Coloured according to NAP content. Soluplus std (green), 10% (brown), 25%(red), 30% (lime) 50% (blue) 100% crystalline NAP (purple)

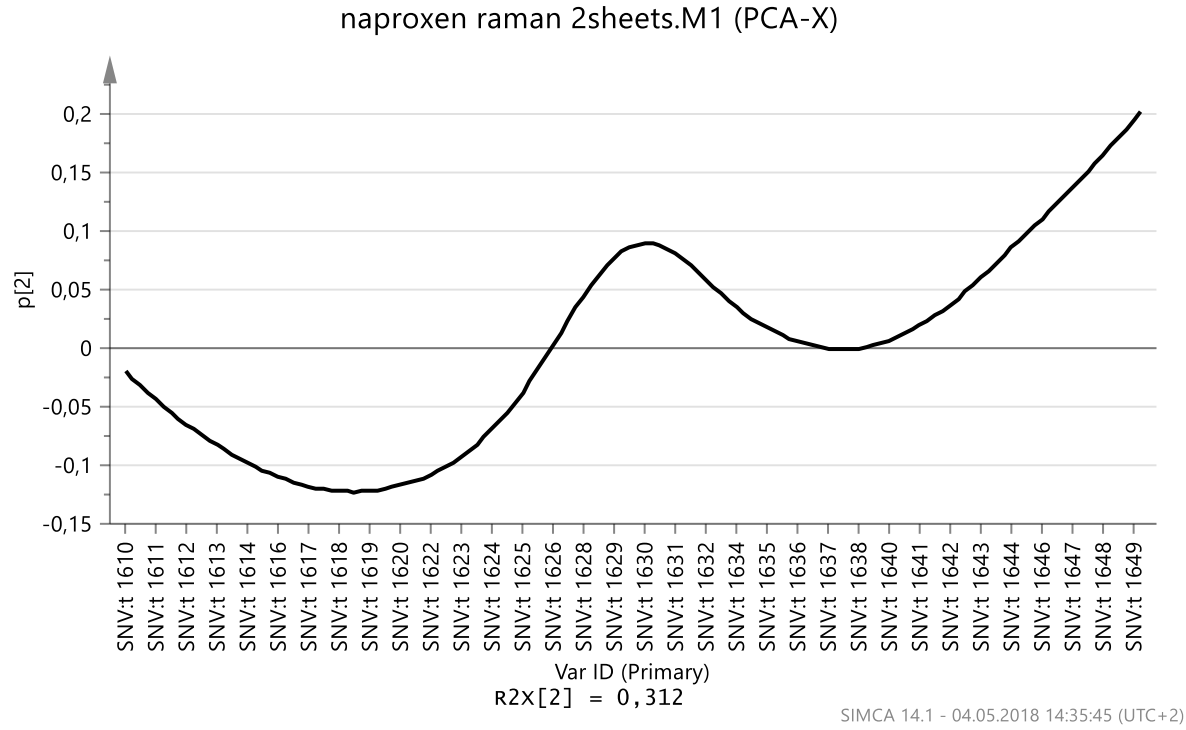

Figure 118 Loadings plot of the second component (PC-2) 31,2% explained variance

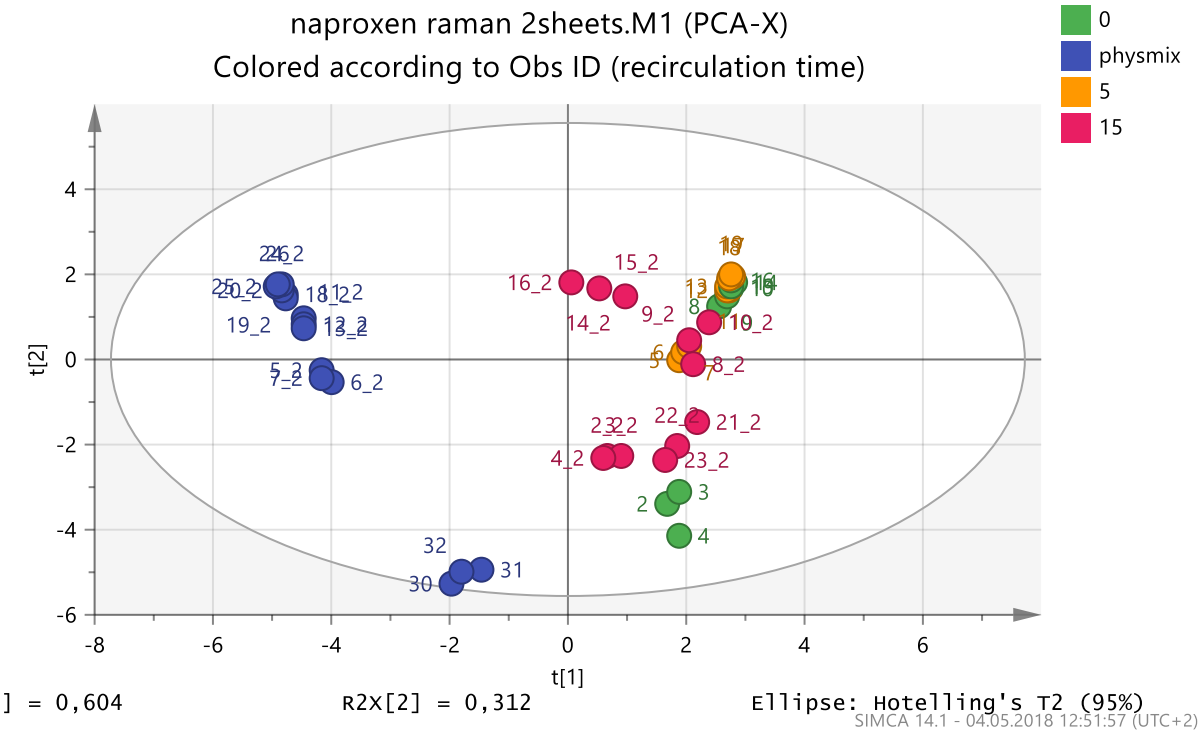

Figure 119 PCA of NAP:Soluplus. Coloured according to recirculation time. No recirculation time, HME (green) 5 minute recirculation time HME (orange) 15minute VCM (red). Physical mixtures as reference (blue)

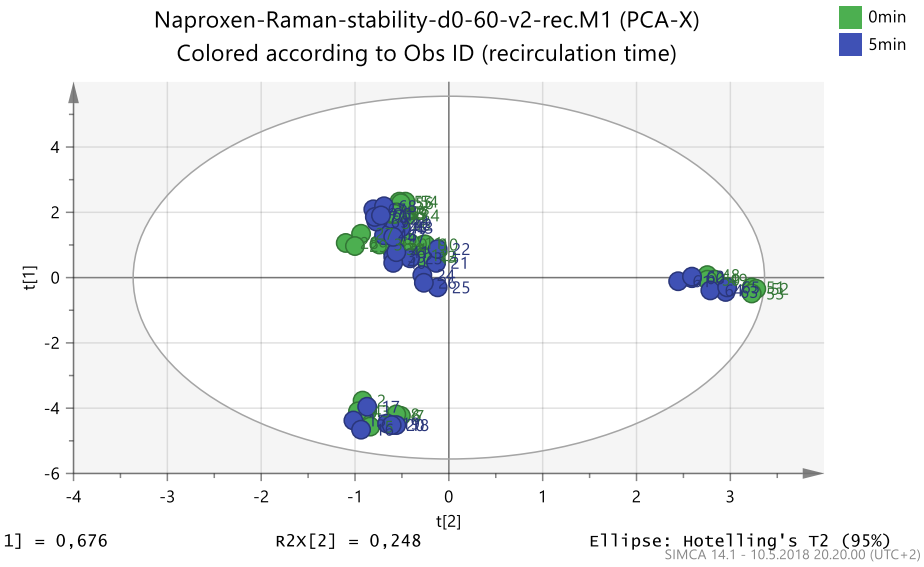

Figure 120 PCA of NAP:Soluplus. Coloured according to recirculation time

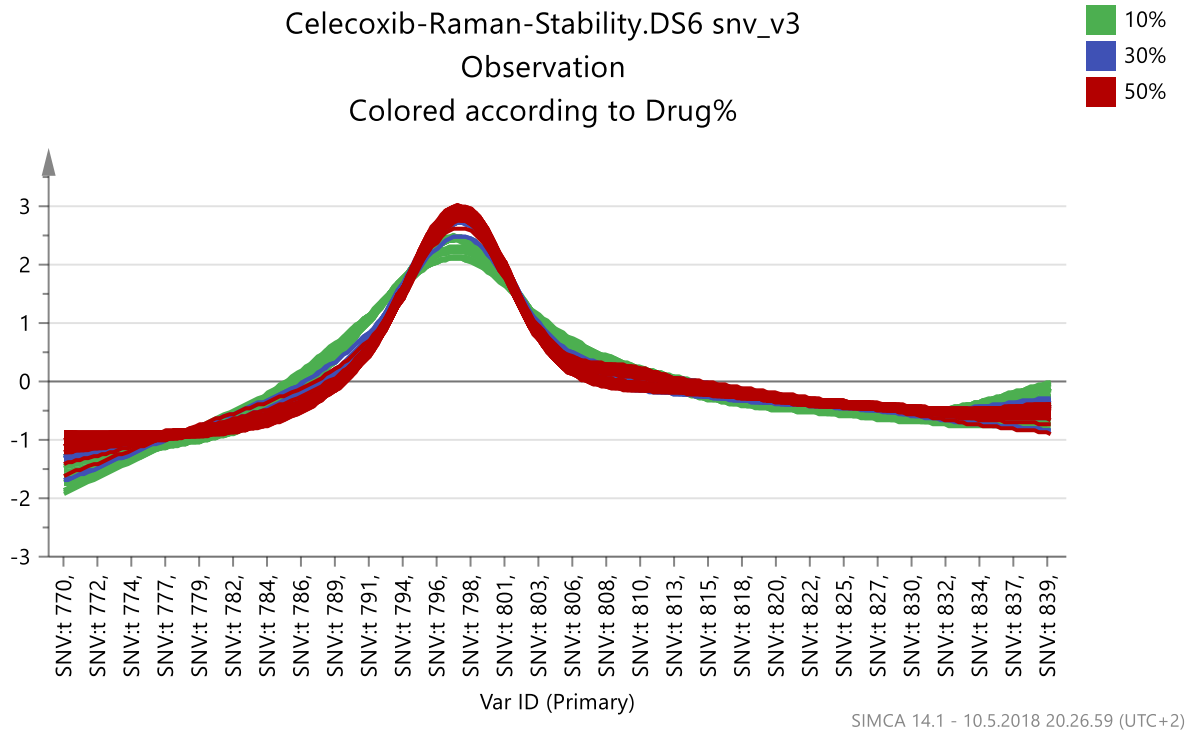

Figure 121 SNV corrected Raman spectra of CCX:Soluplus solid dispersions during storage. Coloured by drug content.

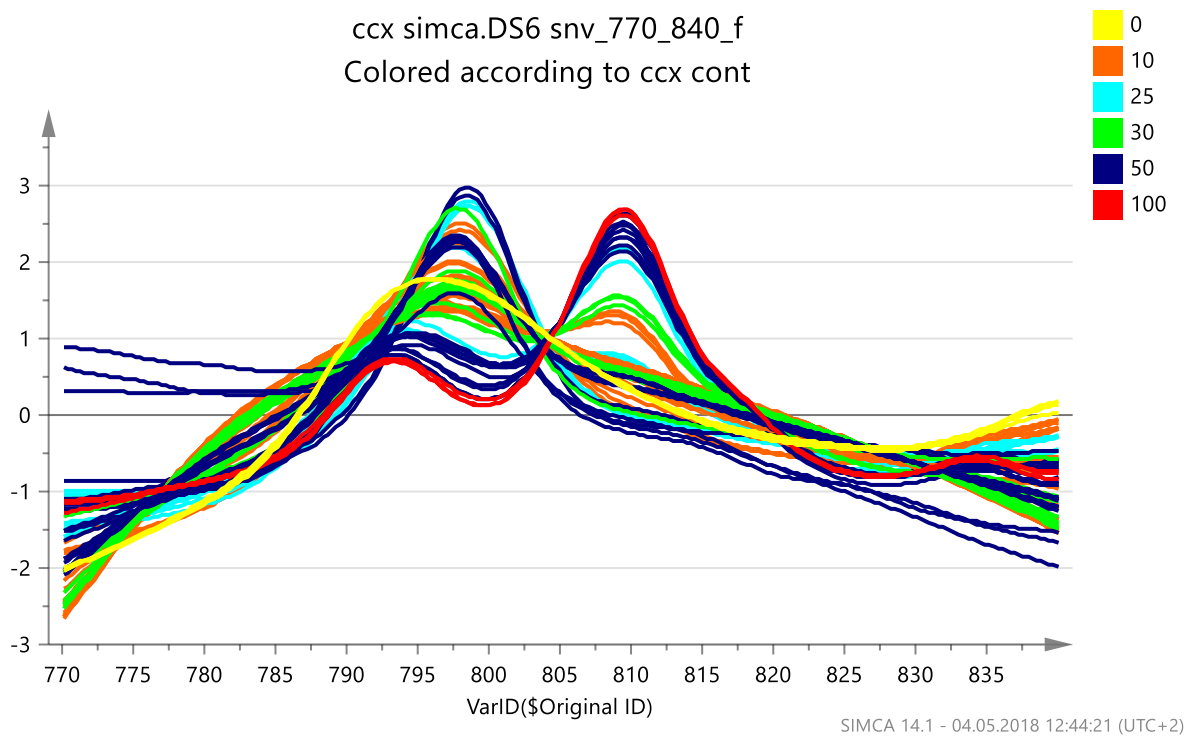

Figure 122 Figure 43 SNV corrected Raman spectra of CCX:Soluplus solid dispersions. Coloured according to CCX content. Soluplus std(yellow), 10% (orange), 25% (teal), 30% (green), 50% (blue). 100% crystalline std (red)

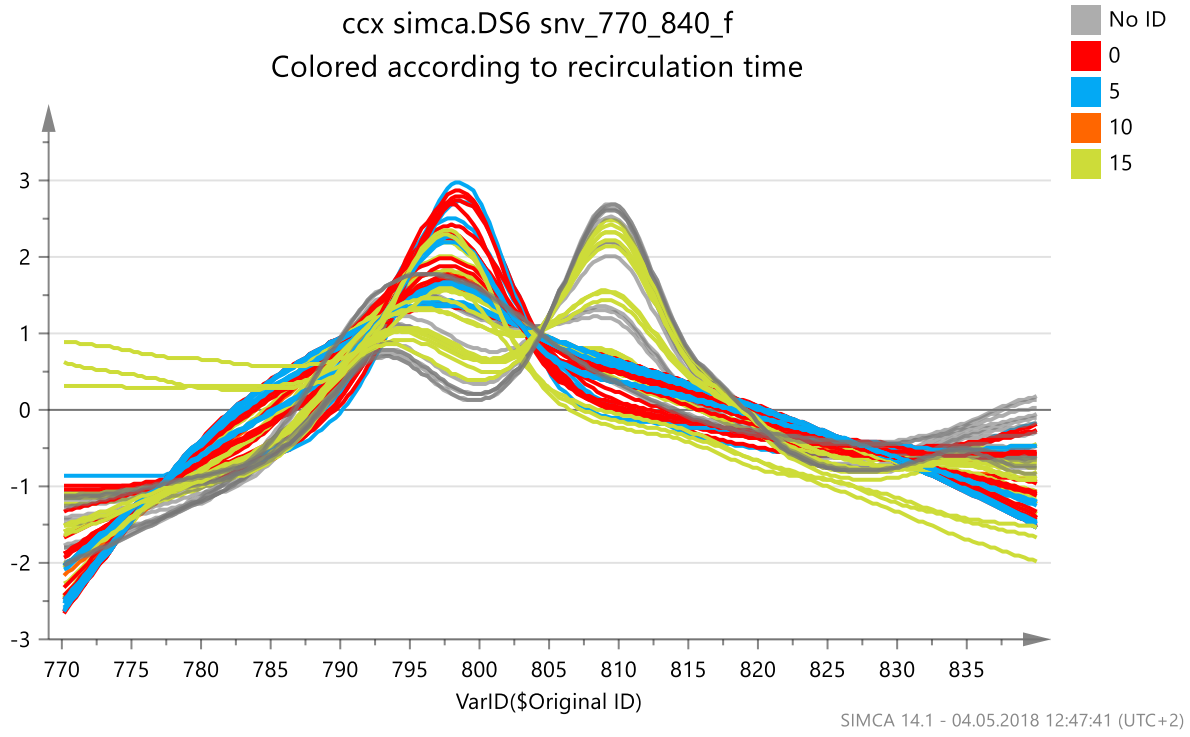

Figure 123 SNV corrected Raman spectra of CCX:Soluplus solid dispersions. Coloured according to recirculation time. No recirculation (red) 5 minute recirculation (blue) 10 minute MeltPrep (oragen) 15 minute MeltPrep(green). Physical mixtures for reference (grey/No ID)

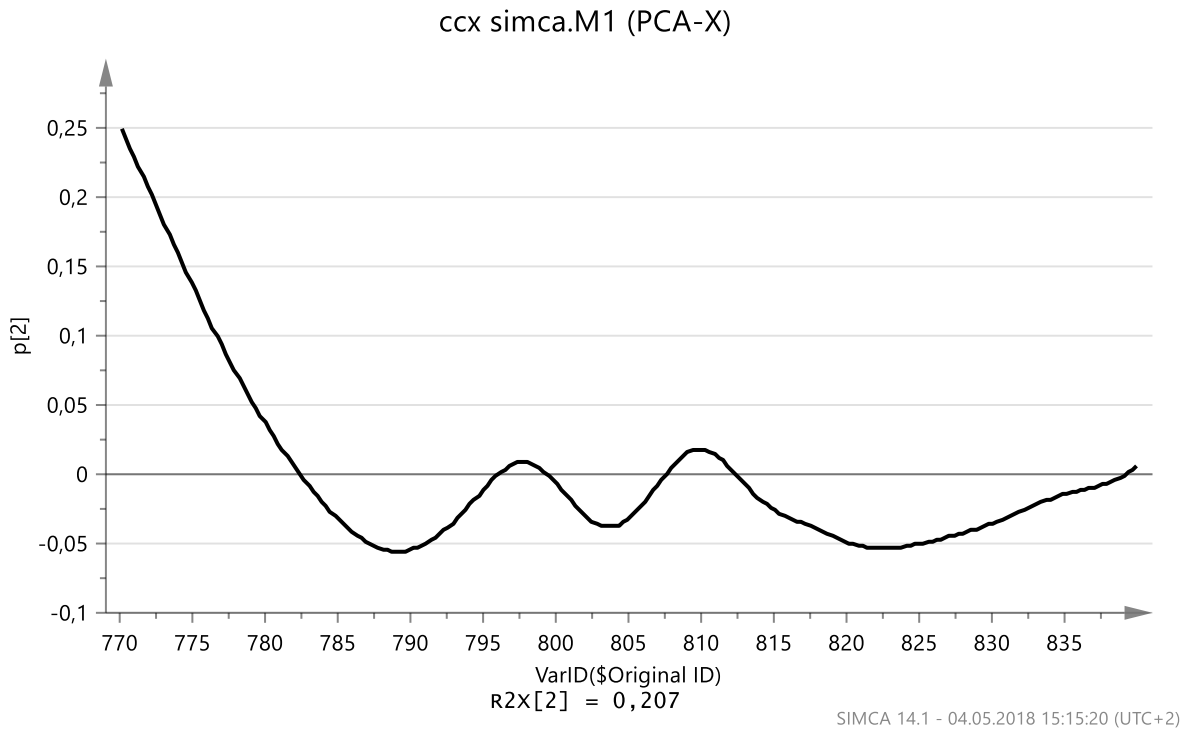

Figure 124 Loadings plot of the second component (PC-2) 20,7% explained variance

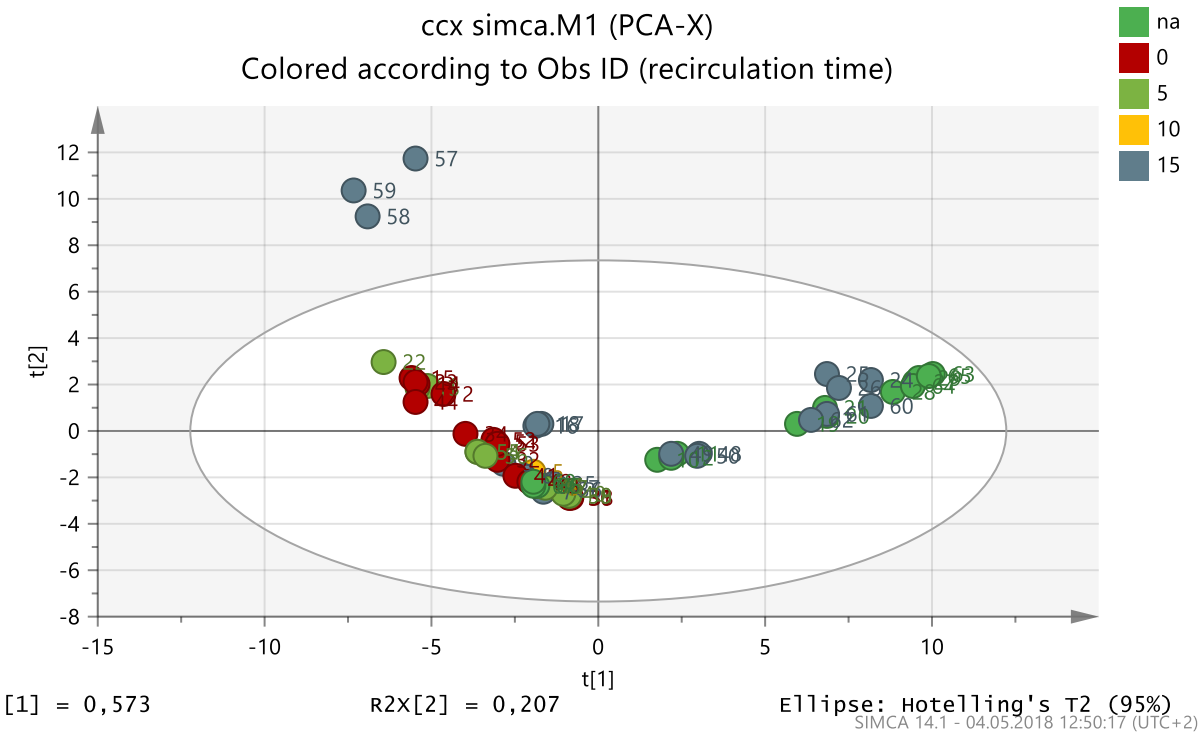

Figure 125 PCA of CCX:Soluplus. Coloured according to recirculation time. No recirculation, HME (red), 5min recirculation HME (olive green). 10 min VCM (yellow) 15min VCM (grey). Physical mixtures as reference,na (green).